Application of novel instrumental analytical approaches for the characterization of surface related phenomena in the context of automotive manufacturing

Dissertation

zur Erlangung des Doktorgrades der Naturwissenschaften

(Dr. rer. nat.)

der Fakultät für Chemie und Pharmazie

der Universität Regensburg

vorgelegt von

Stefan Viehbeck

aus **Dingolfing**

Oktober 2018

Die vorgelegte Dissertation entstand im Zeitraum von November 2014 bis Oktober 2018 in Kooperation des Instituts für Analytische Chemie, Chemo- und Biosensorik der naturwissenschaftlichen Fakultät IV - der Universität Regensburg

und

der Technologie Werkstoff und Verfahrensanalytik der BMW AG.

Die Arbeit wurde angeleitet von: Prof. Dr. habil. Frank-Michael Matysik

Das Promotionsgesuch wurde am 16.10.2018 eingereicht.
Das Kolloquium fand am 17.12.2018 statt.

Vorsitz des Prüfungsausschusses übernahm Prof. Dr. Robert Wolf. Erstgutachter war Prof. Dr. Frank-Michael Matysik, Zweitgutachter war Herr Prof. Dr. Rudolf Bierl und Drittprüfer war PD Dr. Hans-Heiner Gorris.

-„Scientia nihil aliud est quam veritatis imago“-
„Die Wissenschaft ist nichts als das Abbild der Wahrheit.“
Francis Bacon, 1561-1626

Table of contents

Table of contents ..... **I**

List of publications ..... **IV**

Conference contributions ..... **VII**

Declaration of collaboration ..... **VIII**

List of abbreviations ..... **IX**

Graphical Abstract **1**

Introduction **2**

1 Theory **7**
1.1 Materials 7
1.1.1 Carbon Fiber Reinforced Plastics 7
1.1.2 Adhesives 11
1.1.3 References 13
1.2 Analytical techniques 14
1.2.1 Atomic Force Microscopy 14
1.2.2 Chemical Force Microscopy 20
1.2.3 X-ray photolectron spectroscopy 21
1.2.4 DART-Q-ToF-MS 23
1.2.5 References 26
1.3 Mechanical tests 30
1.3.1 Tensile-shear-test 30
1.3.2 Peel-test 31
1.3.3 References 32

2 Experimental **33**
2.1 Chemicals and materials 33
2.2 Measurements 34

3 Results & Discussion 35
3.1 Analytical approach for the formulation of a reference adhesive system 35
3.1.1 Introduction 35
3.1.2 Experimental Procedure 35
3.1.3 Results & Discussion 38
3.1.4 Conclusion 39
3.1.5 References 39
3.2 Evaluation of industrial samples with various surface characterization techniques 40
3.2.1 Introduction 40
3.2.2 Application of direct analysis in real time (DART) and direct inlet probe (DIP-APCI) mass spectrometry in the context of industrial sample analysis 41
3.2.3 AFM 51
3.2.4 XPS 55
3.2.5 References 58
3.3 Method development for self-assembled monolayer functionalization of atomic force microscope cantilevers 62
3.3.1 Introduction 62
3.3.2 Experimental Procedure 62
3.3.3 Results & Discussion 64
3.3.4 Conclusion 66
3.3.5 References 67
3.4 Complementary analytical imaging techniques for the characterization of pretreated carbon fiber reinforced plastics 68
3.4.1 Graphical Abstract 68
3.4.2 Abstract 68
3.4.3 Introduction 69
3.4.4 Experimental Procedure 71
3.4.5 Results & Discussion 73
3.4.6 Conclusion 82
3.4.7 Appendix 83
3.4.8 References 84

3.5 Characterization of environmental aging effects on industrial carbon fiber reinforced plastic building parts 87
3.5.1 Introduction 87
3.5.2 Experimental Procedure 87
3.5.3 Results & Discussion 87
3.5.4 Conclusion 92
3.5.5 References 93
3.6 Evaluation of an industrial approach for improving a surface protecting cavity wax with a combination of different analytical techniques 94
3.6.1 Introduction 94
3.6.2 Experimental Procedure 96
3.6.3 Results & Discussion 99
3.6.4 Conclusion 102
3.6.5 References 103
3.7 Verifaction of urea as aldehyde diminishing component in a newly formulated industrial cavity wax 104
3.7.1 Introduction 104
3.7.2 Experimental Procedure 105
3.7.3 Results & Discussion 105
3.7.4 Conclusion 106
3.7.5 References 106

4 Summary 107

5 Zusammenfassung in deutscher Sprache 109

6 List of Figures 111

List of publications

Peer reviewed articles

Application of direct analysis in real time (DART) and direct inlet probe (DIP-APCI) mass spectrometry in the context of industrial sample analysis

Stefan Viehbeck and Frank-Michael Matysik
Monatshefte für Chemie - Chemical Monthly (2016) 147:1349-1352

Abstract In today′s industry, quick and reliable analytical methods play an important role for quality control. On that account, two emerging techniques, namely direct inlet probe-atmospheric pressure chemical ionization (DIP-APCI) and direct analysis in real time (DART) mass spectrometry, are particularly promising. In case of a DIP-APCI source, small amounts of solid or liquid samples can be studied without sample pre-treatment. A similar system is the DART ion source. In addition to the analysis of solid and liquid samples without preseparation, this ion source offers the possibility to scan the surface of a sample. A method for industrial sample analysis focusing on the study of delamination of coatings from a panel was developed using DIP-APCI-Q-ToF-MS and DART-Q-ToF-MS, respectively. Comparative studies based on the conventional pyrolysis-GC-MS were carried out.

Complementary analytical imaging techniques for the characterization of pretreated carbon fiber reinforced plastics

Stefan Viehbeck, Christian Iffelsberger and Frank-Michael Matysik
Composites Part A: Applied Science and Manufacturing (2018) 113:32-39

Abstract In this work the complementary characterization of pretreatment techniques for adhesive bonding of carbon fiber reinforced plastics (CFRP) is presented. Industrial CFRP plates were pretreated with laser, plasma and corundum blasting abrasive techniques followed by chemical activation. The combined use of atomic force microscopy and chemical force microscopy enabled the characterization of the surface morphology and the specific adhesion force between a chemically functionalized cantilever and the

pretreated surfaces simulating the adhesive bond. Complementary measurements with scanning electrochemical microscopy and X-ray photoelectron spectroscopy supported the experimental findings and delivered additional information about the chemical structure of the surfaces. A comparison of experimental data of mechanical tensile shear strength measurements and the applied analytical methods revealed a valid correlation of microscopic and macroscopic techniques.

Corrosion protection agent and method for the preservation of a cavity

Stefan Viehbeck, Günther Mayer, Johann Troffer, BMW AG
European Patent: EP3344708, published 11.07.2018

Abstract Die vorliegende Erfindung betrifft ein Korrosionsschutzmittel, das insbesondere in der Hohlraumkonservierung Anwendung findet, also in Hohlräumen, wie sie z.B. in Fahrzeugkarosserien vorzufinden sind. Darüber hinaus betrifft die vorliegende Erfindung auch ein Verfahren zum Konservieren eines Hohlraumes.

Hohlraumkonservierungen sind insbesondere aus dem Fahrzeugbau bekannt und bieten nach Applikation, beispielsweise auf ein metallisches Element, einen guten Schutz vor Korrosion, durch auf das metallische Element einwirkendes Wasser oder eine feuchtigkeitshaltige Umgebung. Übliche Hohlraumkonservierungsmittel enthalten Wachse oder Harze sowie Korrosionsschutzadditive, die durch Dispergieren in Lösungsmitteln applizierfähig gemacht werden. Nach dem Abtrocknen, Härten und ggf. Vernetzen des Hohlraumkonservierungsmittels bildet das Hohlraumkonservierungsmittel auf der applizierten Oberfläche einen vor Korrosion schützenden Film. Nachteilig an herkömmlichen Hohlraumkonservierungsmitteln ist, dass sie eine lange Trocknungs- bzw. Vernetzungsdauer und oftmals eine nicht vollständige Durchtrocknung zeigen. Dies erhöht die Verfahrenskosten für die Konservierung und erfordert oftmals eine manuelle Nachbehandlung zur Entfernung von Resten der Hohlraumkonservierung.

Ausgehend von diesem Stand der Technik ist es Aufgabe der vorliegenden Erfindung, ein Korrosionsschutzmittel bereitzustellen, das sich durch eine hohe, und gezielt steuerbare Trocknungs- bzw. Härtungsrate und Vernetzung auszeichnet. Darüber hinaus ist es Aufgabe der vorliegenden Erfindung, ein Verfahren zum Konservieren eines Hohlraumes anzugeben, das zeitsparend und einfach, ohne hohen technischen Aufwand umsetzbar ist

und durch dessen Anwendung ohne aufwendige Nacharbeit ein gleichmäßiger Korrosionsschutzfilm erhalten werden kann.

Corrosion inhibitors

Stefan Viehbeck, Günther Mayer, Johann Troffer, BMW AG
German Patent: DE102016210913A1, application 2017-12-21

Abstract Die vorliegende Erfindung betrifft ein Korrosionsschutzmittel, das insbesondere in der Hohlraumkonservierung Anwendung findet, also in Hohlräumen, wie sie beispielsweise in Fahrzeugkarosserien vorzufinden sind. Hohlraumkonservierungen sind insbesondere aus dem Fahrzeugbau bekannt und bieten nach Applikation, beispielsweise auf ein metallisches Element, einen guten Schutz vor Korrosion wenn auf dieses metallische Element Wasser oder eine feuchtigkeitshaltige Umgebung einwirkt. Übliche Hohlraumkonservierungen enthalten Wachse, Fette, Öle oder Harze, sowie Korrosionsschutzadditive, die durch Dispergieren in Lösungsmitteln applizierfähig gemacht werden. Gerade die verwendeten Wachse, Fette oder Öle werden z.B. durch oxidative Härtung haftend gemacht. Hierbei entstehen Aldehyde als Spaltprodukte. Aufgrund der gesundheitsschädigenden und geruchsbeeinträchtigenden Wirkung der Aldehyde wären Korrosionsschutzmittel, die eine Freisetzung von Aldehyden verhindern oder zumindest reduzieren, von Vorteil. Ausgehend von diesem Stand der Technik ist es somit Aufgabe der vorliegenden Erfindung, ein Korrosionsschutzmittel bereitzustellen, das sich durch eine niedrige Freisetzungsrate von Aldehyden auszeichnet und daher anwendungssicher, gesundheitsunbedenklich sowie geruchsoptimiert ist.

Conference contributions

Oral presentations

ANAKON 2017, 3.-6.4.2017, Tübingen
Analytical characterization of lightweight car parts with chemical force microscopy and DART-Q-TOF-MS
Stefan Viehbeck and Frank-Michael Matysik

Modern analytical chemistry 2015, 22.-23.09.2015 Prague
Comparison of two direct ion sources coupled to a MS system (DART-MS and DIP-MS)
Stefan Viehbeck and Frank-Michael Matysik

XPS User Meeting 2018, 14.-17.05.2018 Eibelstadt
Industrial application of XPS at an automotive company
Stefan Viehbeck

Poster presentations

ANAKON 2015, 23.-26.3 2015, Graz, Austria
Comparison of two direct ion sources coupled to a MS system (DART-MS and DIP-MS)
Stefan Viehbeck and Frank-Michael Matysik

Declaration of collaboration

Most of the theoretical and experimental work presented in this thesis was carried out solely by the author. In some cases, however, the practical implementation of concepts and the performance of measurements were carried out in collaboration with other researchers and individuals. In accordance with § 8 Abs. 1 Satz 7 of the Ordnung zum Erwerb des akademischen Grades eines Doktors der Naturwissenschaften (Dr. rer. nat.) an der Universität Regensburg vom 18. Juni 2009 (Änderungssatzung vom 6. Februar 2014), this section details the nature of these collaborations. This list is sorted according the sections of this thesis.

3.4 Complementary analytical imaging techniques for the characterization of pretreated carbon fiber reinforced plastics
Experimental work regarding SECM was done in collaboration with Christian Iffelsberger at the facilities of University Regensburg. Further measurements and experiments such as AFM, CFM, XPS, macroscopic tests and optical microscopy were done solely by the author. The authors contributed equally for interpretation and writing. The research was done under supervision and guidance of Prof. Dr. Frank-Michael Matysik.

3.6 Evaluation of an industrial approach for improving a surface protecting cavity wax with a combination of different analytical techniques
The experimental work was done in collaboration with Günther Mayer. Both authors contributed equally to the experimantal work and novelty of the invention. The research was done under supervision of Johann Troffer, Christian Lang and Prof. Dr. Frank-Michael Matysik.

3.7 Verifaction of urea as aldehyde diminishing component in a newly formulated industrial cavity wax
The experimental work was done in collaboration with Günther Mayer. Both authors contributed equally to the experimantal work and novelty of the invention. The research was done under supervision of Johann Troffer, Christian Lang and Prof. Dr. Frank-Michael Matysik.

List of abbreviations

AFM Atomic force microscopy

CFRP Carbon fiber reinforced plastic

DART Direct analysis in real time

DFCM Dynamic fluid compression molding

DIP-APCI Direct inlet probe - Atmospheric pressure ionization

ESCA Electron spectroscopy for chemical analysis, synonymous for XPS

FT-IR Fourier-transform infrared Spectroscopy

GC Gas chromatography

HPLC High performance liquid chromatography

PAN Polyacrylonitrile

PUR Polyurethane

Q-ToF-MS Quadrupole Time-of-flight mass spectrometry

RTM Resin transfer molding

SECM Scanning electrochemical microscopy

XPS X-ray photoelectron spectroscopy

Graphical Abstract

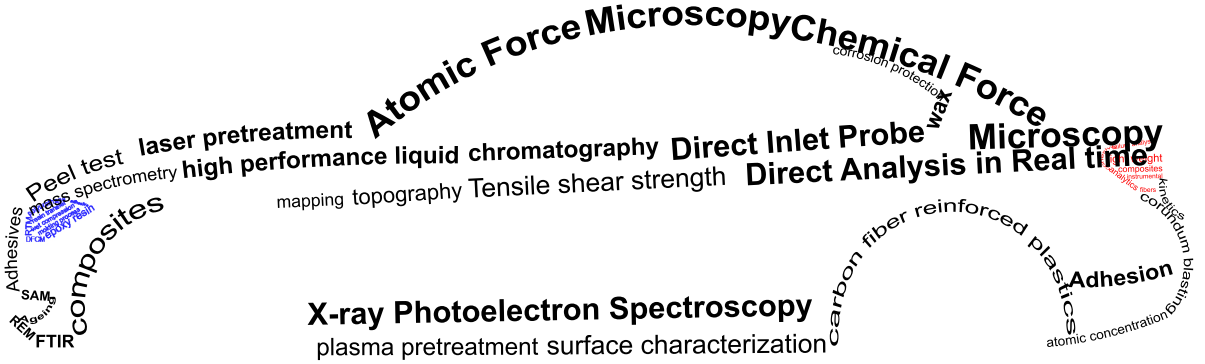

Introduction

Chemical analysis plays a major role in today's society. With high demands on quality[1][2], increasing regulations[3], health issues[4] and environmental pollution[5][6][7], chemical analysis was implemented as a crucial supporting pillar in the identification and evaluation of the aforementioned issues. Besides applications in well known branches, such as food[8][9][10] or the pharmacy industry[11][12], other industries have a high demand for quality and quality control. Leading companies in the premium sector of the automotive industry have an especially high quality requirement[13][14][5]. This has been a considerable challenge for analytical research with ever-increasing numbers of products[15][16][17]. It is enormously important to have fast and reliable analytical techniques to handle complex problem definitions, in addition to routine analysis. The task, however, gets more complex with the increasing diversity of materials installed in modern vehicles. Simple metal or plastic components may have unexpected behavior, due to the production process, adhesives or coatings, which may contribute to detechments and materials which lead to increased pollutant emission[18]. Even newly developed materials, such as fuel cells[19], battery technology[20] or composites[21] must have composition and functionality verified. Thus, analysis and quality control are essential parts of the remediation, verification and identification of issues in the development and manufacturing process. As a result, the automotive industry is increasingly focused on analytical techniques of a broad range of materials with a focus on surface characterization. Typically, a laboratory is equipped with techniques from all fields of analysis. An important field is liquid and gas chromatography coupled with mass spectrometry for the analysis of materials and textiles, additives and coatings. Inductively coupled plasma - optical emission spectrometry (ICP-OES), or ion chromatography (IC), and fourier-transform infrared spectroscopy (FT-IR) are also used for the quality control of materials. Material evaluations of physical parameters are typically done with mechanical tests, such as tensile strength, peel tests or rheology measurements. Computer tomography is used for detailed material-structure analysis and high resolution mass spectrometry is used for material composition analysis.

With a broad selection of available analytical techniques, it is important to focus on the expedient methods and implement techniques that are complimentary to the corresponding task. It is crucial to adopt analytical techniques in industrial production, especially for newly developed materials.

Due to the variety of materials installed in a modern car, the attachment and joining of two substrates is an important factor. For coatings and adhesives, the surface of the material to which each is applied plays a vital role in the manufacturing process. To understand the complex mechanism of adhesion when joining diverse materials, many factors must be considered, such as roughness, technical cleanliness of the surface, as well as chemical interactions and mechanisms (from covalent bonding to weak boundary interactions)[22][23][24]. For these delicate mechanisms and interactions, analytical techniques with a high sensitivity and a capacity for detailed surface characterization are required. Thus, new methods, ideally with little sample preparation, must be investigated. Here, the methods that should be taken into account include the field of direct ion sources coupled with mass spectrometry[25], atomic force microscopy[26] and chemical characterization of the outer molecular layer of a surface using X-ray photoelectron spectroscopy[27].

Preliminary studies[28][29] have shown that atomic force microscopy in combination with chemically modified probing tips was promising for the evaluation of adhesion forces and material surfaces. Thus, a large part of this research is focused on the development of an atomic force microscopy (AFM) method for industrial automotive applications, along with an evaluation of the surface quality in composite bonding.

References

[1] H. Yichen, K. Weijun, Y. Xihui, X. Liwei, W. Jing, and Y. Meihua, "GC-MS combined with chemometric techniques for the quality control and original discrimination of Curcumae longae rhizome: Analysis of essential oils," *Journal of Separation Science*, vol. 37, no. 4, pp. 404–411, 2013.

[2] D. Doutre, B. Gariépy, J. P. Martin, and G. Dubé, "Aluminium Cleanliness Monitoring: Methods and Applications in Process Development and Quality Control BT - Essential Readings in Light Metals: Volume 3 Cast Shop for Aluminum Production," pp. 296–304, Cham: Springer International Publishing, 2016.

[3] K. Ravindra, R. Sokhi, and R. Van Grieken, "Atmospheric polycyclic aromatic hydrocarbons: Source attribution, emission factors and regulation," *Atmospheric Environment*, vol. 42, no. 13, pp. 2895–2921, 2008.

[4] A. Le Cigne, L. Chieze, A. Beaussart, S. El-Kirat-Chatel, Y. F. Dufrene, S. Dedieu, C. Schneider, L. Martiny, J. Devy, and M. Molinari, "Analysis of the effect of LRP-1 silencing on the invasive potential of cancer cells by nanomechanical probing and adhesion force measurements using atomic force microscopy," *Nanoscale*, vol. 8, no. 13, pp. 7144–7154, 2016.

[5] C. Moschet, I. Wittmer, J. Simovic, M. Junghans, A. Piazzoli, H. Singer, C. Stamm, C. Leu, and J. Hollender, "How a Complete Pesticide Screening Changes the Assessment of Surface Water Quality," *Environmental Science & Technology*, vol. 48, no. 10, pp. 5423–5432, 2014.

[6] D. Ašperger, V. Tišler, M. Zrnčić, D. Mutavdžić Pavlović, S. Babić, A. J. M. Horvat, and M. Kaštelan-Macan, "HPLC-DAD-FLD Determination of Veterinary Pharmaceuticals in Pharmaceutical Industry Wastewater with Precolumn Derivatization Using Fluorescamine," *Chromatographia*, vol. 77, no. 15, pp. 1059–1066, 2014.

[7] S. L. Wright and F. J. Kelly, "Plastic and Human Health: A Micro Issue?," *Environmental Science & Technology*, vol. 51, no. 12, pp. 6634–6647, 2017.

[8] E. Dorta, M. González, M. G. Lobo, C. Sánchez-Moreno, and B. de Ancos, "Screening of phenolic compounds in by-product extracts from mangoes (Mangifera indica L.) by HPLC-ESI-QTOF-MS and multivariate analysis for use as a food ingredient," *Food Research International*, vol. 57, pp. 51–60, 2014.

[9] E. Crawford and B. Musselman, "Evaluating a direct swabbing method for screening pesticides on fruit and vegetable surfaces using direct analysis in real time (DART) coupled to an Exactive benchtop orbitrap mass spectrometer," *Analytical and Bioanalytical Chemistry*, vol. 403, no. 10, pp. 2807–2812, 2012.

[10] X. He, J. Li, W. Zhao, R. Liu, L. Zhang, and X. Kong, "Chemical fingerprint analysis for quality control and identification of Ziyang green tea by HPLC," *Food Chemistry*, vol. 171, pp. 405–411, 2015.

[11] S. Alipour, A. Mohammadi, and F. Ahmadi, "Captopril fast disintegrating tablets for children: formulation and quality control by HPLC," *Trends in Pharmaceutical Sciences*, vol. 3, no. 3, 2017.

[12] M. Petrović, B. Škrbić, J. Živančev, L. Ferrando-Climent, and D. Barcelo, "Determination of 81 pharmaceutical drugs by high performance liquid chromatography coupled to mass spectrometry with hybrid triple quadrupole-linear ion trap in different types of water in Serbia," *Science of The Total Environment*, vol. 468-469, pp. 415–428, 2014.

[13] A. M. Beale, F. Gao, I. Lezcano-Gonzalez, C. H. F. Peden, and J. Szanyi, "Recent advances in automotive catalysis for NOx emission control by small-pore microporous materials," *Chem. Soc. Rev.*, vol. 44, no. 20, pp. 7371–7405, 2015.

[14] D. Hoyle, *Automotive Quality Systems Handbook*. Oxford: Elsevier Butterworth-Heinemann, 2 ed., 2005.

[15] B. D. Agarwal, L. J. Broutman, and K. Chandrashekhara, *Analysis and performance of fiber composites*. Wiley & Sons, 4 ed., 2018.

[16] Y. Li, J. Yang, and J. Song, "Design principles and energy system scale analysis technologies of new lithium-ion and aluminum-ion batteries for sustainable energy electric vehicles," *Renewable and Sustainable Energy Reviews*, vol. 71, pp. 645–651, 2017.

[17] Y. Nakagawa, K.-i. Mori, and T. Maeno, "3D printing of carbon fibre-reinforced plastic parts," *The International Journal of Advanced Manufacturing Technology*, vol. 91, no. 5, pp. 2811–2817, 2017.

[18] M. André and M. Rapone, "Analysis and modelling of the pollutant emissions from European cars regarding the driving characteristics and test cycles," *Atmospheric Environment*, vol. 43, no. 5, pp. 986–995, 2009.

[19] S. P. Jiang, "Thermally and Electrochemically Induced Electrode/Electrolyte Interfaces in Solid Oxide Fuel Cells: An AFM and EIS Study," 2015.

[20] M. Metzger, C. Marino, J. Sicklinger, D. Haering, and H. A. Gasteiger, "Anodic Oxidation of Conductive Carbon and Ethylene Carbonate in High-Voltage Li-Ion Batteries Quantified by On-Line Electrochemical Mass Spectrometry," *Journal of The Electrochemical Society*, vol. 162, no. 7, pp. A1123–A1134, 2015.

[21] C. Unterweger, J. Duchoslav, D. Stifter, and C. Fürst, "Characterization of carbon fiber surfaces and their impact on the mechanical properties of short carbon fiber reinforced polypropylene composites," *Composites Science and Technology*, vol. 108, pp. 41–47, 2015.

[22] A. Baldan, "Adhesion phenomena in bonded joints," *International Journal of Adhesion and Adhesives*, vol. 38, pp. 95–116, 2012.

[23] A. V. Pocius, *Adhesion and Adhesives Technology: An Introduction*. Munich: Carl Hanser Verlag, 3 ed., 2012.

[24] J. Schultz and M. Nardin, *Adhesion Promotion Techniques: Technological Applications*. New York: Marcel Dekker Inc., 2002.

[25] R. B. Cody, "Observation of Molecular Ions and Analysis of Nonpolar Compounds with the Direct Analysis in Real Time Ion Source," *Analytical Chemistry*, vol. 81, no. 3, pp. 1101–1107, 2009.

[26] G. Binnig and C. F. Quate, "Atomic Force Microscope," *Physical Review Letters*, vol. 56, no. 9, pp. 930–933, 1986.

[27] K. Siegbahn and K. Edvarson, "β-Ray spectroscopy in the precision range of 1 : 105," *Nuclear Physics*, vol. 1, no. 8, pp. 137–159, 1956.

[28] C. D. Frisbie, L. F. Rozsnyai, A. Noy, M. S. Wrighton, and C. M. Lieber, "Functional Group Imaging by Chemical Force Microscopy," *Science*, vol. 265, no. 5181, pp. 2071–2074, 1994.

[29] S. Raman, T. Utzig, T. Baimpos, B. Ratna Shrestha, and M. Valtiner, "Deciphering the scaling of single-molecule interactions using Jarzynski's equality," *Nature Communications*, vol. 5, p. 5539, 2014.

1 Theory

1.1 Materials

1.1.1 Carbon Fiber Reinforced Plastics

Carbon fiber composites have unique characteristics, when compared to other building materials of the automotive manufacturing process. The composites have a high tensile strength to weight ratio, a low coefficient of linear thermal expansion, high fatigue strengths and high thermal conductivity; all of which provide technical advancements for the automotive industry[1].

The polymeric fibers containing carbon have a diameter of 7 µm, made of polyacrylonitrile (PAN), petroleum, bitumen or cellulose. To manufacture the precursors, liquid monomeric acrylonitrile is first polymerized with co-monomers, such as methacrylic acid. Additional initiators and redox-systems control the polymerization. A typical PAN precursor has a molecular weight of 80000 - 100000 g/mol and 94 - 99 w.% of acrylonatirile with 3000 single acrylonitrile units per PAN molecule. In a spinning process (Fig. 1.1) the fibers are hardened and elongated and the PAN molecules are forced in the direction of the fibers. A spool of several 100 kg is produced as a result, with 1000 - 320000 single fibers in one string. The fabrication of carbon fibers begins with stabilizing the precursor fibers at 200 - 300°C in air. A carbonation at 1300 - 1500°C follows under inert conditions, and the graphitization process is completed at 1800°C. Depending on the application, the surface is electrochemically activated and a finishing treatment is applied before the mechanical parameters can be influenced (shear strength, compatibility to matrix, elasticity)[2].

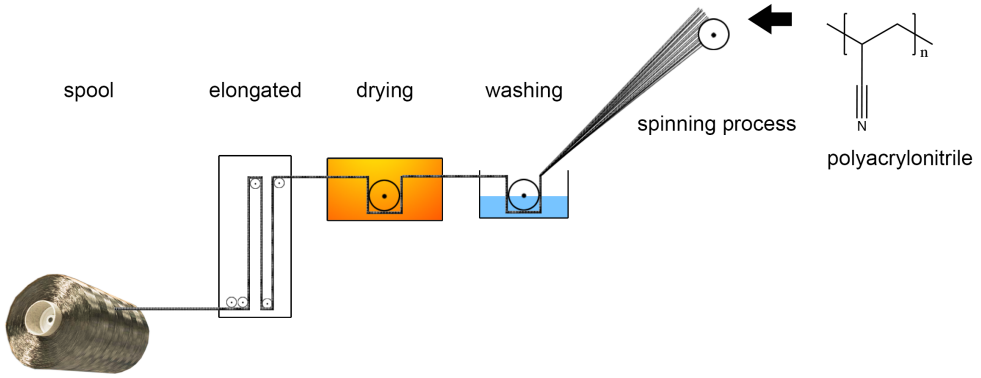

Figure 1.1: Industrial manufacturing process of fibers - polymerization, spinning, washing, drying, elongating, spool, adapted from [2]

Apart from the fibers, the matrix system influences the properties of the composite. There are two different types of polymeric matrix systems used - thermoset and thermoplastic polymers. The most common thermosets for carbon composite materials are epoxy resins. For industrial applications, the high flexibility in mechanical properties through the use of different chemical crosslinking in epoxy polymerization is a notable advantage. Crucial parameters of the matrix include the long-term performance, glass transition temperature, moisture absorption, robustness and stability.[2]

The supply of raw material is very important in the mass production of CFRP; thus, preforms are used in industrial manufacturing. These preorganized textile structures of fibers are already impregnated with resin and stored in stacks. The structure of the layer depends on the particular part. For optically visible parts, a tissue structure is used and for structural components, biaxial or multiaxial textiles are used. In addition to the visual appearance, the physical performance is also influenced by the woven fiber structure.

For more advanced composites, the industry developed preimpregnated reinforcements (also called prepreg). Different manufacturing techniques, such as compression molding, autoclave molding and vacuum bag molding use these semi-finished composite layers. For the automotive sector, where reproducible and well-defined body parts are crucial to production, two techniques are used: resin transfer molding (RTM) and wet compression molding. The production process can vary for both techniques, however the RTM concept relies “on the philosophy of manufacturing in which the resin and fibers are held apart

until the last possible moment"[3]. The RTM process uses the textile preforms in well defined stacks with specific textile structure (Fig. 1.2). The stacks are added into a press of the body part mold and formed under pressure while resin is injected through one or more channels into the mold. The reaction of the resin takes place at increased temperatures; hence, the mold in the press is heated[2].

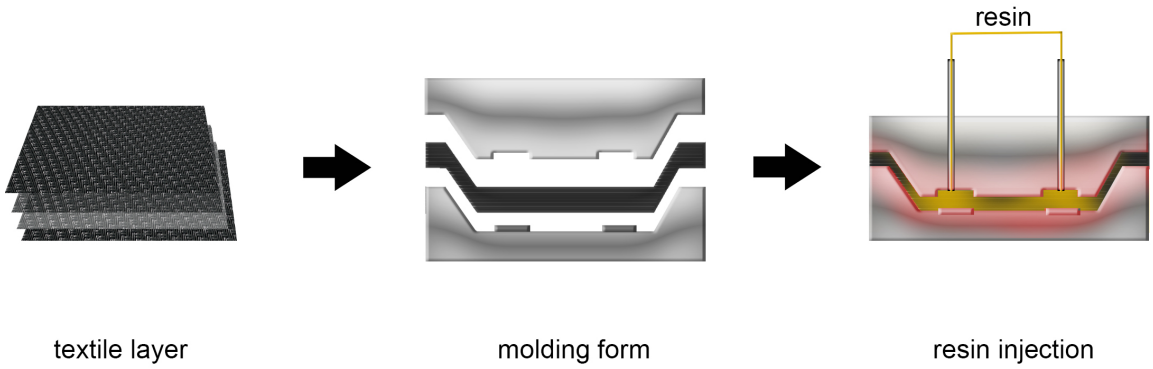

Figure 1.2: Resin transfer molding - industrial approach, adapted from [2]

Wet compression molding is used for less complex parts, where mass production and a fast process are the focus. Recently, an improved compression molding technique called dynamic fluid compression molding (DFCM)[4] was introduced. Standard wet compression is limited in its process and product complexity, whereas the DFCM technique produces RTM-like quality but with increased speed. Both production methods, standard and dynamic fluid compression molding, use similar steps: a wet fabric insertion, a molding process under pressure with curing time and a de-molding phase. Standard wet compression molding needs a resin overflow, but DFCM combines vaccum and dynamic mold pressure for void-free impregnation (Fig. 1.3). Thus, DFCM is an alternative to the RTM process[4].

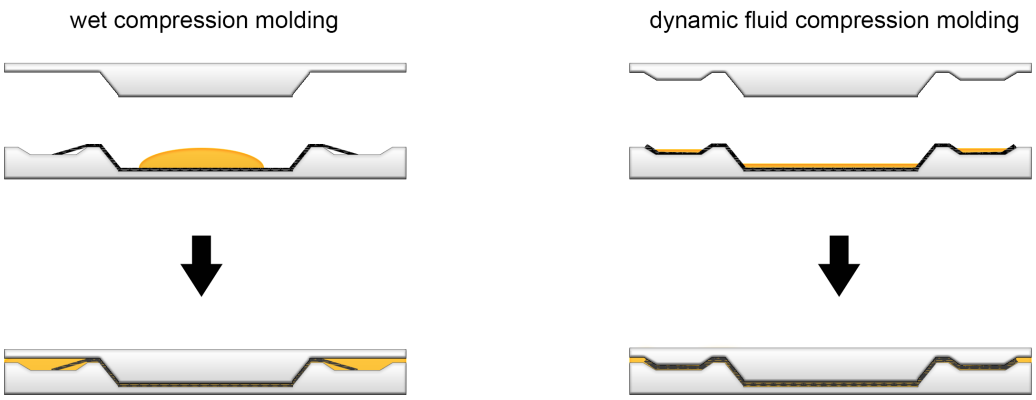

Figure 1.3: Wet compression molding - industrial approach, adapted from [2]

1.1.2 Adhesives

Emulating nature's genius, the practical use of adhesives has been known to mankind for many centuries. In 3000 B.C. glues consisting of herbal or animal pastes were used. Over time many different applications were discovered, and applicable adhesives for specific uses were formulated. Only since the 1940s has the development in technology and mechanism of adhesives rapidly progressed[5]. An adhesive is the general term for a material that joins two substrates together when applied at the interface. An adhesive can take different forms, such as glue, paste, cement, tape etc.. Depending on the application, an adhesive may be liquid with one or two components, or a film with a reaction mechanism, such as acrylic adhesive, epoxy or urethane-based adhesives[5].

The concept of adhesion relies on the interaction of two boundaries in contact with similar or different compositions. The phase of the adhesive can be solid, liquid or gaseous. For the mechanism of adhesion, several different concepts must be understood[6][7][8]:

- Covalent bonding in a chemical reaction
- Mechanical interlocking
- Formation of an electrical double layer
- Adsorption or wetting
- Diffusion
- Weak boundary interactions
- Acid-base interactions

In most cases, the application of adhesives is in a liquid state, where a wetting of the surface occurs. Depending on the surface tension of the adhesive and the adherend, the molecules are adsorbed on the surface. While curing, the adhesive solidifies and the interface between adhesive and surface adheres. This mechanism is based on a physical bond (e.g. adsorption, wetting, van-der-Waals interactions, electrostatic bonding), a chemical reaction (absorption - covalent bonding) and mechanical interlocking (depending on the roughness of the surface). Many different types of adhesives exist. Here,

the polyaddition of a two-component polyurethane adhesive is regarded in Equation 1.1.

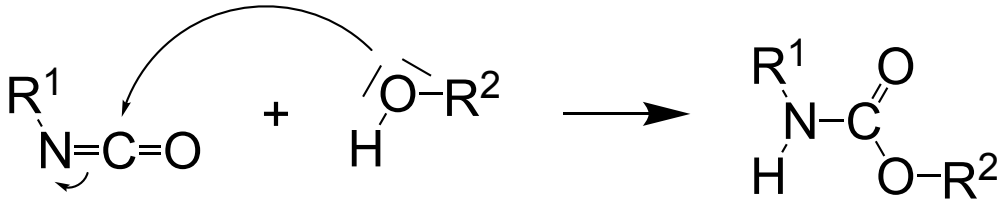

(1.1)

For industrial applications, a homogenous mixture of two separate components initiates the reaction. The first component is a prepolymeric polyol mixture with multiple additives and the second is a prepolymeric isocyanate component. Depending on the amount of alcohol and isocyanate functional groups as well as the chain length in the prepolymeric form, the reactivity and the physical parameters can be influenced, inlcuding elasticity, viscosity, reactivity, curing time and fracture strain. The formulation of an adhesive is adjusted to the individual area of application. For automotive manufacturing, adhesives are optimized regarding fracture strain and reactivity for curing in tightly-scheduled production. In most cases, the adhesives are boosted with an additional catalyst. The reaction is further enhanced and controlled with additional energetic injection. In some cases, infrared heaters are used as an indirect source of heat. The part is brought into contact with infrared heaters at the outer side and the applied adhesive reaction on the inner side is accelerated by the increase in temperature.

1.1.3 References

[1] P. K. Mallick, *Fiber-Reinforced Composites: Materials, Manufacturing, and Design*, vol. 19. CRC Press, 3 ed., 2007.

[2] H. Jäger and T. Hauke, *Carbonfasern und ihre Verbundwerkstoffe*. München: Moderne Industrie, 2010.

[3] K. Potter, *Resin Transfer Moulding*. London: Chapman & Hall, 1 ed., 1997.

[4] Huntsman, "Dynamic Fluid Compression Molding A new process for composite mass-production," 2016.

[5] A. J. Kinloch, *Adhesion and Adhesives: Science and Technology*. New York: Chapman & Hall, 1 ed., 1987.

[6] A. Baldan, "Adhesion phenomena in bonded joints," *International Journal of Adhesion and Adhesives*, vol. 38, pp. 95–116, 2012.

[7] A. V. Pocius, *Adhesion and Adhesives Technology: An Introduction*. Munich: Carl Hanser Verlag, 3 ed., 2012.

[8] J. Schultz and M. Nardin, *Adhesion Promotion Techniques: Technological Applications*. New York: Marcel Dekker Inc., 2002.

1.2 Analytical techniques

1.2.1 Atomic Force Microscopy

In 1982, Gerd Binnig and Heinrich Rohrer developed the scanning tunneling microscope (STM) - the first scanning probe microscope. This revolutionary microscopic technique was the first of its kind with an imaging resolution at atomic level[1][2]. Binning and Rohrer were rewarded with the Nobel Prize in Physics in 1986. In the following years, similar methods using a mechanical scanning tip over a surface were developed. Atomic force microscopy (AFM) was introduced by Binnig, Quate and Gerber in 1986. In contrast to the STM, the AFM is not limited to electrically conducting surfaces. It can scan insulating materials with a lateral resolution of 30 Å and a vertical resolution of 1 Å[3]. Resembling a phonograph, a sharp probing tip is scanned over a surface and the topography of the sample is recorded, measuring the deflection of the probing tip. For the AFM, this sharp probing tip is mounted at the end of a soft cantilever spring[4]. Distinguishing from other microscopic techniques the AFM tip is in contact with the surface. Atomic-range forces between the tip and the sample surface are measured by detecting the deflection of the cantilever. Due to the sensibility and the depth of information, different measurement modes are possible.

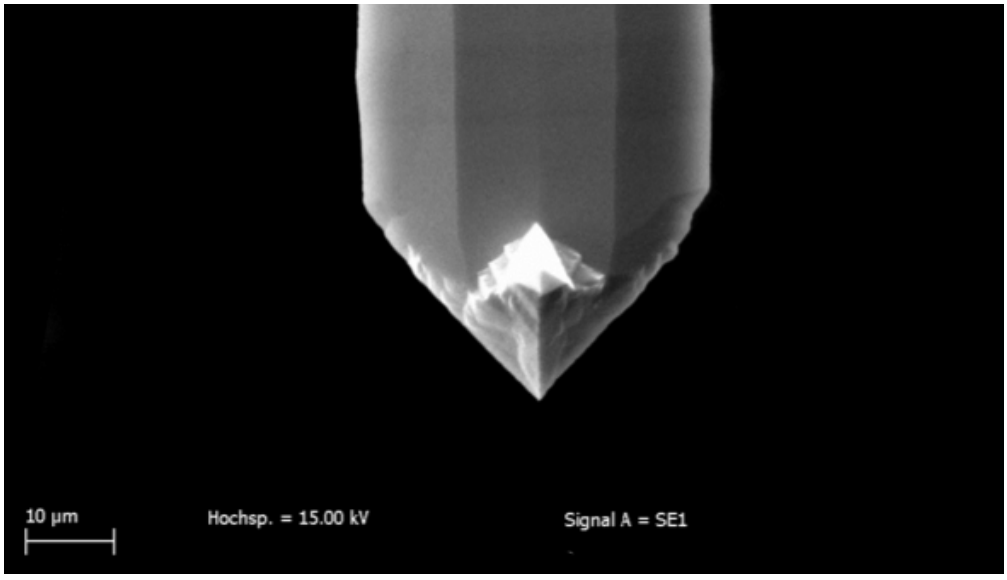

Figure 1.4: Scanning electron microscope (SEM) image of a monolithic silicon Tap-300 Al-G cantilever, force constant 40 N/m, length 125 µm, width 30 µm, radius $<$ 10 nm

Due to its enormous variety of measuring modes, AFM has been applied in numerous scientific fields, including topographical mapping under atmospheric conditions[5] and highly complex measuring modes in a liquid medium for modern molecular and cell biology[6][7]. Further studies have analyzed materials on the molecular[8] or even submolecular level[9]. From electrical nanoimprinting with conducting atomic force microscopy[10] to force spectroscopic measurements to detect cardiovascular diseases in patients[11], many useful applications have been found.

Due to the ability to scan in X,Y and Z directions, the AFM extends the horizontal measuring range of optical or scanning microscopes. Compared to other techniques (Fig. 1.5), the AFM performs at length scales from sub-nanometer to 100 µm, and outperforms other imaging techniques in horizontal and especially in vertical scanning resolution. Optical microscopy often complements AFM, since the lower length-scale of optical microscopy overlaps with the maximum length-scale of the AFM. Hence a correlation results in a large dynamic range with a mm scale from the optical microscopic image to a µm scale with the AFM[12].

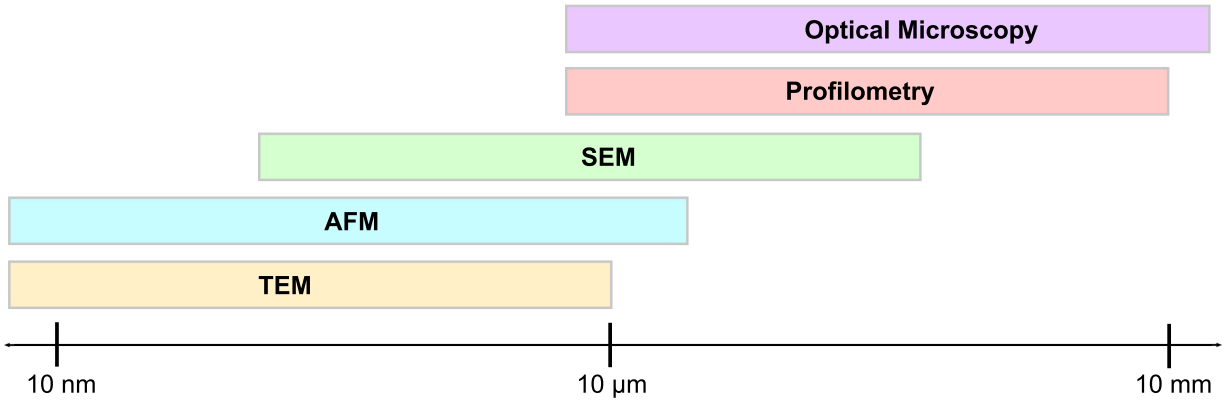

Figure 1.5: Comparison of various microscopic techniques and the resolution (adapted from [12])

A modern AFM (e.g. Flex AFM, company Nanosurf) is illustrated in Fig. 1.6. A housing **1** isolates the device from environmental influences and an active vibration isolation platform **2** protects against vibration disturbances. On top of the isoplatform is an X,Y,Z-automatized sample stage **3**. The main section of the AFM has two integrated optical cameras **4** for adjusting and moving the cantilever to the surface. A laser **5** is adjusted to the top of the cantilever **6** and reflected to a detector **7**. Next to the cantilever is a piezoelectric

transducer and a force transducer. The piezoelectric transducer converts electrical potential into mechanical motion and vice versa, resulting in an electrical potential when the piezo (piezoelectric transducer) receives a mechanical change. For the AFM, the piezo is generally made of synthetic ceramic material (or crystalline, amorphous or polymeric material). The AFM benefits from the sensitivity of the piezo element, since small changes in the geometry of the material (e.g. 0.1 nm) can be detected while applying a potential across two opposite sides of the piezo (e.g. 1 V). The force transducer detects the force between the AFM probe and the surface. Usually the cantilever with an integrated tip is used as the force transducer. Due to the different force constant of the cantilever, the sensitivity of the interaction with the surface can be controlled. Additionally, an optical lever is installed, in this case a laser beam, which is reflected at the top end of the cantilever towards a photodetector. Thus, a deflection of the cantilever results in a change of the laser position on the detector. The high sensitivity of the AFM is due to a feedback controller, which regulates the movements between probe and surface. It reads the signal from the force transducers and drives the piezo to maintain the probe sample-distance.[12]

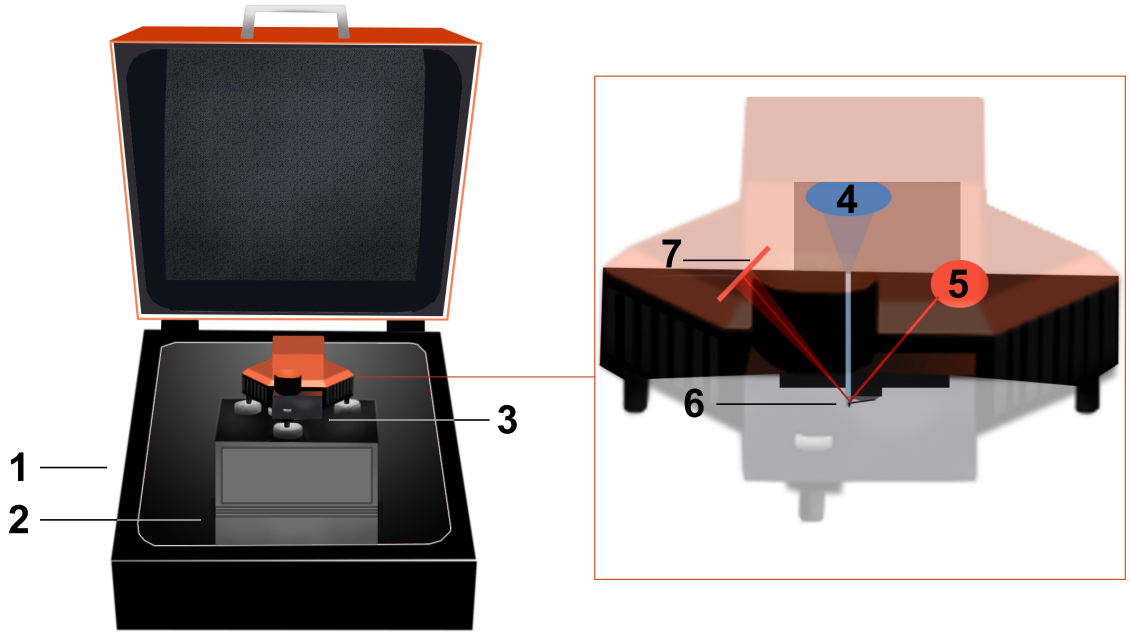

Figure 1.6: Scheme of a commercially available AFM (Flex AFM - company nanosurf)

With the large variety of different techniques, such as electric force, force spectroscopy,

kelvin probe, nanoindentation and scanning thermal microscopy, the concepts rely on either static or dynamic oscillation of the AFM cantilever. For topographical measurements, the static deflection measurement is called contact mode and the oscillating measurement is called tapping mode.

With contact mode, high resolution topographical images can be produced in a short time. Here, the deflection of the cantilever directly correlates with the topography of the sample. In a force distance curve, the difference between contact mode and other static modes (e.g. force spectroscopy) is illustrated in Figure 1.7. Depending on the distance and the strength of interaction forces, the probe is attracted by the surface. An accelerated contact to the surface occurs (snap-in), followed by a repulsive regime, as the cantilever is approached. A force is applied to the surface, such that an indentation occurs while the cantilever bends. Accordingly, while retracting an attractive force (adhesion) withholds the cantilever until a deferred snap-off occurs. For contact mode, the setpoint is usually fixed in a repulsive regime, so the cantilever stays in contact with the surface.

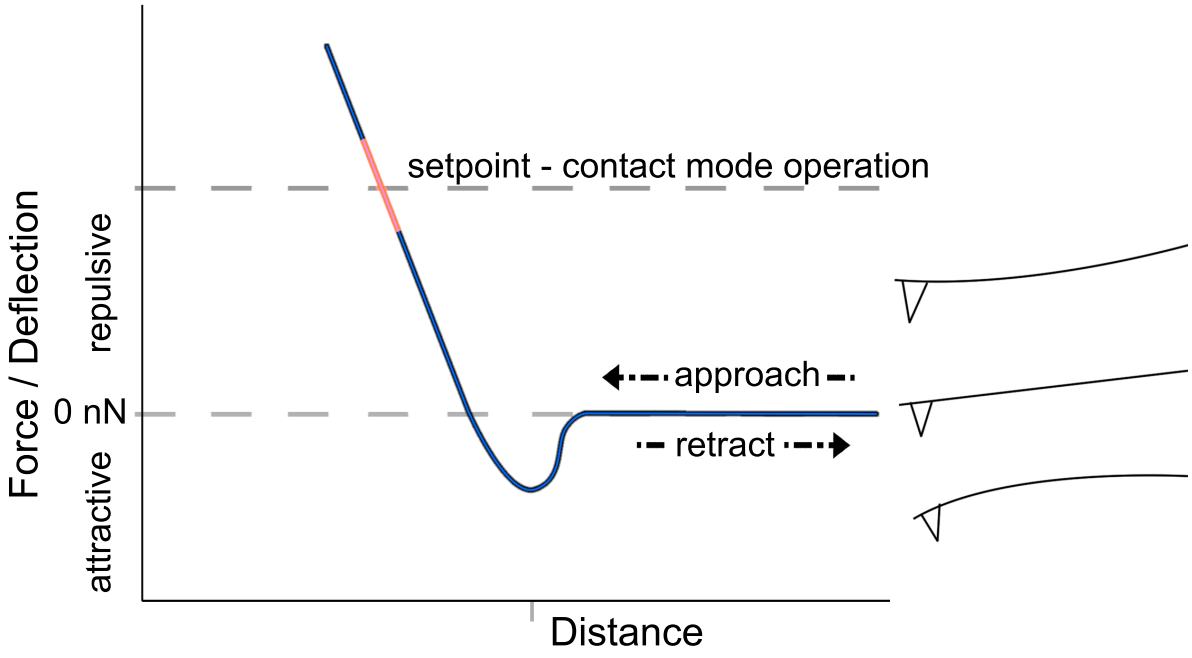

Figure 1.7: Force-distance curve with contact mode operation in repulsive region, showing cantilever deflection at each regime, adapted from [12]

Due to constant contact, the cantilever or the sample may be damaged or changed. In

addition to the applied force, a lateral force acts on both the probe and the sample. The forces applied to the surface by the cantilever can be described by Hooke's law (Equation 1.2:

$$F = -k * D \tag{1.2}$$

where $F =$ force $[\mathrm{N}]$, $k =$ probe force constant $[\mathrm{N/m}]$, $D =$ deflection distance $[\mathrm{m}]$.

For most topographical measurements, the oscillating mode is used (also referred to as the tapping mode or the intermittent contact mode). Here, an additional piezoelectric element oscillates the cantilever, and a calibration of the frequency is done before each measurement. Usually the frequency is set to the resonant frequency of the cantilever with a definable amplitude, depending on the roughness. While scanning over a surface, changes in the vibration amplitude, due to the topography of the sample are detected; i.e. the vibration amplitude is reduced in close proximity to the surface. The set point is what defines the maximum amplitude while the cantilever oscillates close to the surface. To avoid damage to the probe or the sample, the set point and thus the vibration amplitude, should be set high, yet not too high so as to avoid artifacts and problems while recording small changes in amplitude. For material contrast, not only the change in amplitude is recorded but also the delay in the phase of the oscillation. IIdeally, with a completely homogeneous surface, only the interacting forces impact the probe and the phase does not change. In reality, different materials interact differently with the probe, such that a phase shift will be recorded when the surface material changes. Thus, differences in topography and composition of the surface can be imaged.

In the case of force spectroscopy, the additional information of the snap-in (Fig. 1.8 B), due to van der Waals interaction and adhesion forces (Fig. 1.8 D) are used, while approaching (Fig. 1.8 A to B) and retracting (Fig. 1.8 C to D) the cantilever. Each measuring spot is individually approached and retracted, thus the x- and y- positions stay constant, while the probe approaches and retracts in z-direction. The force data is used for spectroscopy, whereas the slope data is used for nanoindentation[12].

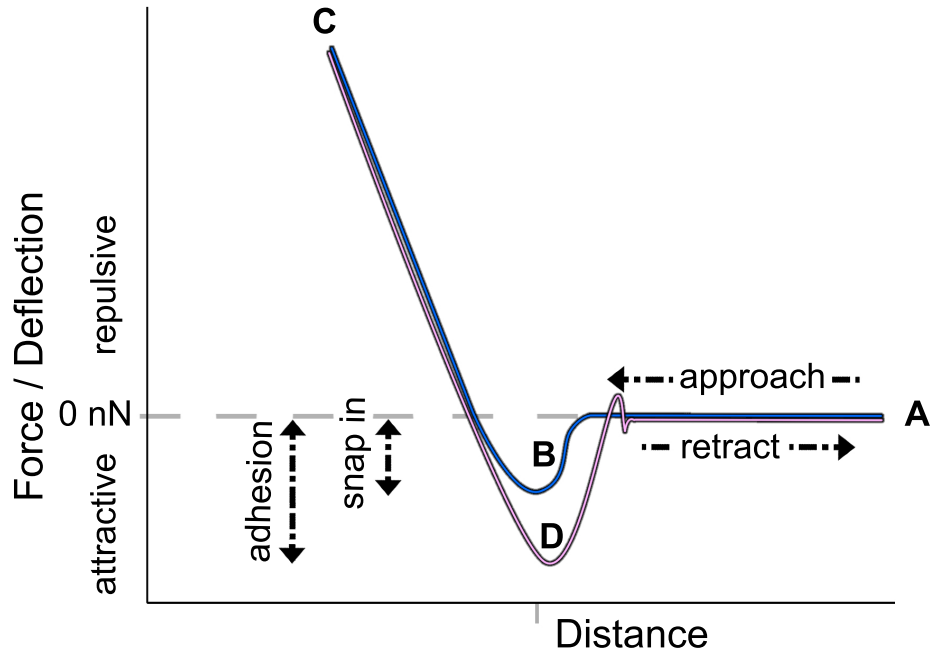

Figure 1.8: Force-distance curve for spectroscopic measurements, A to B approach, at B snap-in occurs, C user defined stop, in contact with sample untill D - snap-off occurs, adapted from [12]

1.2.2 Chemical Force Microscopy

A variation of force spectroscopy with AFM - chemical force microscopy - was introduced in 1994 by Charles Lieber[13][14]. Lieber used chemically-modified probe tips and measured the adhesive and friction forces between probe and organic monolayers. Since then, this method of modifying cantilevers has been used in several fields, such as material science[15] and bioanalysis[16][17][18]. The concept of CFM is to measure specific interactions between the probe and the sample. Since AFM detects even small changes in the attraction and adhesion forces, specific interactions can be measured. The measuring principle resembles force spectroscopy with AFM, however in this case the cantilever is modified with functional chemical groups. Depending on the type of interaction, different functional groups can be chosen, yet a stable bond between the probe and the chemical groups must be achieved. As a result, silane or gold cantilevers are chosen; recent studies have shown that nanocrystalline diamond tips can also be used[19]. In this case to gold coated cantilevers within a self-assembled monolayer process, thiol, thioether or disulfide molecules are able to bond to the gold surface[20]. The measured adhesion force is specific to the interaction between the surface molecules and the molecules on the cantilever. Figure 1.9 illustrates CFM with an 11-mercapto-1-undecanol modified cantilever interacting with unknown surface molecules, R-X.

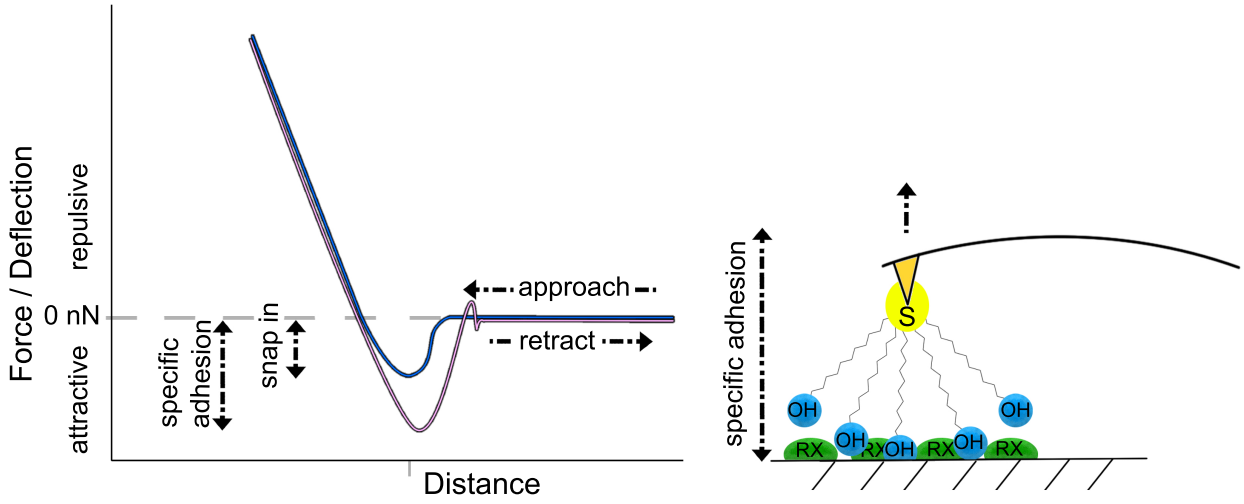

Figure 1.9: Force-distance curve for spectroscopic measurements; illustration of a chemically modified cantilever and the interaction with the surface molecules R-X, adapted from [12]

1.2.3 X-ray photolectron spectroscopy

In modern surface analysis[21], x-ray photoelectron spectroscopy (also known as ESCA or electron spectroscopy for chemical analysis) is an important technique for chemical composition characterization[22], chemical state analysis and determining the electronic state of elements[23]. Essentially, all electrons from the core to the valence level can be studied[24]. The first XPS spectrum was recorded by Kai Siegbahn in 1954[25] who later was rewarded with the Nobel Prize[26] for his contributions[27].

A focused electron beam from a LaB6 scanning electron source creates X-rays on an aluminum anode. The aluminum Kα X-rays are refocused using an ellipsoidal-shaped quartz crystal monochromator and directed towards the sample. While focusing the electron beam on the aluminum anode, the X-ray beam scans over the surface of the sample (Figure 1.10).

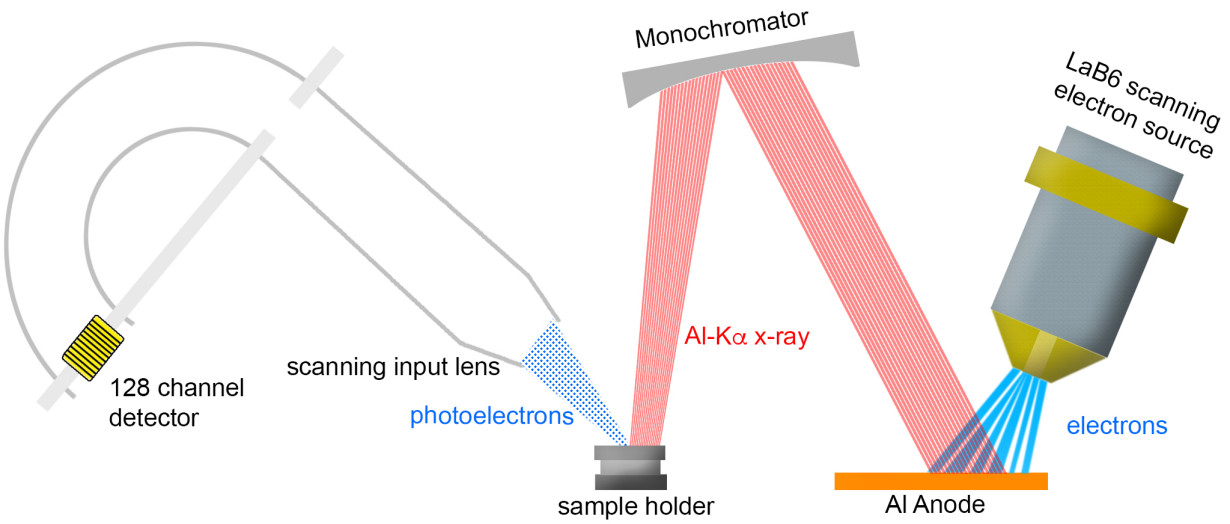

Figure 1.10: XPS set up of commercially available Ulvac Phi - Versa Probe II

The X-ray beam irradiates the sample and photoelectrons are generated (Figure 1.11). An XPS spectrum consists of a plot of the total of detected electrons per energy interval versus kinetic energy. Thus, for each element, a representative and individual spetrum is recorded [28].

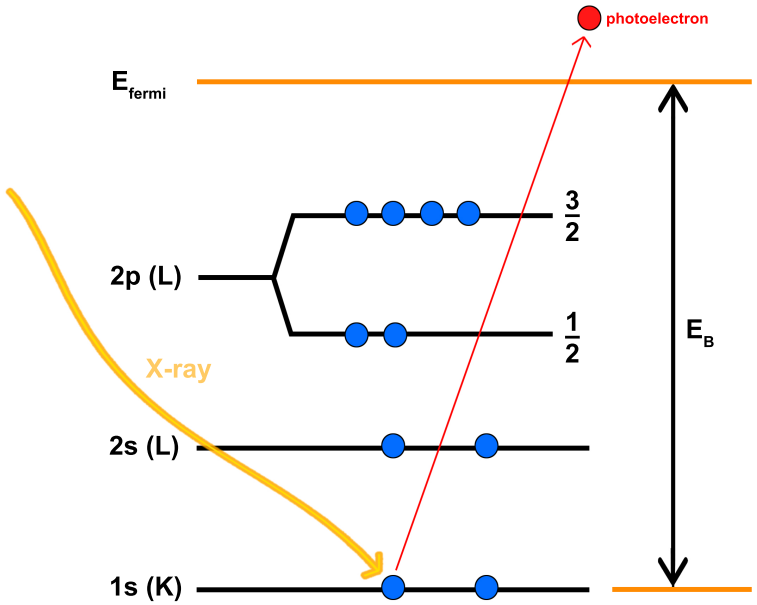

Figure 1.11: Photoelectronic effect, formation of a photoelectron with an X-ray and a 1s electron (adapted from [28])

For qualitative analysis, the binding energy of the electrons is specific to a particular element and the ratio of the signals identifies the element. To determine the binding energy (E_B) of the photoelectrons, the kinetic energy (E_K) is measured and substracted from the Al-Kα X-ray energy ($E_{photon} = 1486.7$ eV). Additionally, a spectrometer-dependent work function is subtracted from the energy of the X-ray photons, as in Equation 1.3. The energy of the fermi level corresponds with a binding energy of zero.

$$E_B = E_{photon} - (E_K + \phi) \tag{1.3}$$

For depth profiling, an argon ion gun is used, particularly for inorganic materials. The voltage can be set between 5 V and 5 kV.

1.2.4 DART-Q-ToF-MS

In 2001, Laramée and Cody developed the first thermal atmospheric ion source in the laboratories of JEOL USA Inc. In the following years it resulted in the DART-Ion source, which has a high sensitivity for gaseous molecules[29]. Additionally, all ioniziable substances, which can be desorbed from a surface, could be analyzed. The DART-Ion source offers a broad field of application for solid, liquid and gasous samples[30][31][32]. The ionization process takes place without elaborate sample pretreatments. Hence, the DART-Ion source delivers results in sort of real time. It also requires a high-resolution mass spectrometer as a detector, since the lack of preliminary separation leads to a large amount of information simultaneously.

The DART-Ion source is an atmospheric pressure ion source and consists of a tube where a continuous gas stream flows through (either nitrogen or helium). It is seperated into different chambers, as shown in Figure 1.12. In the first chamber, an electrical potential of several kilovolts between a needle electrode and a counter electrode initiates an electrical glow discharge producing ions, electrons and the electronic excited-state species of helium or vibronic nitrogen molecules. When exiting the glow discharge chamber, the gas passes through a tube containing a perforated intermediate electrode, a gas heater and a grid electrode behind an insulating cap[33].

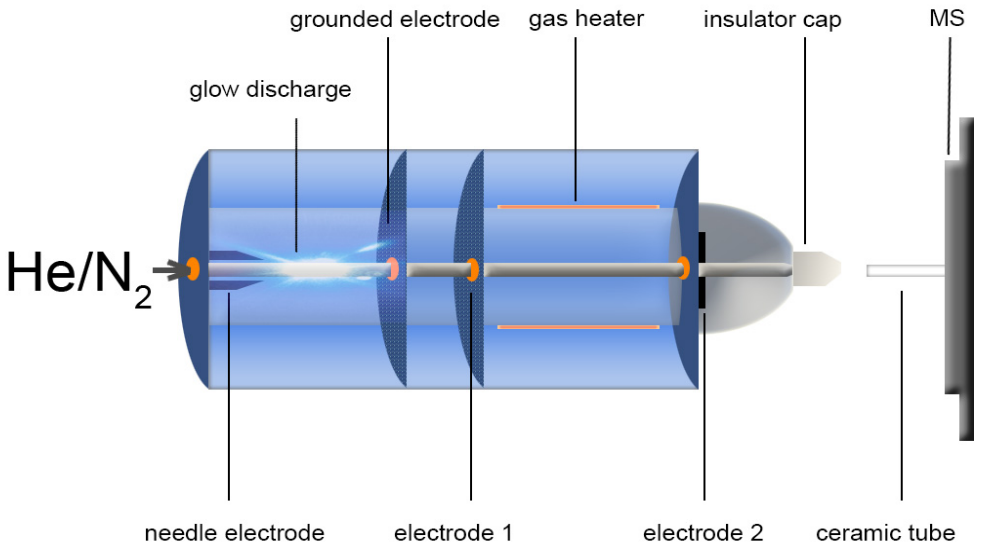

Figure 1.12: DART-Ion source functional principle; first chamber: energetic excitement of the gas to a metastable state through glow discharge, second chamber: filtering charged gas molecules, and third chamber: heating process up to 550°C

The exiting gas flow can be aimed at a 45°angle towards the sample surface or directly towards the inlet of the mass spectrometer. Usually a discharge needle potential between 1 kV and 5 kV is set. The potentials of the second perforated electrode and the grid electrode are biased to positive potentials for positive-ion detection and to negative potentials for negative ion detection[33].

As the excited and heated gas flow hits the sample, it desorbs molecules from the surface. Different competing reactions can occur, depending on the parameter settings and the presence or absence of solvents. One such reaction is the Penning Ionisation[34] (Equation 1.4), in which a metastable, excited-state neutral atom or molecule N^* transfers energy to an analyte molecule M, resulting in the formation of a molecular ion $M^{+\bullet}$ and an electron. The reaction will occur if the analyte molecule M has an ionization energy that is lower than the internal energy of the excited neutral N^*. The long-lived helium 2^3S state has an internal energy of 19.8 eV, which is higher than the ionization energies of common

atmospheric gases and organic molecules. [33]

$$N^* + M \rightarrow N + M^{+\bullet} + e^- \tag{1.4}$$

The ionisation process is assisted by the atmospheric conditions and the humidity in the air. The excited helium in the 2^3S state ionizes the humidity, and protonated water clusters will be formed (Equation 1.5).

$$He(2^3S) + nH_2O \rightarrow [(H_2O)_{n-1} + H]^+ + OH^\bullet + He(1^1S) \tag{1.5}$$

Proton transfer to produce the protonated molecule [M + H]$^+$ will occur if the analyte molecule M has a higher proton affinity than the ionized water clusters (Equation 1.6) [33].

$$M + [(H_2O)_n + H]^+ \rightarrow [M + H]^+ + nH_2O \tag{1.6}$$

An inlet tube assists the formed ions into the mass spectrometer.

1.2.5 References

[1] G. Binnig, H. Rohrer, C. Gerber, and E. Weibel, "Surface studies by scanning tunneling microscopy," *Physical review letters*, vol. 49, no. 1, pp. 57–61, 1982.

[2] G. Binnig and H. Rohrer, "Scanning tunneling microscopy," *Surface Science*, vol. 126, no. 1-3, pp. 236–244, 1983.

[3] G. Binnig and C. F. Quate, "Atomic Force Microscope," *Physical Review Letters*, vol. 56, no. 9, pp. 930–933, 1986.

[4] D. Rugar and P. Hansma, "Atomic Force Microscopy," 1990.

[5] S. Tualu, A. J. Ghazai, S. Stach, A. Hassan, Z. Hassan, and M. Tualu, "Characterization of surface roughness of Pt Schottky contacts on quaternary n-Al0.08In0.08Ga0.84N thin film assessed by atomic force microscopy and fractal analysis," *Journal of Materials Science: Materials in Electronics*, vol. 25, no. 1, pp. 466–477, 2014.

[6] Y. F. Dufrêne, T. Ando, R. Garcia, D. Alsteens, D. Martinez-Martin, A. Engel, C. Gerber, and D. J. Müller, "Imaging modes of atomic force microscopy for application in molecular and cell biology," *Nature Nanotechnology*, vol. 12, no. 4, pp. 295–307, 2017.

[7] K. Haase and A. E. Pelling, "Investigating cell mechanics with atomic force microscopy," *Journal of The Royal Society Interface*, vol. 12, no. 104, 2015.

[8] B. Schuler, G. Meyer, D. Peña, O. C. Mullins, and L. Gross, "Unraveling the Molecular Structures of Asphaltenes by Atomic Force Microscopy," *Journal of the American Chemical Society*, vol. 137, no. 31, pp. 9870–9876, 2015.

[9] C. Moreno, O. Stetsovych, T. K. Shimizu, and O. Custance, "Imaging Three-Dimensional Surface Objects with Submolecular Resolution by Atomic Force Microscopy," *Nano Letters*, vol. 15, no. 4, pp. 2257–2262, 2015.

[10] S. Goswami, S. Nandy, A. N. Banerjee, A. Kiazadeh, G. R. Dillip, J. V. Pinto, S. W. Joo, R. Martins, and E. Fortunato, "Electro-Typing on a Carbon-Nanoparticles-Filled Polymeric Film using Conducting Atomic Force Microscopy," *Advanced Materials*, vol. 29, no. 47, pp. 1–9, 2017.

[11] A. F. Guedes, F. A. Carvalho, I. Malho, N. Lousada, L. Sargento, and N. C. Santos, "Atomic force microscopy as a tool to evaluate the risk of cardiovascular diseases in patients," *Nature Nanotechnology*, vol. 11, no. 8, pp. 687–692, 2016.

[12] P. Eaton and P. West, *Atomic Force Microscopy*. New York: Oxford University Press Inc., 2010.

[13] C. D. Frisbie, L. F. Rozsnyai, A. Noy, M. S. Wrighton, and C. M. Lieber, "Functional Group Imaging by Chemical Force Microscopy," *Science*, vol. 265, no. 5181, pp. 2071 LP – 2074, 1994.

[14] A. Noy, D. V. Vezenov, and C. M. Lieber, "Chemical Force Microscopy," *Annual Review of Materials Science*, vol. 27, no. 3, pp. 381–421, 1997.

[15] J. Wu, F. Liu, G. Chen, X. Wu, D. Ma, Q. Liu, S. Xu, S. Huang, T. Chen, W. Zhang, H. Yang, and J. Wang, "Effect of Ionic Strength on the Interfacial Forces between Oil/Brine/Rock Interfaces: A Chemical Force Microscopy Study," *Energy and Fuels*, vol. 30, no. 1, pp. 273–280, 2016.

[16] S. Iliafar, K. Wagner, S. Manohar, A. Jagota, and D. Vezenov, "Quantifying Interactions between DNA Oligomers and Graphite Surface Using Single Molecule Force Spectroscopy," *The Journal of Physical Chemistry C*, vol. 116, no. 26, pp. 13896–13903, 2012.

[17] D. J. Müller and Y. F. Dufrêne, "Atomic force microscopy: a nanoscopic window on the cell surface," *Trends in Cell Biology*, vol. 21, no. 8, pp. 461–469, 2011.

[18] L. N. Poloni, X. Zhong, M. D. Ward, and T. Mandal, "Best practices for real-time in situ atomic force and chemical force microscopy of crystals," *Chemistry of Materials*, vol. 29, no. 1, pp. 331–345, 2017.

[19] M. E. Drew, A. R. Konicek, P. Jaroenapibal, R. W. Carpick, and Y. Yamakoshi, "Nanocrystalline diamond AFM tips for chemical force spectroscopy: fabrication and photochemical functionalization," *Journal of Materials Chemistry*, vol. 22, no. 25, p. 12682, 2012.

[20] A. Ebner, L. Wildling, R. Zhu, C. Rankl, T. Haselgrübler, P. Hinterdorfer, and H. J. Gruber, *Functionalization of Probe Tips and Supports for Single-Molecule Recognition Force Microscopy*, pp. 29–76. Berlin, Heidelberg: Springer Berlin Heidelberg, 2008.

[21] P. Dietrich, K. Beblo-Vranesevic, M. Kjærvik, W. Unger, K. Schwibbert, K. Hardie, and J. Brown, "XPS surface analysis of bacterial samples," 2018.

[22] V. Gong and R. França, "Nanoscale chemical surface characterization of four different types of dental pulp-capping materials," *Journal of Dentistry*, vol. 58, pp. 11–18, 2017.

[23] G. Corro, E. Vidal, S. Cebada, U. Pal, F. Bañuelos, D. Vargas, and E. Guilleminot, "Electronic state of silver in Ag/SiO2 and Ag/ZnO catalysts and its effect on diesel particulate matter oxidation: An XPS study," *Applied Catalysis B: Environmental*, vol. 216, pp. 1–10, 2017.

[24] J. M. Hollander and W. L. Jolly, "X-Ray Photoelectron Spectroscopy," *Accounts of Chemical Research*, vol. 3, no. 6, pp. 193–200, 1970.

[25] K. Siegbahn and K. Edvarson, "β-Ray spectroscopy in the precision range of 1 : 105," *Nuclear Physics*, vol. 1, no. 8, pp. 137–159, 1956.

[26] K. Siegbahn, "Electron spectroscopy for atoms, molecules, and condensed matter," 1981.

[27] K. Siegbahn, C. Nordling, and A. Fahlman, "ESCA, atomic, molecular and solid state structure studied by means of electron spectroscopy," tech. rep., Almqvist and Wiksell, Uppsala, 1967.

[28] P. E. S. J. F. Moulder, W. F. Stickle and K. D. Bomben, *Handbook of X-ray Photoelectron Spectroscopy*. Chigasaki: ULVAC-PHI and Physical Electronics, 3 ed., 1992.

[29] R. B. Cody, J. A. Laramée, and H. D. Durst, "Versatile New Ion Source for the Analysis of Materials in Open Air under Ambient Conditions," *Analytical Chemistry*, vol. 77, no. 8, pp. 2297–2302, 2005.

[30] M. J. Pavlovich, B. Musselman, and A. B. Hall, "Direct analysis in real timeâĂŤMass spectrometry (DART-MS) in forensic and security applications," *Mass Spectrometry Reviews*, vol. 37, no. 2, pp. 171–187, 2016.

[31] T.-H. Chen, H.-Y. Hsu, and S.-P. Wu, "The detection of multiple illicit street drugs in liquid samples by direct analysis in real time (DART) coupled to Q-orbitrap tandem mass spectrometry," *Forensic Science International*, vol. 267, pp. 1–6, 2016.

[32] E. S. Chernetsova, P. O. Bochkov, M. V. Ovcharov, S. S. Zhokhov, and R. A. Abramovich, "DART mass spectrometry: a fast screening of solid pharmaceuticals for the presence of an active ingredient, as an alternative for IR spectroscopy," *Drug Testing and Analysis*, vol. 2, no. 6, pp. 292–294, 2010.

[33] R. B. Cody, "Observation of Molecular Ions and Analysis of Nonpolar Compounds with the Direct Analysis in Real Time Ion Source," *Analytical Chemistry*, vol. 81, no. 3, pp. 1101–1107, 2009.

[34] F. M. Pennig, "Über Ionisation durch metastabile Atome," *Naturwissenschaften*, vol. 15, p. 818, 1927.

1.3 Mechanical tests

In modern industrial applications, the evaluation and quality control of an adhesive is essential, since small changes in the formulation, contamination or aging effects drastically influence the physical parameters. Hence, quick tests are used to ensure the performance of the adhesive and approve new adhesives through standardized methods. Mechanical tests evaluate an adhesive and the strength of the compound[1].

1.3.1 Tensile-shear-test

A tensile shear test[2][3][4] indicates the maximum strength applicable in parallel to the bond (Fig 1.13). Usually, two types of detatchments are found: a cohesive failure within the adhesive and an adhesive failure in the intersection between the adhesive and substrate. Additionally, the tractive distance and the maximum strength are recorded. Ideally, there is a cohesive failure with a high tensile strength.

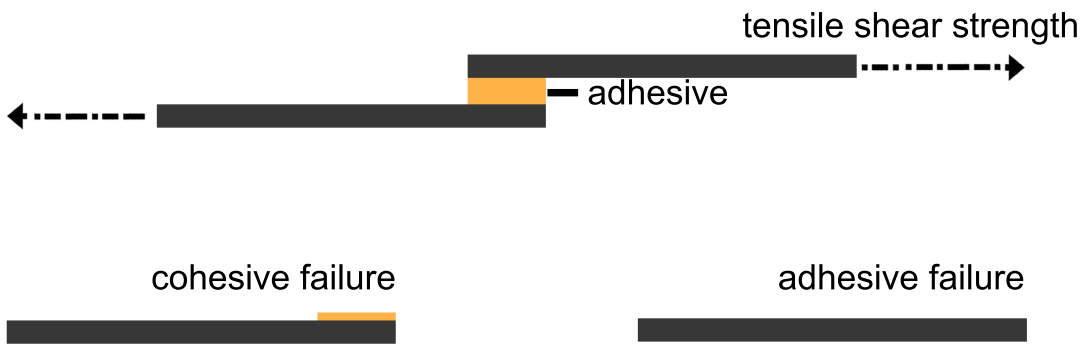

Figure 1.13: Scheme of the tensile shear test

1.3.2 Peel-test

A second test, the peel test[5][6] (Fig. 1.14), evaluates the quality of the adhesive by applying a vertical force. Here, the test is done manually by slicing the outer end of the adhesive with a knife. The adhesive is evaluated based on the failure mechanism; a cohesive failure is desired.

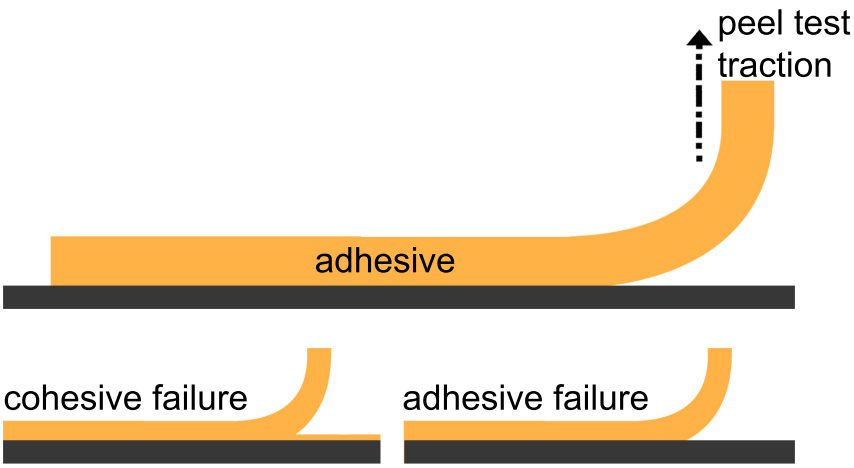

Figure 1.14: Scheme of the peel test

1.3.3 References

[1] A. Ching and B. Oral, "Peel and Shear Fracture Characterization of Debonding in FRP Plated Concrete Affected by Moisture," *Journal of Composites for Construction*, vol. 10, no. 1, pp. 35–47, 2006.

[2] P. E. C. Cardoso, R. R. Braga, and M. R. O. Carrilho, "Evaluation of micro-tensile, shear and tensile tests determining the bond strength of three adhesive systems," *Dental Materials*, vol. 14, no. 6, pp. 394–398, 1998.

[3] S. A. Meguid and Y. Sun, "On the tensile and shear strength of nano-reinforced composite interfaces," *Materials & Design*, vol. 25, no. 4, pp. 289–296, 2004.

[4] W. Zhang, C. Cotton, J. Sun, D. Heider, B. Gu, B. Sun, and T.-W. Chou, "Interfacial bonding strength of short carbon fiber/acrylonitrile-butadiene-styrene composites fabricated by fused deposition modeling," *Composites Part B: Engineering*, vol. 137, pp. 51–59, 2018.

[5] S. Teixeira de Freitas, M. D. Banea, S. Budhe, and S. de Barros, "Interface adhesion assessment of composite-to-metal bonded joints under salt spray conditions using peel tests," *Composite Structures*, vol. 164, pp. 68–75, 2017.

[6] Y. Wei and J. W. Hutchinson, "Interface strength, work of adhesion and plasticity in the peel test BT - Recent Advances in Fracture Mechanics: Honoring Mel and Max Williams," pp. 315–333, Dordrecht: Springer Netherlands, 1998.

2 Experimental

2.1 Chemicals and materials

Adhesive
In chapter 3.1. the formulation of the reference adhesive is described. For all experiments this adhesive was used. The chemical composition is listed in the chapter, as well as the experimantal procedure.

AFM tip modification
The procedure for chemical modification of AFM cantilevers is described in chapter 3.3. For the self assembled monolayer process 11-mercapto-1-undecanol was used (Fig. 2.1). All chemicals and the experimental procedure are described in the corresponding experimental part of the chapter.

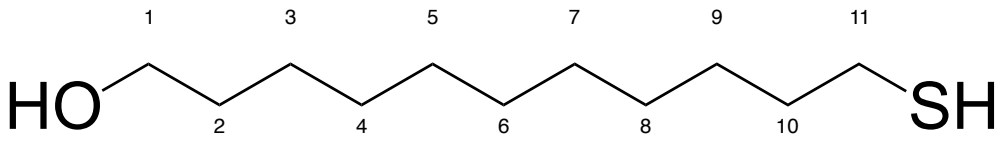

Figure 2.1: For self assembled monolayer process 11-mercapto-1-undecanol was used

Carbon fiber reinforced plastic
All experiments regarding CFRP pretreatment are described in chapter 3.4.. The CFRP plates were industrially manufactured in a RTM process (comparable products available at Rhein Composite GmbH).

Cavity wax
The cavitx wax used in the chapter 3.6. and 3.7. is a commercially available product. For all experiments water based cavity wax was used.

2.2 Measurements

FT-IR
All IR measurements were done with a commercial FT-IR (Thermo - nicolet is50). A macro was programmed to record the reaction process of adhesives over time. Here a FT-IR spectrum was recorded every 30 seconds for 800 minutes. Resulting in a 3D time resolved FT-IR spectrum. For the evaluation of the reaction speed the signal at 2261 cm^{-1} was plotted over time.

DART-Q-ToF-MS
For the analysis with the DART-SVP ion source (IonSense/KR-Analytical), a sample was introduced directly into the excited and heated helium stream. Based on preceding measurements, it was found that 350°C is an appropriate temperature for the study of volatile components used in industrial manufacturing.

AFM
The AFM experiments were done with the Flex AFM system from Nanosurf AG. The topographical measurements were done in tapping mode with Tap300Al-G cantilevers and the force measurements were done with Tap300GB-G and HQ:NSC19/Cr-Au cantilevers.

XPS
All XPS measurements were done with a Ulvac PHI - Versa Probe II. For all experiments the procedure is comparable. At first the samples were stored in a prevacuum chamber till they reached a pressure of 10^{-5} Pa. Afterwards they were transfered to the main chamber of the system (pressure 10^{-7} Pa). The X-ray setting for the survey spectrum was chosen at 25 W, 15 kV with 100 µm. Afterwards a high resolution spectrum was recorded for the respective elements with 100 W, 20 kV and a diameter of 100 µm and a scanning area of 1400 µm. For depth profiling argon sputtering was set to 2x2 kV for 35 minutes and 15 cycles.

3 Results & Discussion

3.1 Analytical approach for the formulation of a reference adhesive system

3.1.1 Introduction

In the automotive sector, raw materials and supply characteristics must ensure large-scale production. This is especially true in emerging sectors, where many suppliers offer similar products. However, most of the knowledge on the product is kept in secret, and this is particularly true for the production of adhesives[1] for automotive applications[2][3]. Hence, for detailed analytical approaches, reference substances must be used[4]. Therefore, different attempts at formulating a two-component polyurethane adhesive will be regarded and an analytical approach[5][6] to qualify the product will be investigated[7].

3.1.2 Experimental Procedure

For all experiments, a two-component polyurethane adhesive was formulated with a composition resembling the isocyanate component containing methylenediphenyl diisocyanate, hexamethylene diisocyanate and bulking agent (e.g. soot).

Formulation A
A prepolymeric alcohol functionalized polybutadiene mixture (52.12 w.%, Polyvest EP HT, EVONIK Resource Efficiency GmbH, Marl, Germany) was used as the reactive polyol. Thiodiethanol (9.2 w.%, Fluka Analytical) was used as the chain extending component. The filler, kaolin (37.95 w.%), and the adhesion agent, trimethoxysilane (0.66 w.%), were

obtained from Sigma-Aldrich. Dimethoxypolysiloxane (0.07 w.%, Sigma-Aldrich) was used as an antifoaming agent (Table 3.1)[7].

Table 3.1: System A: Polyol formulation

System A: Polyol	Amount in w.%
Polyvest	52.12
Thiodiethanol	9.2
Kaolin	37.94
Trimethoxysilane	0.66
Dimethoxypolysiloxane	0.07

All components were homogenized with a Thinky Mixer ARE 250 (Thinky corp., Tokyo, Japan) for two minutes at 2000 RPM.

Formulation B
To improve the crosslinking, 2.0 w.% of pentaerythrit (Sigma-Aldrich) was mixed into Formulation A.

Formulation C
To increase the reaction speed, zirconium(IV)acetylacetonate was used as a catalyst (Sigma-Aldrich)[8]; 0.4 w.% was mixed into Formulation B.

Fourier-Transform Infrared Microspectroscopy (FT-IR)
The reaction of a two-component polyurethane (PUR) adhesive was seen by the decrease in signal from the isocyanate antisymmetric valence stretching at 2250-2300 cm^{-1} (Fig. 3.2). A macro was created to record the reaction process of the adhesive over time. An FT-IR spectrum was recorded every 30 seconds for 800 minutes. This resulted in a 3D time-resolved FT-IR spectrum. For the evaluation of the reaction speed, the signal at 2261 cm^{-1} was plotted over time (Fig. 3.2).

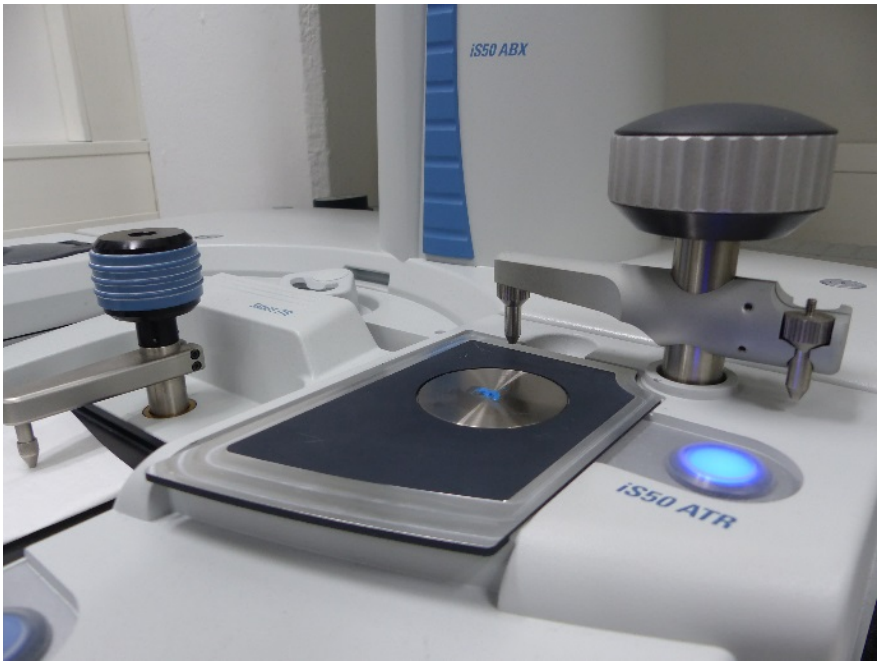

Figure 3.1: Thermo - nicolet is50

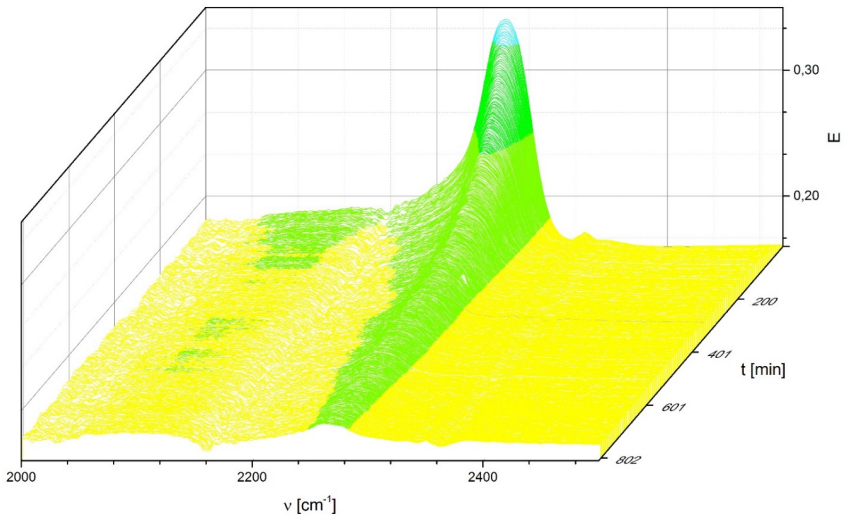

Figure 3.2: FT-IR isocyanate signal and reaction over time

3.1.3 Results & Discussion

The time dependent polymerization of the isocyanate - polyol reaction can be seen in Fig. 3.3. For formulation A (Fig. 3.3 A), it was 250 minutes until most of the isocyanate reacted, though the extinction was still decreasing and no saturation was achieved after 800 minutes of curing time. To increase crosslinking and internal strength, pentaerythrit was added resulting in Formulation B (Fig. 3.3 B). Within the first 100 minutes the isocyanate reaction was enhanced, due to the increased amount of binding partners. However, after 800 minutes the reaction was still in progress. Therefore, a catalyst (zirconium(IV)acetylacetonate) was added to formulation B, which drastically enhanced the reaction (Fig. 3.3 C). Within the first 100 minutes, most of the isocyanate reacted to the polyurethane and after 250 minutes the reaction completed, as the extinction reached saturation. To validate the reaction rate of Formulation C, a commercially available two-component polyurethane adhesive was tested (Fig. 3.3 D). In the first 25 minutes, the reaction rate was drastically increased; however, the adhesive reaction was not complete after 800 minutes of curing time.

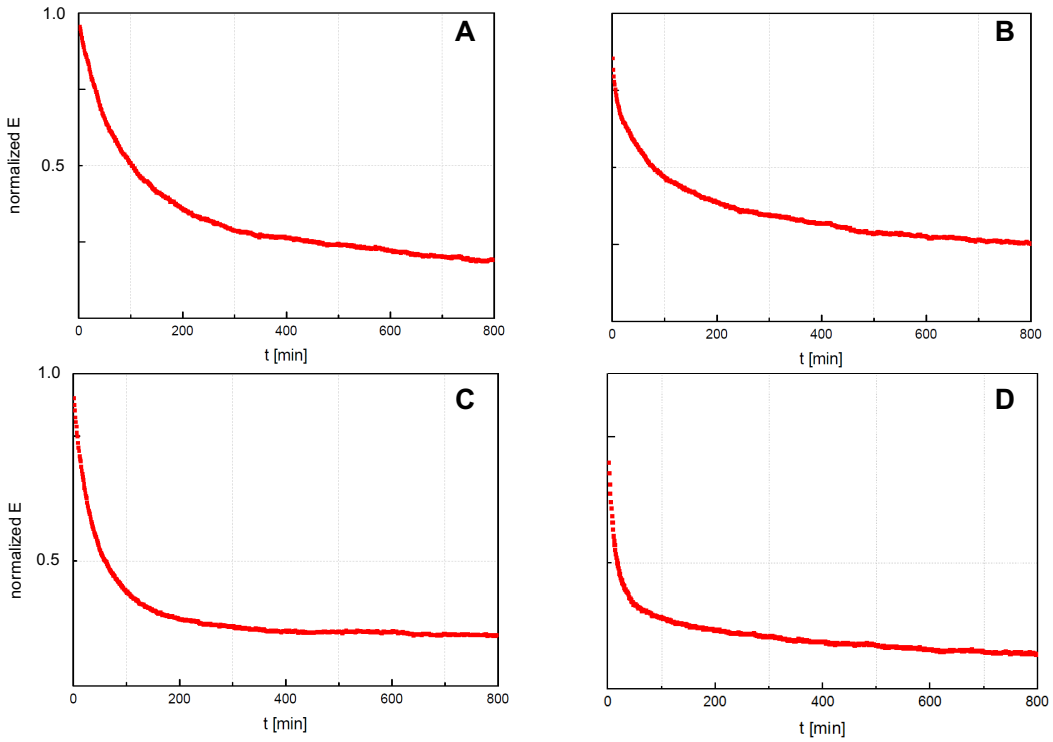

Figure 3.3: Time resolved FT-IR - Isocyanate signal over time, adhesive formulation A - C and industrial adhesive D

3.1.4 Conclusion

A method to monitor the reaction time of a two-component polyurethane adhesive system was successfully introduced. Additionally, a reference adhesive system with known composition was formulated, and will be used for further experiments. The catalytic effect of a metal complex on an adhesive system was shown. A commercially available product was compared to the purchased product, showing adequate similarity.

3.1.5 References

[1] G. Habenicht, *Kleben - Grundlagen, Technologien, Anwendungen*. Springer-Verlag Berlin Heidelberg, 6 ed., 2009.

[2] K. Stephan, "Elastic Bonding in Vehicle Construction," 2005.

[3] A. L. Loureiro, L. F. M. da Silva, C. Sato, and M. A. V. Figueiredo, "Comparison of the Mechanical Behaviour Between Stiff and Flexible Adhesive Joints for the Automotive Industry," *The Journal of Adhesion*, vol. 86, no. 7, pp. 765–787, 2010.

[4] S. Clauß, D. J. Dijkstra, J. Gabriel, O. Kläusler, M. Matner, W. Meckel, and P. Niemz, "Influence of the chemical structure of PUR prepolymers on thermal stability," *International Journal of Adhesion and Adhesives*, vol. 31, no. 6, pp. 513–523, 2011.

[5] H. Wilhelm and U. Kurt, "Über die Kinetik der Reaktion von Hexamethylendiisocyanat mit 2-ethyl-1,3-hexandiol in verschiedenen Lösungsmitteln," *Die Makromolekulare Chemie*, vol. 180, no. 4, pp. 939–948, 1979.

[6] D. Kincal and S. Özkar, "Kinetic study of the reaction between hydroxyl-terminated polybutadiene and isophorone diisocyanate in bulk by quantitative FTIR spectroscopy," *Journal of Applied Polymer Science*, vol. 66, no. 10, pp. 1979–1983, 1997.

[7] B. Müller and W. Rath, *Formulierung von Kleb- und Dichtstoffen: das kompetente Lehrbuch für Studium und Praxis*. Hannover: Vincentz Network, 2004.

[8] W. J. Blank, Z. A. He, and E. T. Hessell, *Catalysis of the isocyanate-hydroxyl reaction by non-tin catalysts*, vol. 35. 1999.

3.2 Evaluation of industrial samples with various surface characterization techniques

3.2.1 Introduction

The automotive industry is in the midst of a transition, with rapidly changing markets, stiffer competition and new technologies[1]. From an old-fashioned metal-dependent industry, the demand to adapt to an eco-minded sustainable product is to be expected. Consequently, many changes are being made under the pretext of Industry 4.0[2]. Besides automation in production[3], digitalization[4], e-mobility[5] and autonomous driving[6], the material composition of the product has changed as well[7]. Whilst iron, steel and aluminum are still implemented, newly developed materials, such as polymeric components are gaining importance[8]. The joining and bonding of these materials with drastically different characteristics is challenging, especially the surface characteristics that influence the compatibility of the materials and thus the quality of the product[9]. Therefore, new and specific analytic techniques must be applied to the diversity of materials. Additionally, the combination of different techniques must be regarded when it comes to surface analysis. Since morphology, chemical composition and physical performance synergize and impact material bonding, different techniques from the areas of mass spectrometry, microscopy and chemical characterization are regarded.

3.2.2 Application of direct analysis in real time (DART) and direct inlet probe (DIP-APCI) mass spectrometry in the context of industrial sample analysis[1]

Stefan Viehbeck, Frank-Michael Matysik

Graphical Abstract

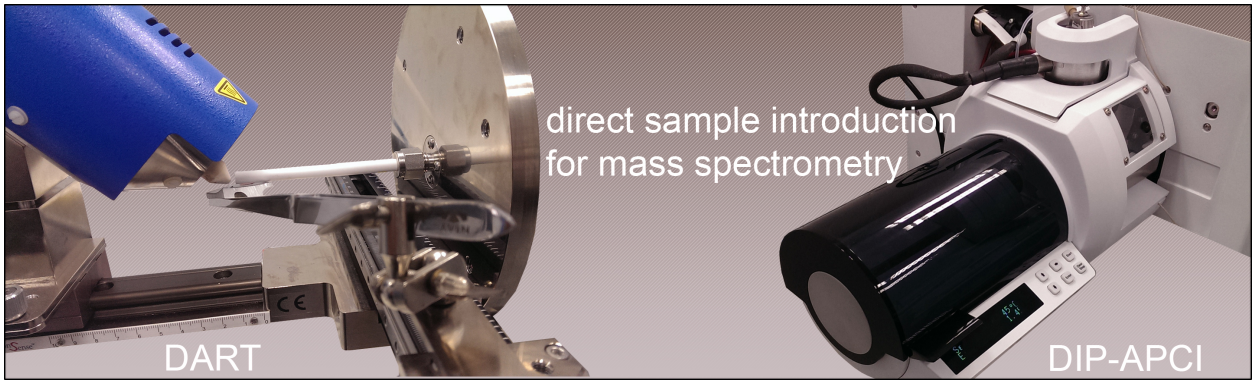

Abstract

In today's industry, quick and reliable analytical methods play an important role for quality control. On that account, two emerging techniques, namely direct inlet probe-atmospheric pressure chemical ionization (DIP-APCI) and direct analysis in real time (DART) mass spectrometry, are particularly promising. In case of a DIP-APCI source, small amounts of solid or liquid samples can be studied without sample pre-treatment. A similar system is the DART ion source. In addition to the analysis of solid and liquid samples without pre-separation, this ion source offers the possibility to scan the surface of a sample. A method for industrial sample analysis focusing on the study of delamination of coatings from a panel was developed using DIP-APCI-Q-ToF-MS and DART-Q-ToF-MS, respectively. Comparative studies based on the conventional pyrolysis-GC-MS were carried out.

1 *Monatshefte für Chemie - Chemical Monthly (2016) 147:1349-1352*

Introduction

In recent years, direct analysis in real time (DART) and direct inlet probe-atmospheric pressure chemical ionization (DIP-APCI) mass spectrometry have attracted increasing attention. These emerging new ionization techniques enable direct analysis of untreated samples without preliminary separation. For the DART ion source, the ionization takes place through penning ionization [10], formation of water clusters, and proton exchange[11]. In particular, DART-MS is already established in several fields of application[12]. For example, recent reports illustrated the great potential for bioanalytical applications[13][14]. Regarding the DIP-APCI source, the ionization process is similar to an APCI source[15]. An auxiliary gas, in this case nitrogen, is ionized by corona discharge[16], followed by the formation of protonated water clusters and proton exchange with volatile analytes. An interesting field of application of DIP-APCI-MS was the development of a non-destructive method for plasticizer screening[17]. In this short communication, we focus on DART-MS and DIP-APCI-MS methods for the qualitative characterization of delamination problems of industrial samples.

Experimental Procedure

The samples were introduced directly into the ion sources without any sample preparation or pre-separation. In the present study, delamination of an e-coat from a car panel was examined (Fig. 3.4). For the analysis with the DART-SVP ion source (IonSense/KR-Analytical) (Fig. 3.5), a sample was introduced directly into the excited and heated helium stream. Based on preceding measurements, it was found that 350°C is an appropriate temperature for the study of volatile phthalate components used in industrial manufacturing. Using lower temperatures for the DART gas stream, the ion yield of phthalates is drastically reduced, and for higher temperatures, the matrix signals increase. On the other hand, for the analysis with the DIP-APCI source (SIM GmbH), small pieces of a sample were scraped off the surface and placed in a crucible on top of the push rod from the DIP-APCI (Fig. 3.6). The temperature control of the ion source was set applying a gradient to ensure a well-defined evaporation of the sample. The first temperature point was set to 300°C and held for 1 min, and the second one to 350°C for 2 min before reaching the maximum of 400°C which was applied for 1 min. The heating rate was variable and was set to 2 K/s. As a mass detector, an Agilent Q-ToF-MS system (Agilent quadrupole time-of-flight 6530) was used in conjunction with both sources. To compare both methods to a conventional analytical approach, parts of the detached materials were brought in contact with glass wool soaked in ethanol. A fraction of the glass wool was placed in

a pyrolysis-GC crucible and analyzed via pyrolysis-GC-MS (Frontier Lab AS-1020E/PY-2020iD-Agilent 7890 A GC-Agilent 5975C inert XL MSD) using a GC column Agilent HP-5MS 30 m, 0.25 mm, 0.25 µm. The pyrolysis process was set to 600°C for 30 s. The temperature program for GC separations was as follows: 40°C for 4 min, then 8°C/ min to 320°C, the final temperature was kept constant for 8 min resulting in a total run time of 47 min.

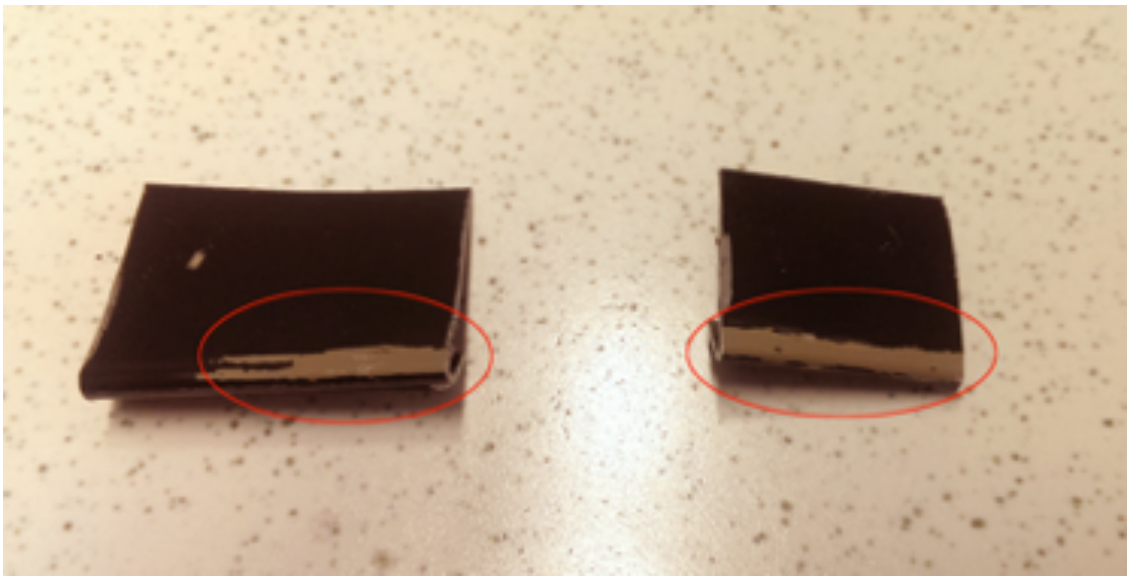

Figure 3.4: Representative samples with delamination phenomena of an e-coat from a car panel

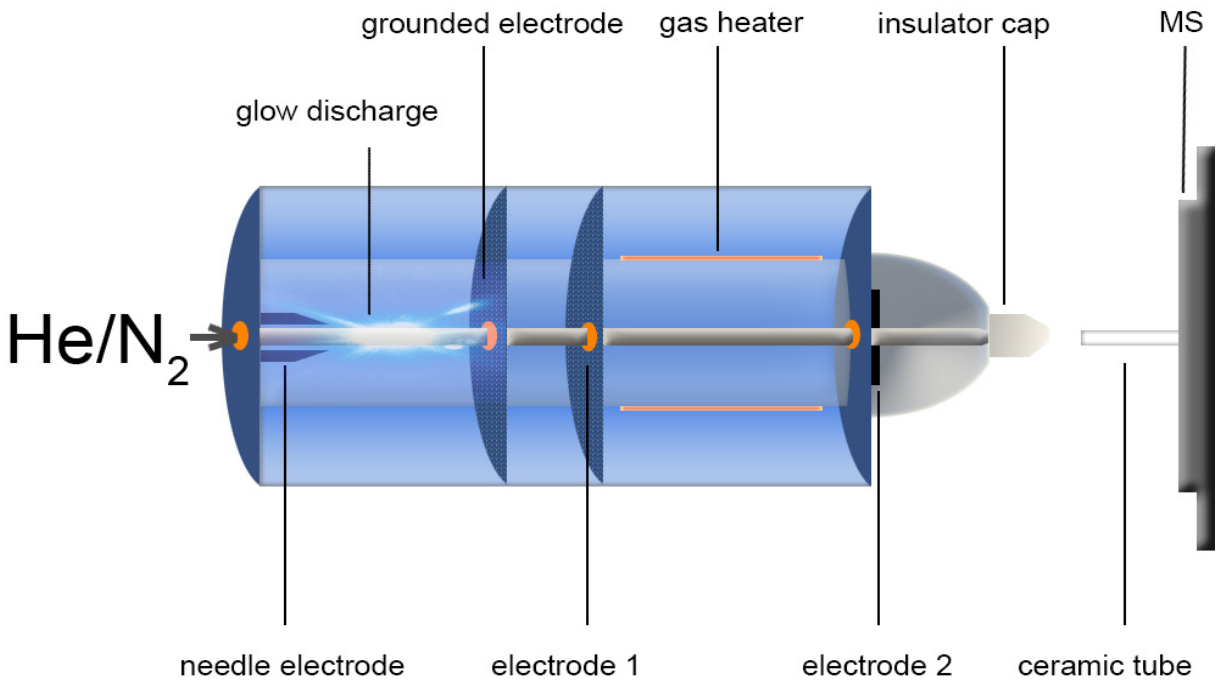

Figure 3.5: DART ion source functional principle, first chamber: energetic excitement of the gas to a metastable state through glow discharge, second chamber: filtering charged gas molecules, and third chamber: heating process-the gas can be heated up to 550°C

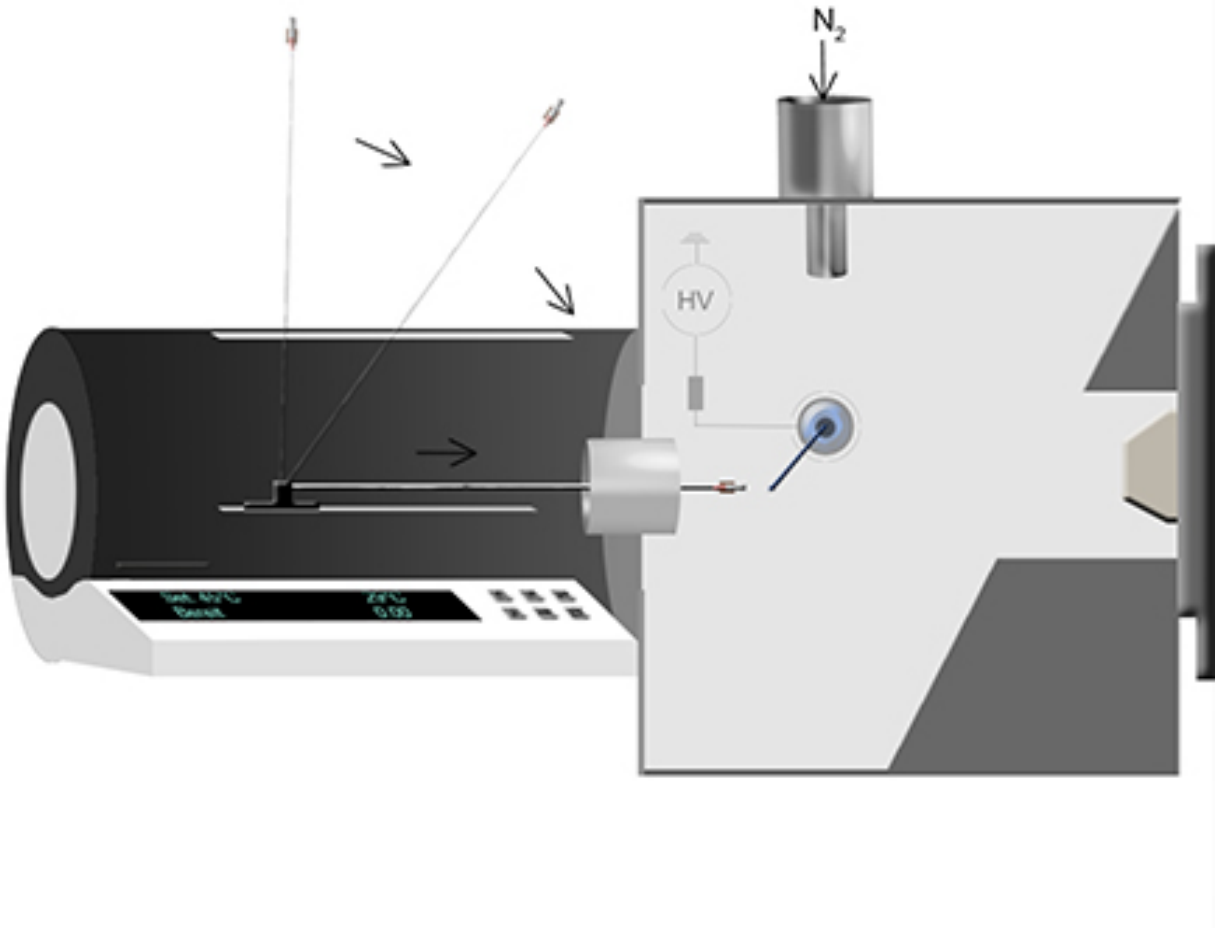

Figure 3.6: DIP-APCI ion source functional principle, push rod with crucible for liquid and solid samples, APCI chamber with corona needle

Results & discussion

DART-MS as well as the DIP-APCI-MS are promising in the field of failure analysis. However, the assessment of these rather new techniques in comparison with traditional methods, such as pyrolysis-GC-MS under industrial conditions, is still open. Thus, industrial samples, in particular several car panels, with delamination of the varnish, were examined. In case of the DART source, all ionizable compounds lead to a simultaneous formation of ions. In contrast, using DIP-APCI, the analytes are introduced to the ion source at different times according to their differences in vapour pressure. This can be helpful in the cases of thermolabile compounds and can reduce ion suppression effects. Despite large background signals found in the DART mass spectrum (Fig. 3.7) as well as in the DIP-APCI mass spectrum (Fig. 3.8), both techniques resulted in a clear signal with m/z of 419. After generating the molecular formula and correlating the results

with additional MS/MS information (Fig. 3.9), the signal was identified as protonated bis(7-methyloctyl)phthalate.

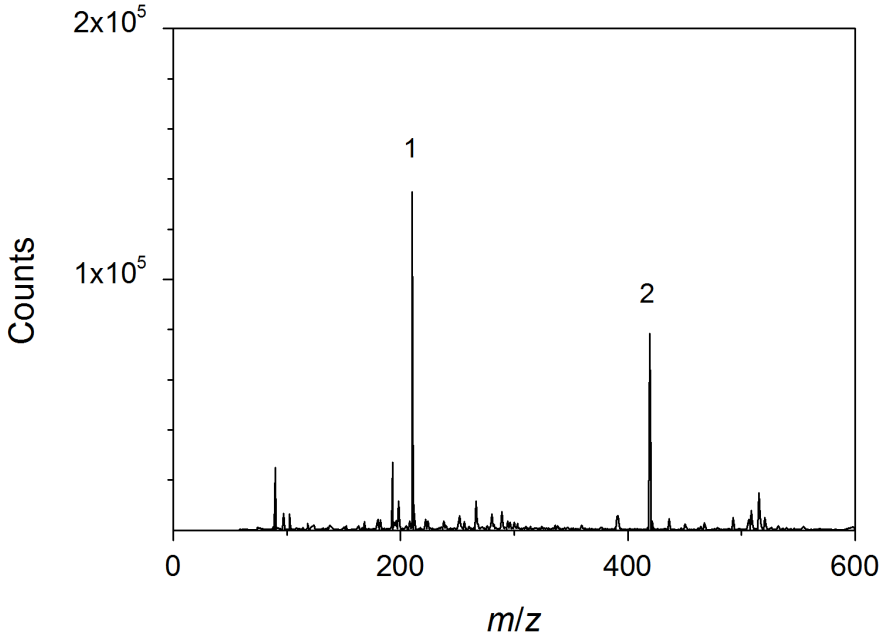

Figure 3.7: DART-Q-ToF-MS mass spectrum of a typical sample; 1 matrix signal from the coating, 2 signal with the m/z of 419.3156 - identified as protonated bis(7-methyloctyl)phthalate

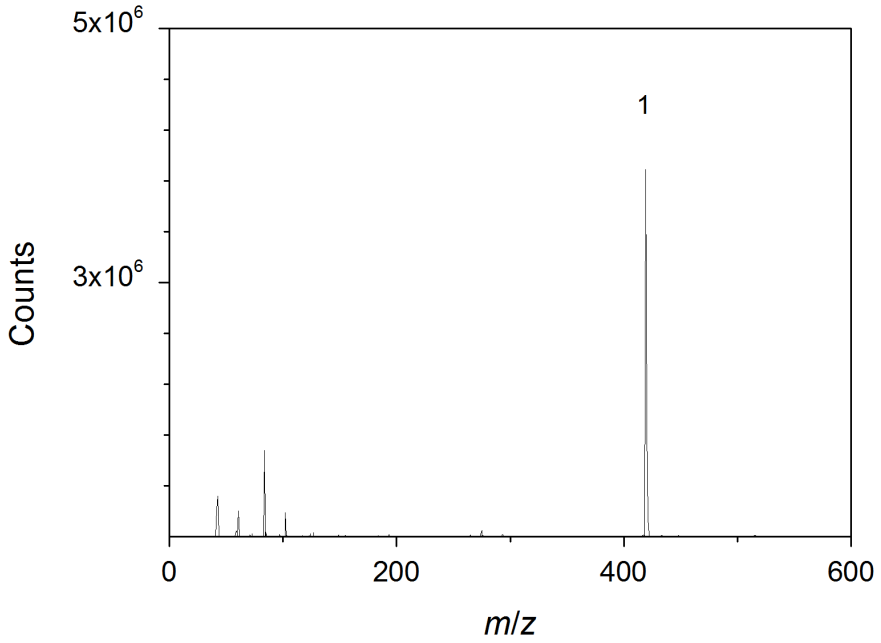

Figure 3.8: DIP-APCI-Q-ToF-MS mass spectrum of a typical sample; 1 signal with the m/z of 419.3154 - identified as protonated bis(7-methyloctyl)phthalate

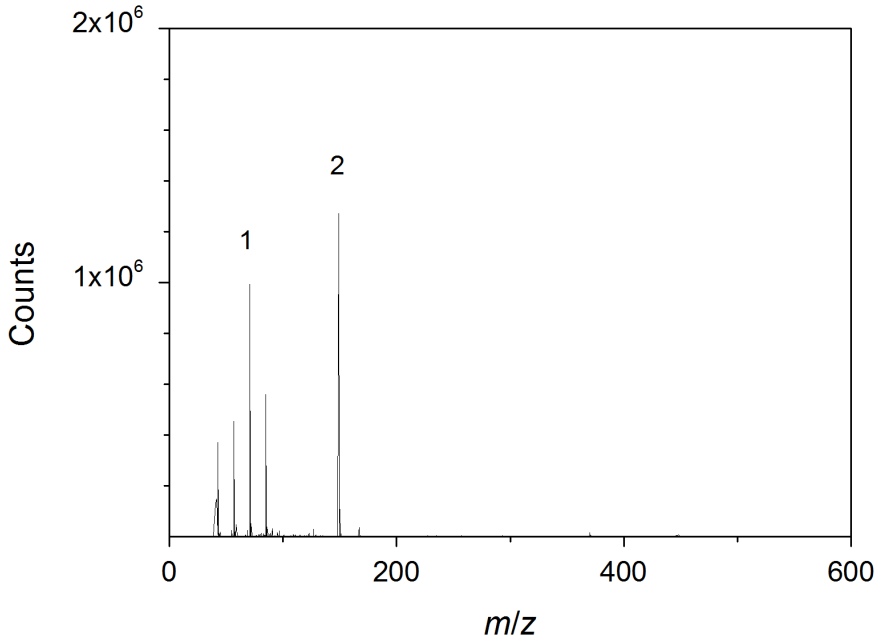

Figure 3.9: Q-ToF-MS/MS mass spectrum of $m/z = 419$; 1 alkyl groups with $m/z = 127$ $[C_9H_{18} + H]^+$, 2 $m/z = 149$ $[C_8H_4O_3 + H]^+$

Contamination or migration of plasticizers to the interface between the substrate and a varnish are often responsible for irregularities and delamination. In the present case, it is assumed that bis(7-methyloctyl)phthalate is the cause for the delamination problem. Hence, both techniques were able to identify the sought substance. An advantage of the DIP-APCI source is the temperature gradient, which is associated with a pronounced pre-separation due to the different evaporation temperatures of the molecules in the sample matrix. Furthermore, only material, which was scraped off the area of the delamination, was added to the DIP-APCI crucible, whereas the size of the measuring point of the DART ion source depends on the distance of the source from the sample, with a minimal spot size of about 1 cm. Thus, the excited helium of the DART ionizes the molecules responsible for the detachment as well as the matrix molecules of the coating surrounding the delamination spot, e.g. the signal in the mass spectrum of the DART ion source with m/z = 210 (Fig. 3.7). For DART-MS, the advantage can be seen in the flexibility of a wide range of samples that can be studied. Even the surfaces of larger samples from the automotive industry can be screened using a DART ion source. The analytical performance of a Q-ToF-MS system offers high mass accuracy and resolution facilitating the identification of compounds of interest. Since no chromatographic separation is used, the enhanced performance of a Q-ToF-MS is very important. For further detailed structural information, MS/MS experiments result in clarification. For an assessment of the benefit of this direct analytical approach, a conventional pyrolysis-GC-MS system was used to analyze the same sample. Due to chromatographic separation, the pyrolysis-GC-MS delivers separate signals for different compounds at different times. As seen in the chromatogram of the pyrolysis-GC-MS measurement (Fig. 3.10), a typical signal for phthalates at 35 min was detected. Correlating the retention time and the extracted MS spectra (Fig. 3.11) with reference data from pure plasticizers, bis(7-methyloctyl)phthalate was identified. In addition, the fragments generated in the electron ionization process indicate a typical phthalate mass spectrum. The peak at m/z = 149 is the base peak of all phthalates other than dimethyl phthalate[18]. As expected, the pyrolysis-GC-MS measurement results in a reliable identification. However, it has to be kept in mind that an extraction step was involved and good extraction efficiency must be ensured. In the present case, the same qualitative information was obtained as by DART-MS/MS and DIP-APCI-MS/MS.

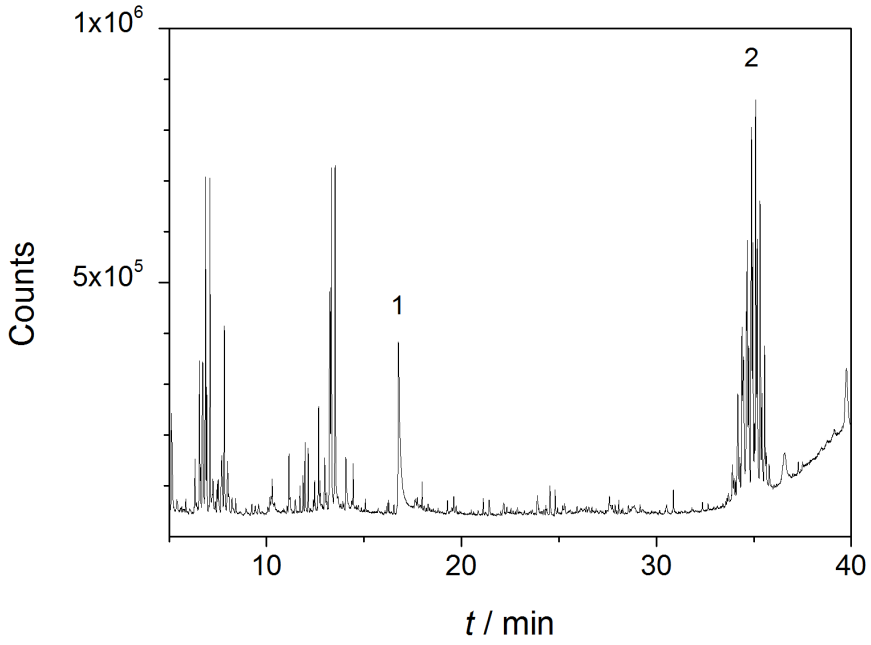

Figure 3.10: Pyrolysis-GC-MS recording corresponding to glass wool containing extracted parts of the sample; 1 phthalic acid (pyrolysis product), 2 bis(7-methyloctyl)phthalate

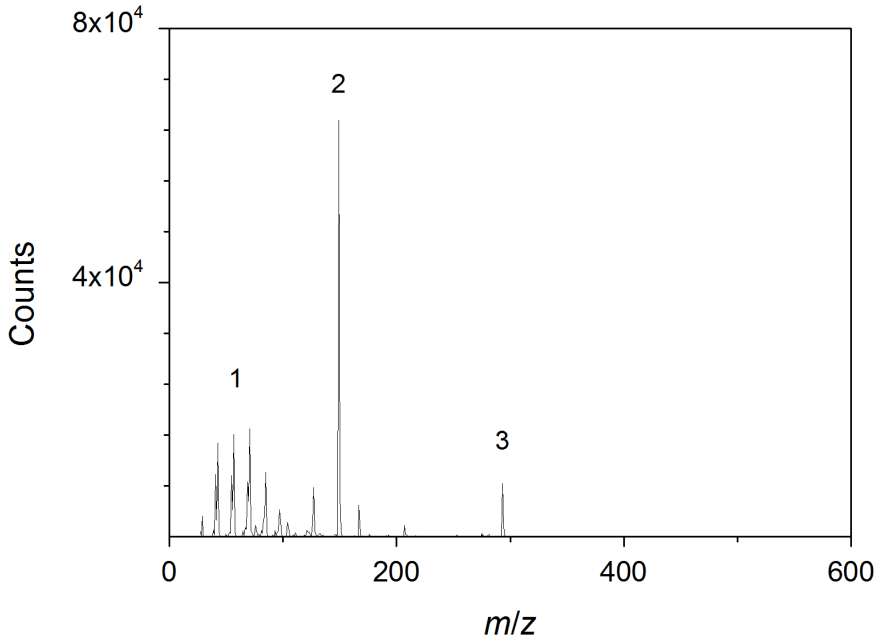

Figure 3.11: Pyrolysis-GC-EI mass spectrum of the signal from the chromatogram shown in Fig. 3.10 at 35 min, by comparison with a reference library identified as bis(7-methyloctyl)phthalate, fragments: 1 alkyl groups; 2 $m/z = 149$ $[C_8H_4O_3 + H]^+$[13]; 3 $m/z = 293$ $[C_{17}H_{24}O_4 + H]^+$

Conclusion

With both DART-MS and DIP-APCI-MS, the working steps and the required time for sample analysis were significantly reduced, due to the elimination of sample preparation or chromatographic pre-separation. Consequently, industrial laboratories can increase sample throughput and enhance the efficiency of analytical operations. However, in the case of trace analysis and severe matrix effects, such as ion suppression, the conventional analytical methods incorporating a chromatographic separation are still indispensable.

3.2.3 AFM

Introduction

In daily industrial quality control, fast and reliable analytical methods are implemented in the process. State-of-the-art optical microscopes are used to characterize irregularities in surfaces[19], inclusions or defects in materials[20] or coatings[21][22]. However, due to the lack of physical contact with the surface, no further information beyond surface irregularity imaging can be gained. For surface contaminations, a correlation between topographical illustration and localization of the contamination can be crucial for quality control, since non-visible contamination results in irregularities in the product. Thus, contact microscopic techniques, such as AFM[23][24][25], will be regarded as supplementary to optical microscopy and chemical characterization[26].

Experimental Procedure

An industrial e-coated aluminum surface with contamination was examined with an atomic force microscope (Nanosurf Flex AFM). A commercially available Tap-300 Al-G cantilever was used. The effects of the contamination were seen as surface defects after applying varnish. Thus, the surface was scanned for topographical irregularities before applying varnish, and the material contrast was measured with AFM. The topography measurement was conducted in tapping mode over an area of 9x9 µm. In the same position, phase monitoring was conducted, where possible phase shifts due to interactions between the cantilever and the surface were measured.

Results and Discussion

Figure 3.12 shows the defect after applying varnish using the AFM camera.

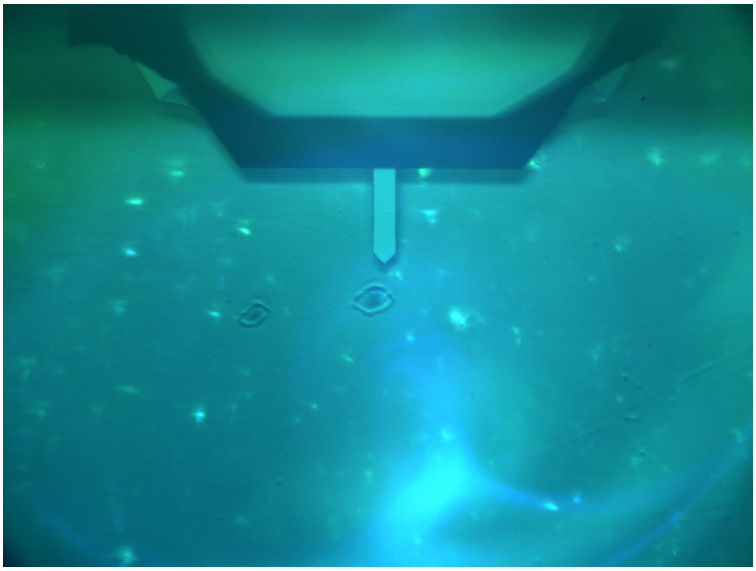

Figure 3.12: AFM camera image of the topographical irregularities after applying varnish

Due to reflections in the varnish the defect was not visible with optical microscopy. The e-coated aluminum surface was mapped before applying varnish in order to gather further topographical information (Figure 3.13). No significant irregularities were measured and the roughness of this industrial manufactured surface was relatively low with areas of 200 nm heights. The phase contrast measurement (Fig. 3.14) showed certain areas with an increased phase shift of 20-40° independent of the topography of the surface. Hence, the contamination on the surface interacted differently with the cantilever as compared with the e-coated surface, resulting in a phase shift.

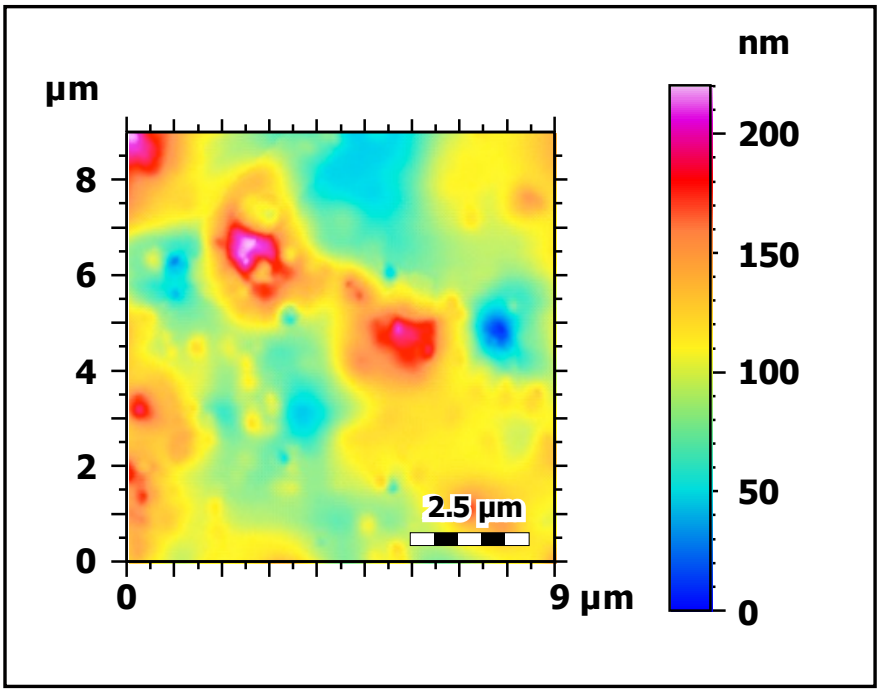

Figure 3.13: Topographical AFM map of the contaminated area

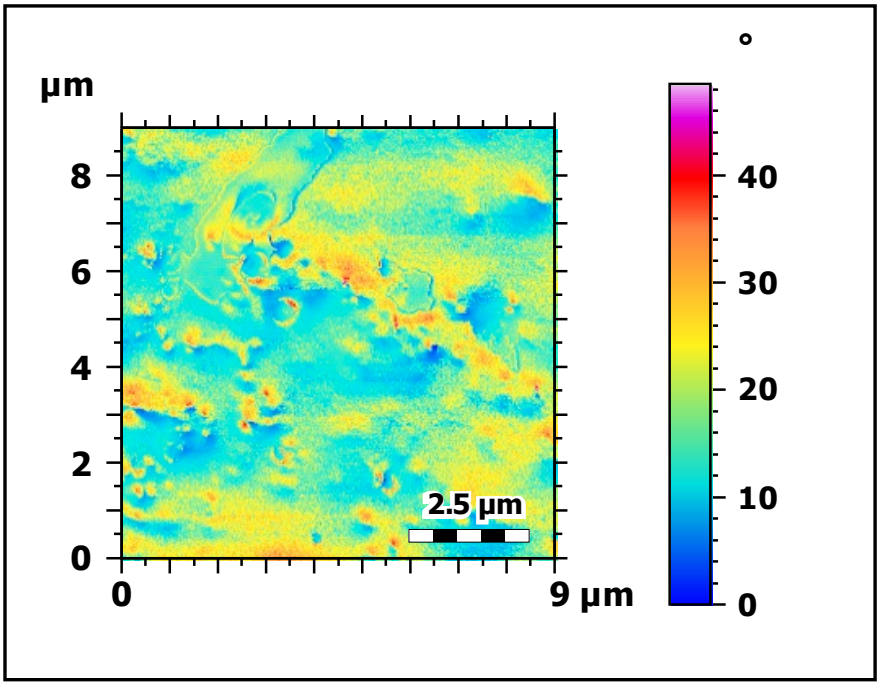

Figure 3.14: AFM - Material contrast imaging of the contaminated area due to different adhesion

To verify the phenomenon seen with the AFM, an additional XPS spectrum of the contaminated area was recorded (Fig. 3.15). Unexpectedly, a contamination with Sn and S was seen.

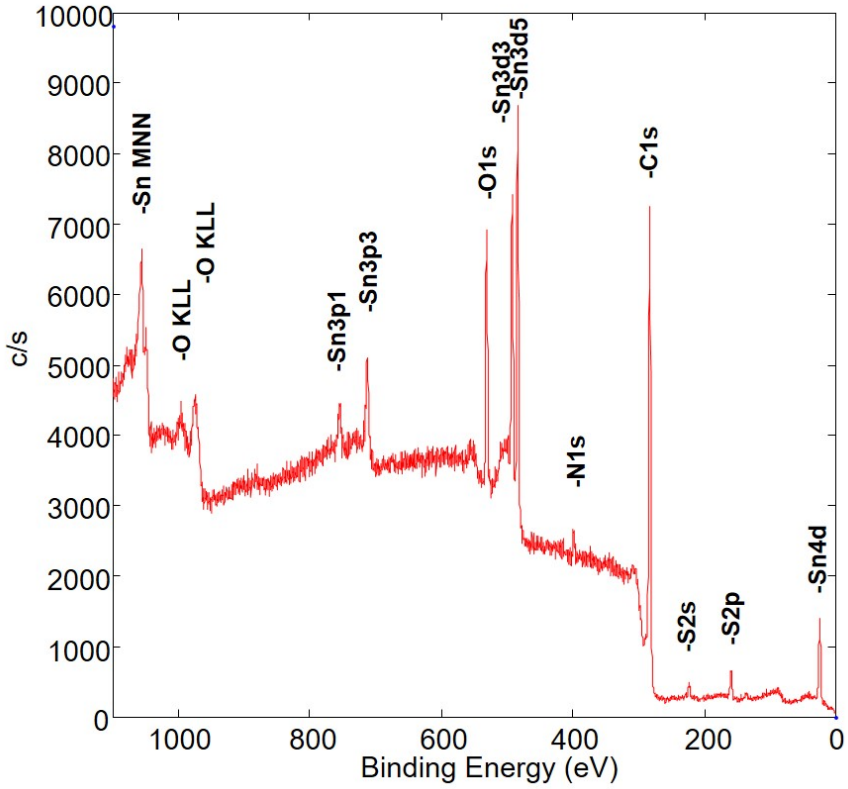

Figure 3.15: XPS spectrum of the contaminated area, showing signals of Sn and S

Conclusion

Topographical scanning in tapping mode and material contrast monitoring resulted in a fast and nondestructive method used to localize surface irregularities. The phase shift was correlated with material contrast and was distinguished from the topography. A regular cantilever can be used to monitor a broad range of applications from coatings and plastics to metal surfaces. Yet for detailed information on the type of interaction and identification of possible detachment mechanisms, the application of specific, surface-dependent methods, such as XPS, should be considered. Using XPS, a sulfur and tin contamination was identified, and in correlation with the AFM phase shift measurement, the area of contamination was successfully circumscribed.

3.2.4 XPS

Introduction

Weight reduction is an important factor in modern car production, and to this end, composite materials[27] and metal alloys[28] (e.g. aluminum alloys[29]) are employed. Thus, aluminum car parts are produced at a large-scale within a foundry. Due to the enormous speed and the large-scale production, surface contamination, such as release agents, oil or dust, is inevitable. Most aluminum parts need to be bonded to other parts and reproducible adhesion must be ensured[30]; a laser can be used to clean the aluminum surface prior to bonding[31]. An advantageous solution to this problem is to use a laser to clean the aluminum surface . The alteration of the surface and the effectivity of the pretreatment must first be evaluated with an instrumental analytical technique. Both quality and safety are dependent on proper bonding. With X-ray photoelectron spectroscopy[32], surface characterization of the top layer is possible, and characterizations of the aluminum bond site as well as the formation of an oxygen layer can be identified[33].

Experimental Procedure

X-ray photoelectron spectroscopy (XPS) was performed with a commercial PHI 5000 VersaProbe II (Ulvac PHI, Hagisono, Chigasaki, Kanagawa, Japan). The aluminum surfaces were studied at several positions with an incoming Al-Kα X-ray of 100 µm at 100 W, 20 kV and 1486 keV. In addition to the sample after pretreatment, a sample before laser pretreatment was analyzed as a reference. First, a survey spectrum was measured to study all components on the surface. A detailed spectrum of five locations was then recorded from each sample: C1s (278-298 eV), O1s (523-543 eV), Al2p (68-88 eV) and Si2p (94-114 eV). To determine the oxygen layer, a depth profile was recorded. Using argon sputtering, several nanometers of the top layer were ablated and a detailed spectrum was recorded. This process was repeated 15 times, resulting in a depth profile of 100 nm.

Results and discussion

The recorded detailed spectra of the surface differed significantly. Quantifying the elements (Table 3.2), the untreated surface showed an increased signal of carbon (45 Atom. %) compared to the laser pretreated surface (6 Atom. %). A distinct aluminum oxide layer was seen on the pretreated surface (oxygen 64 Atom. % and aluminum 26 Atom. %). The depth profile of the pretreated surface (Fig. 3.16) showed a constant homogeneous aluminum oxide layer, and the carbon signal decreased after the first sputter sequence.

The carbon signal decreased with each sputter profile and the aluminum signal increased, as shown for the untreated surface in Figure 3.17. Only the first 25 nm showed an Al_2O_3 layer. At 60 nm, most of the surface was removed and the aluminum material signal was seen. Besides carbon, a contamination of silicon was found with increased amounts at further depths. Here, contaminations of carbon from oils, dust and human handling were found, as well as a constant layer of release agent seen in the silicon signal. With the laser pretreated surface, neither of the contaminations were present in higher amounts.

Table 3.2: XPS surface analyzis of untreated and pretreated aluminum

Elements:	C1s	O1s	Al2p	Si2p
	Atom. %	Atom. %	Atom. %	Atom. %
Untreated surface	45	38	12	5
Pretreated Surface	6	64	26	4

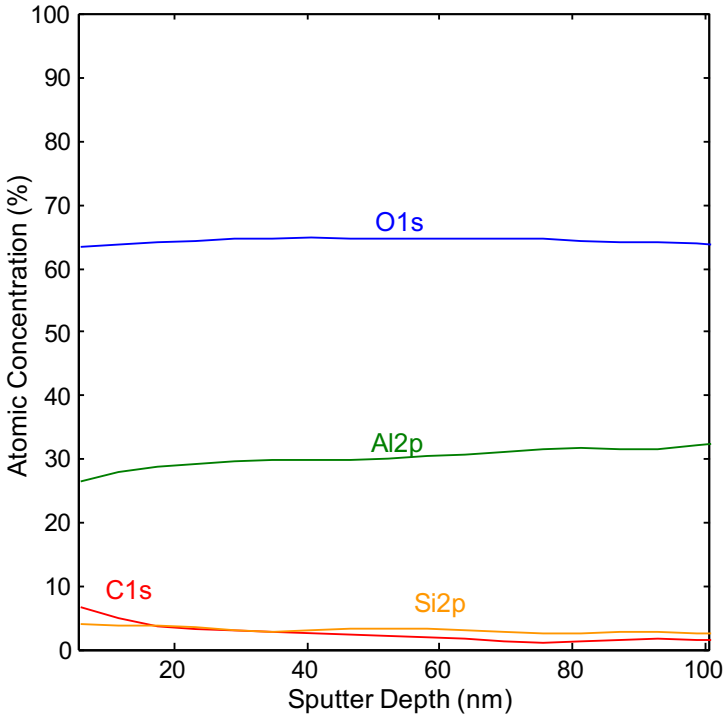

Figure 3.16: XPS profile: pretreated surface

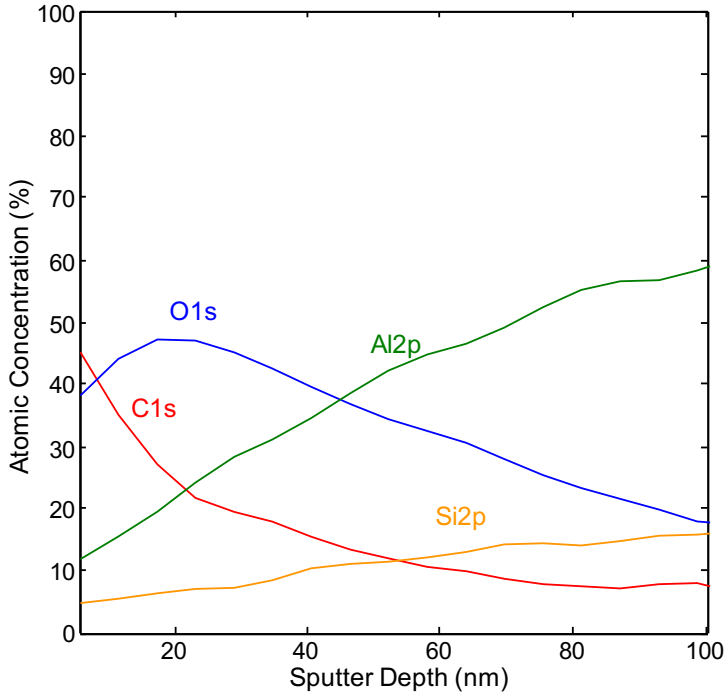

Figure 3.17: XPS profile: pretreated surface

Conclusion

Due to mechanical and non-sterile handling, the necessity of a cleaning process in the form of a pretreatment can be seen. XPS provided detailed information to evaluate the surface regarding chemical components in the first layer. The rather unique ability to create a depth profile using argon sputtering was useful for the analysis of oxygen layers. Thus, a method for the characterization of surface modifications after mechanical pretreatment processes was established.

3.2.5 References

[1] A. Grau, M. Indri, L. L. Bello, and T. Sauter, "Industrial Robotics in Factory Automation : from the Early Stage to the Internet of Things," *IECON 2017 - 43rd Annual Conference of the IEEE Industrial Electronics Society*, pp. 6159–6164, 2017.

[2] E. Hofmann and M. Rüsch, "Industry 4.0 and the current status as well as future prospects on logistics," *Computers in Industry*, vol. 89, pp. 23–34, 2017.

[3] M. Smater and J. Zieliński, "Automatization and Robotisation as a Lever for Process and Product Quality in SME," *Solid State Phenomena*, vol. 220-221, pp. 1001–1007, 2015.

[4] M. Wollschlaeger, T. Sauter, and J. Jasperneite, "The Future of Industrial Communication: Automation Networks in the Era of the Internet of Things and Industry 4.0," *IEEE Industrial Electronics Magazine*, vol. 11, no. 1, pp. 17–27, 2017.

[5] S. Robert, "E-Mobility and the Energy Transition," *Angewandte Chemie International Edition*, vol. 56, no. 37, pp. 11019–11022, 2017.

[6] W. Brenner and A. Herrmann, *An Overview of Technology, Benefits and Impact of Automated and Autonomous Driving on the Automotive Industry BT - Digital Marketplaces Unleashed*. Berlin, Heidelberg: Springer Berlin Heidelberg, 2018.

[7] D. K. Koli, G. Agnihotri, and R. Purohit, "Advanced Aluminium Matrix Composites: The Critical Need of Automotive and Aerospace Engineering Fields," *Materials Today: Proceedings*, vol. 2, no. 4, pp. 3032–3041, 2015.

[8] A. K. Naskar, J. K. Keum, and R. G. Boeman, "Polymer matrix nanocomposites for automotive structural components," *Nature Nanotechnology*, vol. 11, p. 1026, 2016.

[9] M. A. Wahab, *Joining Composites with Adhesives: Theory and Applications*. DEStech Publications, Inc., 2016.

[10] F. M. Penning, "Über Ionisation durch metastabile Atome," *Naturwissenschaften*, vol. 15, p. 818, 1927.

[11] R. B. Cody, "Observation of Molecular Ions and Analysis of Nonpolar Compounds with the Direct Analysis in Real Time Ion Source," *Analytical Chemistry*, vol. 81, no. 3, pp. 1101–1107, 2009.

[12] J. H. Gross, "Direct analysis in real time - a critical review on DART-MS," *Analytical and Bioanalytical Chemistry*, vol. 406, no. 1, pp. 63–80, 2014.

[13] C. Wang, H. Zhu, Z. Cai, F. Song, Z. Liu, and S. Liu, "Newborn screening of phenylketonuria using direct analysis in real time (DART) mass spectrometry," *Analytical and Bioanalytical Chemistry*, vol. 405, no. 10, pp. 3159–3164, 2013.

[14] E. S. Roberts, B. A. Boudreau, D. W. Brown, K. L. McQuade, and E. E. Remsen, "Analysis of carbohydrates in Fusarium verticillioides using size-exclusion HPLC - DRI and direct analysis in real time ionization - time-of-flight - mass spectrometry (DART-MS)," *Anal. Methods*, vol. 8, no. 3, pp. 673–681, 2016.

[15] S. Krieger, A. von Trotha, K. S.-Y. Leung, and O. J. Schmitz, "Development, optimization, and use of an APCI source with temperature-controlled vaporization of solid and liquid samples," *Analytical and Bioanalytical Chemistry*, vol. 405, no. 4, pp. 1373–1381, 2013.

[16] D. I. Carroll, I. Dzidic, R. N. Stillwell, K. D. Haegele, and E. C. Horning, "Atmospheric pressure ionization mass spectrometry. Corona discharge ion source for use in a liquid chromatograph-mass spectrometer-computer analytical system," *Analytical Chemistry*, vol. 47, no. 14, pp. 2369–2373, 1975.

[17] K. Sonja and S. O. J., "Non-destructive plasticizer screening using a direct inlet probe-atmospheric pressure chemical ionization source and ion trap mass spectrometry," *Rapid Communications in Mass Spectrometry*, vol. 28, no. 17, pp. 1862–1870, 2014.

[18] R. Davis and M. Frearson, *Mass spectrometry - analytical chemistry by open learning*. Chichester/New York: Wiley, 1987.

[19] G. U. Kothiyal, M. Singaperumal, R. S. Sirohi, and M. P, "Characterization of surface topography by confocal microscopy: II. The micro and macro surface irregularities," *Measurement Science and Technology*, vol. 11, no. 3, p. 315, 2000.

[20] Y. Ma, Y. Yang, T. Sugahara, and H. Hamada, "A study on the failure behavior and mechanical properties of unidirectional fiber reinforced thermosetting and thermoplastic composites," *Composites Part B: Engineering*, vol. 99, pp. 162–172, 2016.

[21] K. Adamsons, "Chemical depth profiling of automotive coating systems using slab microtome sectioning with IR/UV-VIS spectroscopy and optical microscopy," *Journal of Coatings Technology*, vol. 74, no. 924, p. 47, 2002.

[22] L.-P. Sung, J. Jasmin, X. Gu, T. Nguyen, and J. W. Martin, "Use of laser scanning confocal microscopy for characterizing changes in film thickness and local surface morphology of UV-exposed polymer coatings," *JCT Research*, vol. 1, no. 4, pp. 267–276, 2004.

[23] P. Bertrand-Lambotte, J. L. Loubet, C. Verpy, and S. Pavan, "Nano-indentation, scratching and atomic force microscopy for evaluating the mar resistance of automotive clearcoats: study of the ductile scratches," *Thin Solid Films*, vol. 398-399, pp. 306–312, 2001.

[24] G. González, W. Stracke, Z. Lopez, U. Keller, A. Ricker, and R. Reichelt, "Characterization of Defects and Surface Structures in Microporous Materials by HRTEM, HRSEM, and AFM," *Microscopy and Microanalysis*, vol. 10, no. 2, pp. 224–235, 2004.

[25] R. S. McLean and B. B. Sauer, "Tapping-Mode AFM Studies Using Phase Detection for Resolution of Nanophases in Segmented Polyurethanes and Other Block Copolymers," *Macromolecules*, vol. 30, no. 26, pp. 8314–8317, 1997.

[26] S. Y. Lang, Y. Shi, Y. G. Guo, D. Wang, R. Wen, and L. J. Wan, "Insight into the Interfacial Process and Mechanism in Lithium-Sulfur Batteries: An In Situ AFM Study," *Angewandte Chemie - International Edition*, vol. 55, no. 51, pp. 15835–15839, 2016.

[27] K. Friedrich and A. A. Almajid, "Manufacturing Aspects of Advanced Polymer Composites for Automotive Applications," *Applied Composite Materials*, vol. 20, no. 2, pp. 107–128, 2013.

[28] G. S. Cole and A. M. Sherman, "Light weight materials for automotive applications," *Materials Characterization*, vol. 35, no. 1, pp. 3–9, 1995.

[29] J. Hirsch, "Recent development in aluminium for automotive applications," *Transactions of Nonferrous Metals Society of China*, vol. 24, no. 7, pp. 1995–2002, 2014.

[30] G. Meschut, V. Janzen, and T. Olfermann, "Innovative and Highly Productive Joining Technologies for Multi-Material Lightweight Car Body Structures," *Journal of Materials Engineering and Performance*, vol. 23, no. 5, pp. 1515–1523, 2014.

[31] A. W. AlShaer, L. Li, and A. Mistry, "The effects of short pulse laser surface cleaning on porosity formation and reduction in laser welding of aluminium alloy for automotive component manufacture," *Optics & Laser Technology*, vol. 64, pp. 162–171, 2014.

[32] E. Paparazzo, "XPS analysis of iron aluminum oxide systems," *Applied Surface Science*, vol. 25, no. 1, pp. 1–12, 1986.

[33] T. Dimogerontakis, R. Oltra, and O. Heintz, "Thermal oxidation induced during laser cleaning of an aluminium-magnesium alloy," *Applied Physics A*, vol. 81, no. 6, pp. 1173–1179, 2005.

3.3 Method development for self-assembled monolayer functionalization of atomic force microscope cantilevers

3.3.1 Introduction

Most industrial applications are only verified by mechanical tests. Due to lack of time, most issues are solved by applying a solution, without analyzing the cause. This is especially true with the introduction of new materials, where macroscopic tests are applied to verify the functionality of the material. In the realm of adhesives, standard tests, such as peel tests, tensile strength tests, rheology or scoop tests, are used to verify the bond between an adhesive and a substrate[1][2][3]. However, in the case of a detachment, or for the qualification of a new application (e.g. bonding CFRP with adhesive), great efforts are made to achieve a reliable and well-understood process. In addition to the macroscopic and mechanical approach, it is important to consider scientific and analytical approaches, due to the rapid development of new materials[4][5]. Thus, compromises between basic research and industrial applications have to be made. In this chapter, experimental approaches were used to apply force spectroscopy using AFM to the simulation of the interaction between an adhesive and a suitable substrate[6][7].

3.3.2 Experimental Procedure

All AFM measurements made using a commercial AFM (Nanosurf - FlexAFM). The topographical measurements were made in the tapping mode with Tap300Al-G cantilevers, and the force measurements were made with Tap300GB-G and HQ:NSC19/Cr-Au cantilevers. The modification with functional alcohol groups was made via a self-assembled monolayer (SAM) process (Figure 3.18 B).

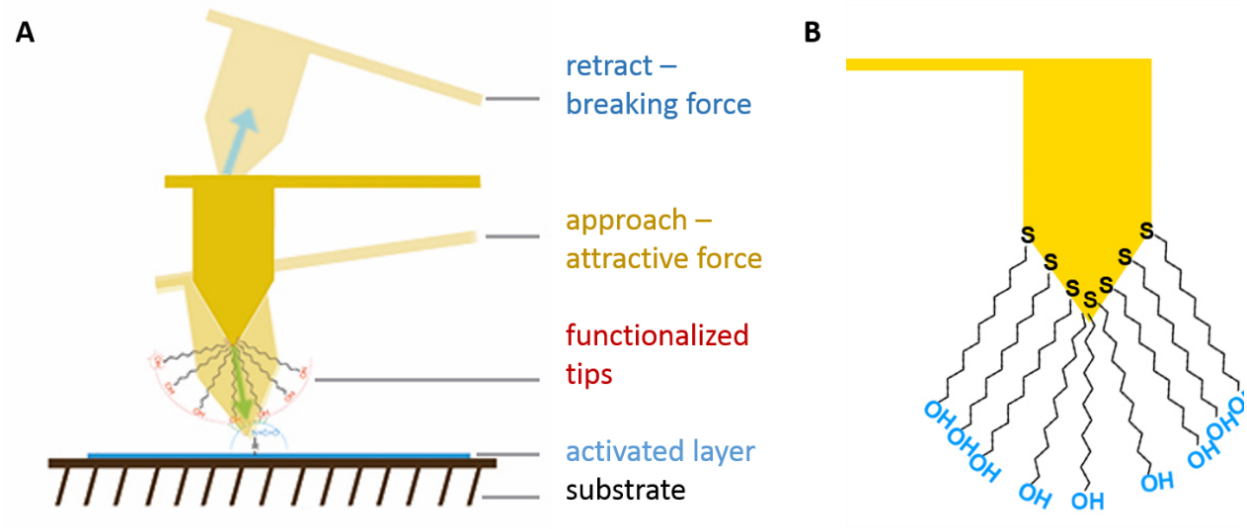

Figure 3.18: Schematic representation of the principle of AFM/CFM measurements (A) and functionalized cantilever (B)

A 5 mM solution of 11-mercapto-1-undecanol in ethanol (Sigma-Aldrich) was used. The cap of a micro vial was used To facilitate the handling, and it provided an ideal storage space for the cantilever and the thiol solution. The respective vial was filled with argon gas and used as a cap to ensure a clean reaction environment; it was stored for 48 hours (Figure 3.19). XPS measurements were made to verify successful monolayer formation.

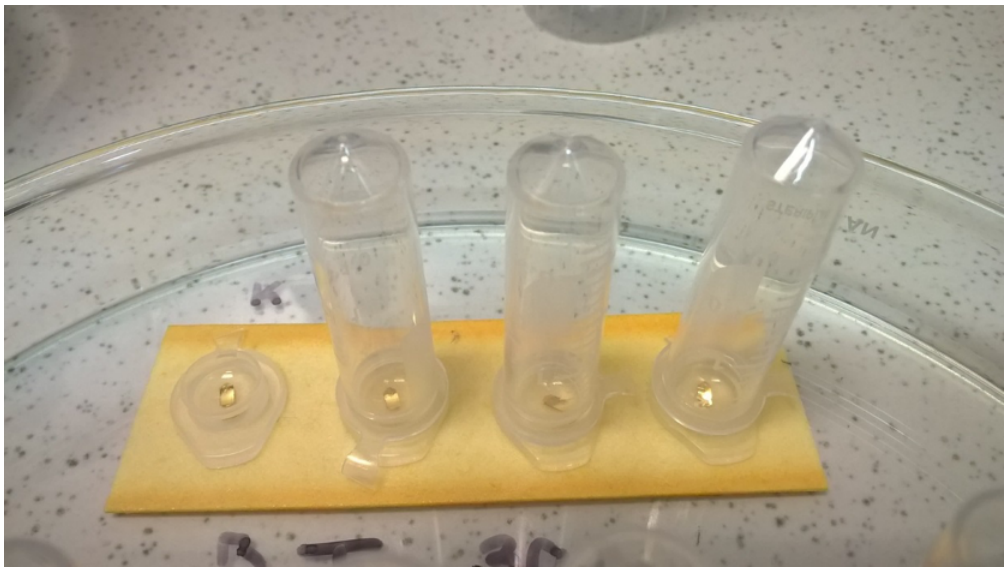

Figure 3.19: Preparation of self-assembled monolayer on cantilever tips.

During CFM measurements, the functionalized cantilever approached the surface with a constant speed and the interaction force (e.g. van der Waals interactions) between the surface and the cantilever was detected. At a certain distance the cantilever was deflected and attracted to the surface, which can be seen in a force distance diagram. During the retracting process, the cantilever interacted with the surface and was retarded, due to adhesion forces. Consequently, two forces arose with force spectroscopy - the attractive force for approaching the surface and the adhesion force for retracting the cantilever[8]. By using functionalized cantilevers, specific interaction forces were detected (Figure 3.18 A).

XPS experiments:
X-ray photoelectron spectroscopy (XPS) was performed with a commercial Phi 5000 VersaProbe III (Ulvac PHI, Hagisono, Chigasaki, Kanagawa, Japan). A detailed spectrum for C1s (278-298 eV), O1s (523-543 eV) and S2p (155-175 eV) were recorded.

3.3.3 Results & Discussion

The XPS spectrum of the modified cantilever differed significantly from the untreated reference cantilever (Fig. 3.20 A and B). The C1s signal (Fig. 3.20 A) of the modified cantilever showed carbon-to-oxide bonding at 288 eV. After comparing the signal with the literature, an alcohol-to-carbon bond was suggested[9]. This correlates with the O1s signal, since an oxygen-to-carbon bond was seen at 536 eV. Thus, a successful cantilever modification was achieved.

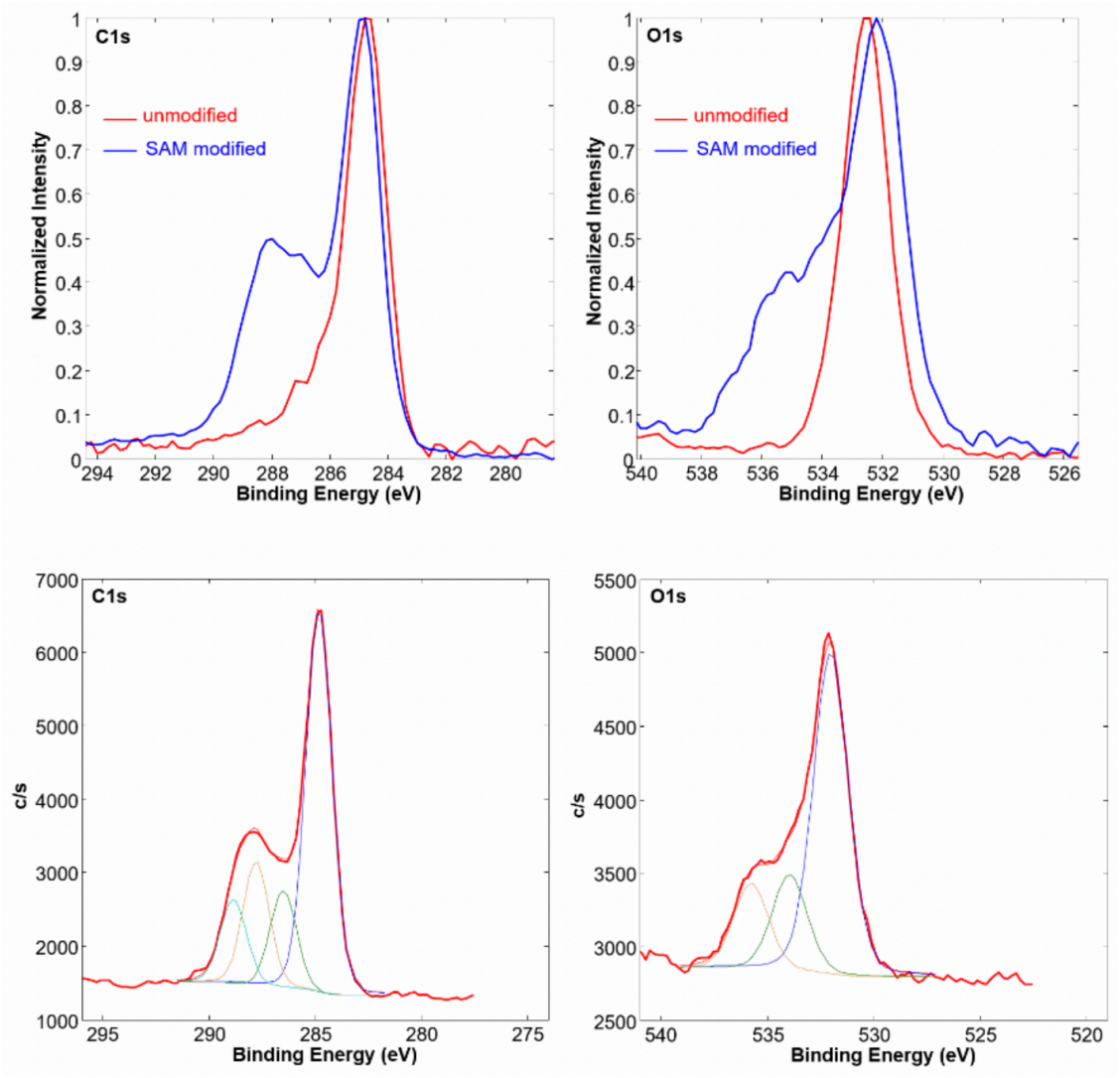

Figure 3.20: XPS spectra of unmodified AFM cantilevers and cantilevers with SAM modification used for CFM measurements.

To test the modified cantilever a CFRP plate, pretreated by corundum blasting, was chemically activated and compared to an unmodified cantilever. The unmodified cantilever detected adhesion forces between 10 nN and 50 nN with no significant area information (Fig. 4B). The SAM modified cantilever showed increased adhesion forces of up to 250 nN and a detailed area map with activated domains (Fig. 4A). With the modified tip, the chemical interaction increased the depth of information gained via force measurement.

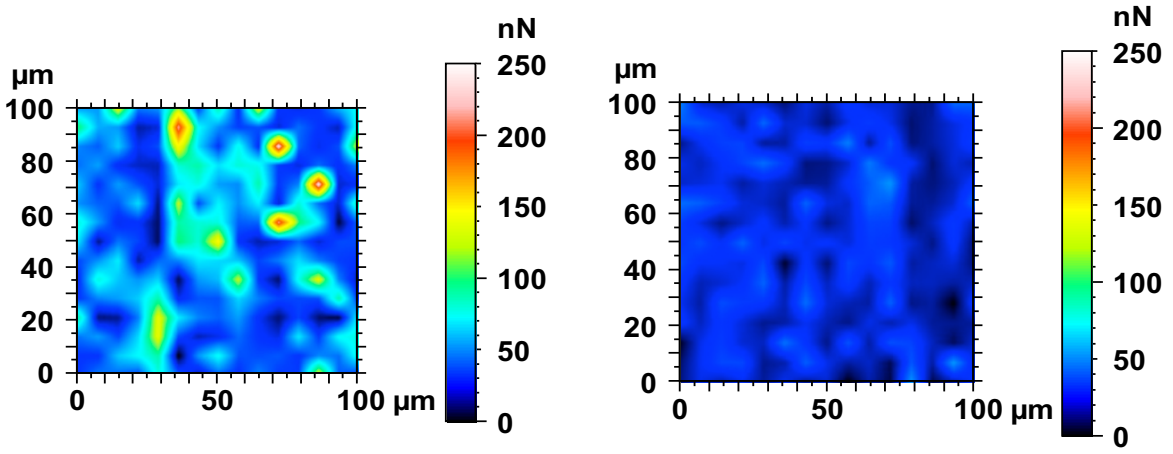

Figure 3.21: Measurement with B unmodified gold cantilever and A modified gold cantilever.

3.3.4 Conclusion

The procedure and preparation of thiol self-assembled monolayer for AFM cantilevers was successfully applied and verified with XPS measurements. The use of micro vials for the SAM process was reliable and easy to apply to the modification of multiple cantilevers. This scientific approach was implemented for real industrial samples. Further studies must be done to show the utility of specific interaction measurements on different surface types. A reliable process of cantilever modification, verification and application was established.

3.3.5 References

[1] K. Uehara and M. Sakurai, "Bonding strength of adhesives and surface roughness of joined parts," *Journal of Materials Processing Technology*, vol. 127, no. 2, pp. 178–181, 2002.

[2] S. A. Meguid and Y. Sun, "On the tensile and shear strength of nano-reinforced composite interfaces," *Materials & Design*, vol. 25, no. 4, pp. 289–296, 2004.

[3] T. Ferracin, C. M. Landis, F. Delannay, and T. Pardoen, "On the determination of the cohesive zone properties of an adhesive layer from the analysis of the wedge-peel test," *International Journal of Solids and Structures*, vol. 40, no. 11, pp. 2889–2904, 2003.

[4] M. Sharma, S. Gao, E. Mäder, H. Sharma, L. Y. Wei, and J. Bijwe, "Carbon fiber surfaces and composite interphases," *Composites Science and Technology*, vol. 102, pp. 35–50, 2014.

[5] R. Tao, M. Alfano, and G. Lubineau, "Laser-based surface patterning of composite plates for improved secondary adhesive bonding," *Composites Part A: Applied Science and Manufacturing*, vol. 109, pp. 84–94, 2018.

[6] N. Zheng, J. He, J. Gao, Y. Huang, F. Besenbacher, and M. Dong, "Adhesion force measured by atomic force microscopy for direct carbon fiber-epoxy interfacial characterization," *Materials & Design*, vol. 145, pp. 218–225, 2018.

[7] A. Beaussart, T. C. Ngo, S. Derclaye, R. Kalinova, R. Mincheva, P. Dubois, P. Leclere, and Y. F. Dufrene, "Chemical force microscopy of stimuli-responsive adhesive copolymers," *Nanoscale*, vol. 6, no. 1, pp. 565–571, 2014.

[8] A. Noy, D. V. Vezenov, and C. M. Lieber, "Chemical Force Microscopy," *Annual Review of Materials Science*, vol. 27, no. 3, pp. 381–421, 1997.

[9] P. E. S. J. F. Moulder, W. F. Stickle and K. D. Bomben, *Handbook of X-ray Photoelectron Spectroscopy*. Chigasaki: ULVAC-PHI and Physical Electronics, 3 ed., 1992.

3.4 Complementary analytical imaging techniques for the characterization of pretreated carbon fiber reinforced plastics[2]

Stefan Viehbeck, Christian Iffelsberger, Frank-Michael Matysik

3.4.1 Graphical Abstract

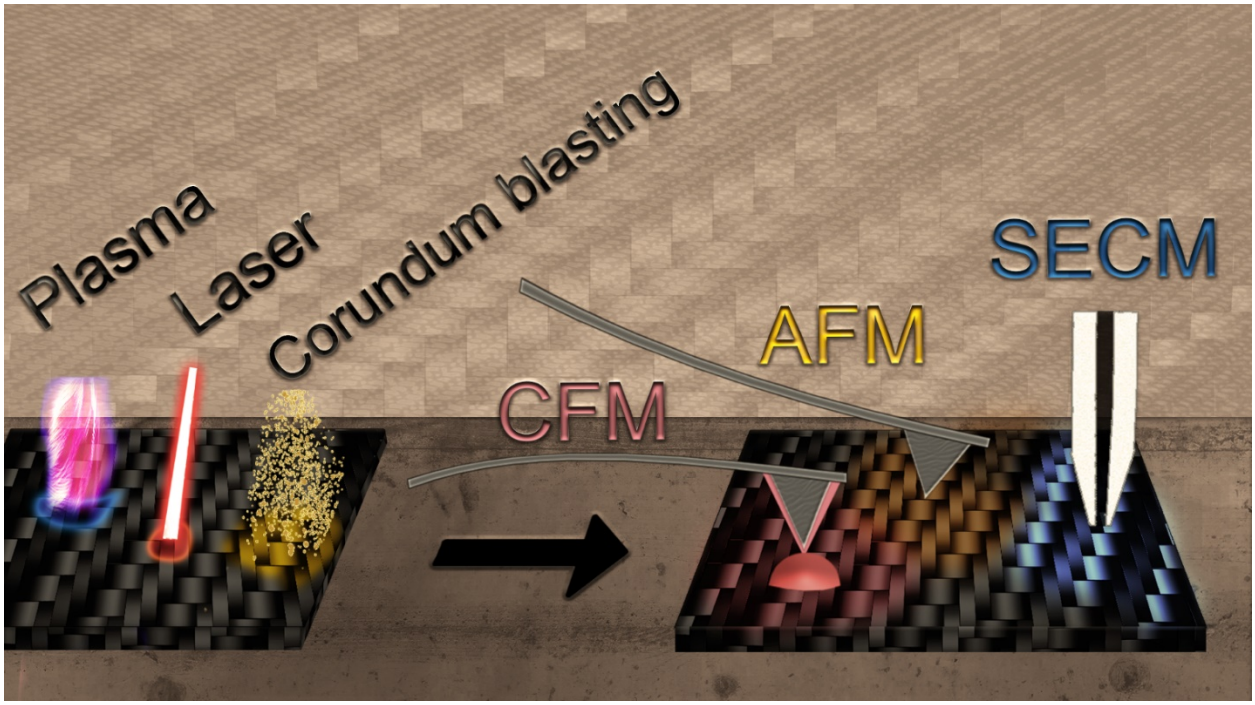

3.4.2 Abstract

In this work the complementary characterization of pretreatment techniques for adhesive bonding of carbon fiber reinforced plastics (CFRP) is presented. Industrial CFRP plates were pretreated with laser, plasma and corundum blasting abrasive techniques followed by chemical activation. The combined use of atomic force microscopy and chemical force

2 *Composites Part A: Applied Science and Manufacturing (2018) 113:32-39*

microscopy enabled the characterization of the surface morphology and the specific adhesion force between a chemically functionalized cantilever and the pretreated surfaces simulating the adhesive bond. Complementary measurements with scanning electrochemical microscopy and X-ray photoelectron spectroscopy supported the experimental findings and delivered additional information about the chemical structure of the surfaces. A comparison of experimental data of mechanical tensile shear strength measurements and the applied analytical methods revealed a valid correlation of microscopic and macroscopic techniques.

3.4.3 Introduction

Carbon fiber reinforced plastics (CFRP) represent an attractive class of composite material consisting of carbon fibers immersed in a surrounding plastic matrix. The combination of the materials can strengthen their individual properties so that CFRP possess a greater ratio of modulus and tensile strength to their weight, a lower thermal coefficient and a higher internal damping compared to steel or lightweight alloys such as aluminum or titanium[1]. These characteristics lead to a broad field of commercial and industrial applications including military and commercial aircrafts, automotive, space and sporting goods[2] to name just a few examples. In the automotive industry CFRP components are used to construct body parts, chassis or engine components of lighter weight and with a better stability. The special chemical composition of workpieces consisting of CFRP requires different joining methods than conventional aluminum, steel or iron parts. Riveting, welding or screwing are not suitable for composite lightweight car manufacturing[3]. In addition to that, adhesive bonding won't adhere properly on a recently manufactured CFRP part. Since large scale and automated production/compression tools require release agents and thereby contaminate the surface of the manufactured parts. Different pretreatment techniques are used to remove the release agent and activate the surface to enable adhesive bonding. The quality aspect of the CFRP bonding is regarded as a crucial safety issue. Thus, new methods for quality evaluation are needed. Currently only macroscopic measurements such as tensile shear strength and peel tests are applied to evaluate the adhesive bonding[4]. The surface is evaluated according to the fracturing and conclusively regarding the efficiency of the surface pretreatment technique. For detailed information on the impact of the surface pretreatment techniques and possible consequences

for the adhesive bonding, further investigations and new analytical methods must be established. In scanning probe microscopy, the information is generated through interactions between a probe, which is scanned across a substrate. The result of this measuring process is expressed as an image[5]. Beside the topographical mapping[6] atomic force microscopy (AFM) possesses the potential for the detection of interacting forces between the cantilever and a surface[7][8]. Especially for biochemical applications this measuring mode is often combined with a chemically modified cantilever[9]. Using this chemical force microscopy (CFM) recent studies show the specific interaction of functional groups and a biolayer[10]. The strength of AFM, the atomic[11][12] or molecular[13] resolution, is often compromised by the restriction to relatively small surface areas. For studying atomic or molecular effects and correlating them with macroscopic surface properties the uniformity of the studied surface is a prerequisite. From the practical point of view the microscopic surface properties are often determined by many various effects occurring at different spots across the surface. This aspect is a limitation of many high-resolution scanning probe techniques for studying workpieces at industrial scale and size. The lack of representative characterization of larger surface areas can be considered as a disadvantage of AFM in the context of industrial applications. Scanning electrochemical microscopy (SECM), developed and characterized by A.J. Bard and coworkers[14], is an alternative scanning probe technique. SECM has found a wide range of applications ranging from biological surfaces[15][16] to novel inorganic materials[17]. Usually the studied substrate is fixed in an electrochemical cell and immersed in a solution containing an electroactive compound as mediator substance. In the amperometric measurement mode the current of an electrochemical reaction occurring at the UME is used as signal to generate analytical information about the (electro)chemical activity and/or topographical details of the scanned surface, in a noninvasive way[18]. In SECM the probe is an ultra-microelectrode (UME) with an electrode diameter of 25 µm or less resulting in a limited resolution compared to AFM. SECM is well suited for studying properties of inhomogeneous surfaces within areas of a few square mm [19]. This is particularly attractive for surfaces which can hardly be characterized by optical methods. In addition, surfaces exhibiting regions with different (electro)chemical properties like CFRP are ideal substrates for SECM studies. With its ability to scan across rather large surface areas SECM provides additional information to AFM. A classical amperometric measuring principle is the feedback mode[14], with its two possibilities to influence the signal. In negative feedback, isolating surface regions hinder the mass transport of the mediator towards the UME resulting in a decreased current. A conductive substrate, however, leads to an enhanced current due to redox cycling between

probe and substrate. As with other scanning probe techniques the resolution of the SECM depends on the probe size. Mathematical expressions for the analytical treatment of the measured currents are described in literature[20] and a comprehensive review of applications and experimental parameters for SECM studies was published recently by Polcari et al.[21]. Further surface techniques such as X-ray photoelectron spectroscopy[22][23] or ToF-SIMS[24] complement previous methods with information on the chemical composition of the surface. In this work, advanced scanning probe techniques such as AFM/CFM and SECM were used for the characterization of the surface of CFRP plates and to correlate the effects of different activation procedures such as corundum blasting, plasma and laser activation prior to chemical activation of the CFRP/CFRP bonding. X-ray photoelectron spectroscopy was applied for additional characterization the chemical composition of the CFRP surface.

3.4.4 Experimental Procedure

Chemicals & Materials

Industrial CFRP plates, a commercially available material (Rhein Composite GmbH), were used after a resin transfer molding process. Different pretreatment techniques were applied to activate the CFRP surface and to remove the release agent and surface contamination. In detail, the following mechanical pretreatment methods were applied: (i) corundum blasting (4-5 bar, 120 grit, (ii) CO_2-laser activation ($\lambda = 10.6$ µm with 80 W), and (iii) atmospheric plasma treatment ($\sim 200°C$ with 10 kV). All techniques were applied with optimized settings as used under industrial conditions for comparable composites. In addition to mechanical pretreatment a chemical activator[25] (e.g. organometallic compound) was subsequently used to activate functional surface groups and to catalyze the reaction of an adhesive to the surface. The AFM and CFM studies were done either after mechanical pretreatments or after mechanical pretreatments combined with chemical activation. Prior to all scanning probe experiments the CFRP plates were cut into squares with an area of a few square cm. The obtained squares were cleaned with ultrapure water and isopropanol (MS grade, Merck KGaA, Darmstadt, Germany). For a better correlation of the optical, SECM and AFM/CFM measurements the examined surface areas were restricted by laying a square (1 cm^2) of a pierced (⌀ 2.1 mm) silicone foil with a thickness of 100 µm (Elastosil, Wacker Chemie AG, Burghausen, Germany) on the CFRP surface. The roughness of the corundum blasting treated sample made a fixation

of the silicone foil with a fast curing 2-componenent epoxy resin (UHU GmbH & Co. KG, Buhl, Germany) necessary. All imaging experiments were performed within the restricted area. For all SECM experiments an aqueous solution of 1.5 mM ferrocene methanol (FcMeOH, 99 %, ABCR, Karlsruhe, Germany) as mediator and 0.2 M KNO_3 (analytical grade, Merck KGaA, Darmstadt, Germany) as supporting electrolyte were used. The solution was prepared in ultrapure water with a resistivity higher than 18 MΩ cm^{-1} (membraPure, Bodenheim, Germany). As adhesive system a two-component polyurethane mixture (1:1) was used. The first component was formulated as a multicomponent polyol mixture[26]. A prepolymeric alcohol functionalized polybutadiene mixture (52.5 w.%, Polyvest EP HT, EVONIK Resource Efficiency GmbH, Marl, Germany) was used as reactive polyol. Thiodiethanol (9.0 w.%, Fluka Analytical) was used as chain extending component. The filler, kaolin (35.7 w.%), and the adhesion agent, trimethoxysilan (0.4 w.%), were obtained from Sigma-Aldrich. Dimethoxypolysiloxan (0.04 w.%, Sigma-Aldrich) was used as antifoaming agent. Pentaerythrit (2.0 w.%, Sigma-Aldrich) was used for crosslinking. To increase the reaction speed zirconium(IV)acetylacetonate was used as catalyst (0.4 w.%, Sigma-Aldrich)[27]. All components were homogenized with a Thinky Mixer ARE 250 (Thinky corp., Tokyo, Japan) for 2 minutes at 2000 rpm. The second component was a prepolymeric MDI isocyanate mixture (DOW Chemicals). Each component was filled in a cartridge and applied with the help of a two-component adhesive gun with multi-chamber mixing nozzle.

Instrumentation & Measurements

All AFM measurements were done with a commercial AFM (Nanosurf - FlexAFM). The topographical measurements were done in tapping mode and with Tap300Al-G cantilevers. For each cantilever calibrations of the deflection-sensitivity and the spring constant were done. The chemical modification of the cantilever and the evaluation of the SAM process is described in Results & Discussion - Chapter 3.3.

SECM imaging was performed with a commercial SECM system CHI 920C (CH Instruments, Austin, USA) in a two-electrode setup with a Pt wire ($\varnothing$ 0.5 mm) as counter and quasi-reference electrode. All potentials refer to this quasi-reference electrode. A Pt-disk ultra-microelectrode with an electrode diameter of 25 µm and an RG of 2-3 was used as SECM probe. The probe was fabricated according to the procedure described elsewhere[17]. Prior to the imaging the substrate was levelled until a tilt less than 10 µm per mm^2 was achieved. The imaging for the reference, laser- and plasma-activated sample

was performed at a tip-to-substrate distance of d< 10 µm, according to the measured current (I_M) of 60 % in relation to the current measured in the bulk phase ($I_\infty \approx$). For the corundum blasting treated sample IM was 125 % relative to $I_\infty \approx$ corresponding to a tip-to-substrate distance of about 17 µm. The scan speed was 100 µm s^{-1} with a pixel size of 4 µm. After imaging by scanning probe techniques optical images of the studied area were taken using a Leica M205 C stereo microscope.

Tensile shear strength experiments:
For macroscopic characterization, tensile shear strength measurements were conducted. For all tensile shear tests the substrates were cut into plates with a width of 45 mm and a length of 100 mm. The adhesive was applied onto the two substrates with a two-component adhesive gun and a multi chamber mixing nozzle. The two plates overlapped and adhered with an area of 45 mm x 20 mm. After 7 days of curing the complementary ends of both plates were fixed in the tensile shear testing device and sheared with a constant speed of 0.4 mm s^{-1}. Five independent measurements were done and the result is calculated as mean value.

XPS experiments:
X-ray photoelectron spectroscopy (XPS) was performed with a commercial system Phi 5000 VersaProbe III (Ulvac PHI, Hagisono, Chigasaki, Kanagawa, Japan). The same samples as used for the SECM experiments were studied at several positions with an incoming Al-Kα X-Ray of 100 µm with 100 W and 20 kV. First, a survey spectrum was measured to study all components on the surface (Fig. 3.28). Afterwards a detail spectrum with 3 spots on each sample for C1s (278-298 eV), O1s (523-543 eV), N1s (391-411 eV), Si2p (94-114 eV) and Sn3d5 (480-500 eV) was recorded.

3.4.5 Results & Discussion

Untreated CFRP surface.
The optical characterization of the untreated CFRP plate is shown in Figure 3.22 A. It shows surface defects induced by mechanical stress. As expected, in the scanning electrochemical microscopy image (Fig. 3.22 B), recorded with a 25 µm UME in 1.5 mM FcMeOH (bulk phase current of $I_\infty \approx$ 5.5 nA, supporting information, Fig. 3.29), the predominant negative feedback signal indicates a complete isolation of the carbon fiber by the epoxy resin. At spots where the epoxide layer is damaged the exposed carbon fibers show a positive

feedback. The adhesion force measured before the chemical activation (Fig. 3.22 C) was predominantly in the range of 10 to 25 nN at some spots adhesion forces of up to 60 nN were measured. After chemical activation the chemical force measurements (Fig. 3.22 D) showed an increase for the adhesion at the examined area proving the effectiveness of the chemical activation process.

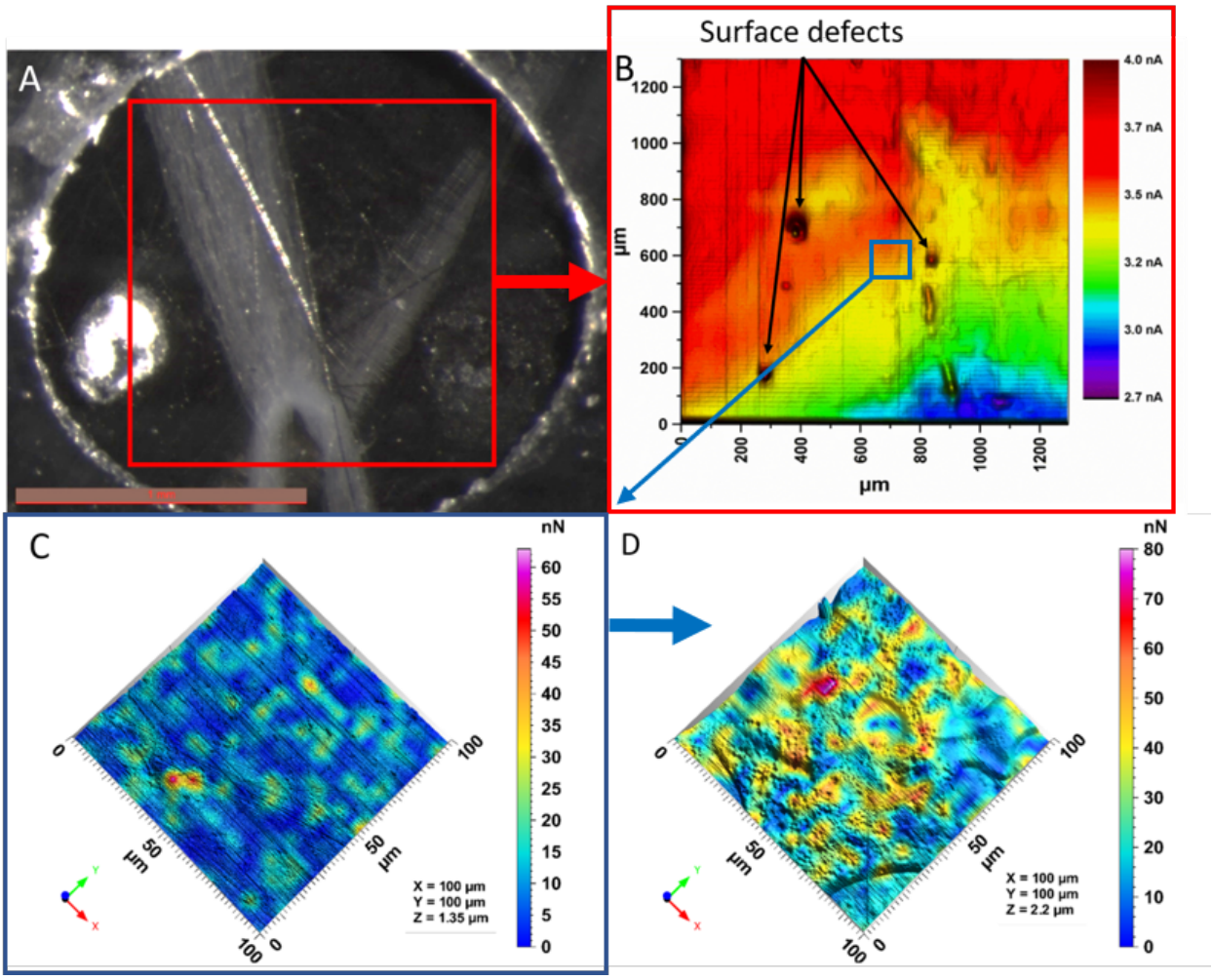

Figure 3.22: Characterization of untreated CFRP. (A) Optical image of the CFRP, the red square corresponds to the area imaged by SECM. (B) SECM false color image of the CFRP. AFM topography and adhesion force (false coloring) images before (C) and after (D) chemical activation.

Plasma pretreated CFRP surface.

In case of plasma activation the optical image shown in Figure 3.23 A indicates an increased roughness and topographical changes of the CFRP surface associated with several surface defects. With the SECM (Fig. 3.23 B) a significantly increased current is shown in the

plasma pretreated area. The intense energy of the plasma burned the epoxy resin and exposed carbon fibers at the outermost layer. Thus, the fibers are clearly imaged by a positive feedback response. The diameter of the 7 µm carbon fibers is magnified by the larger probe diameter of 25 µm. The generally increased current within the activated area could be derived from graphite depositions due to pyrolysis of the epoxy resin. Further surface defects can be seen in the SECM image. For both AFM images (Fig. 3.23 C, Fig. 3.23 D) a localization within a defined area of the SECM image was possible. The topographical information gained with AFM indicated an increased roughness for the plasma activated area (Fig. 3.23 C-1) with a carbon fiber of about 7 µm in width (Fig. 3.23 C-2). Regarding the surface and the adhesion force, no significant influence can be found between the fiber and the detected forces. However, the topographical image of the plasma activated area correlates well with a slightly increased adhesion force of 30-50 nN which compares to forces of 20-30 nN (Fig. 3.23, C-3) for partially activated areas. Thus, the overall adhesion force in the plasma activated area is significantly increased. In addition, several spots with adhesion forces up to 140 nN were detected within the plasma pretreated area. With additional chemical activation 3.23 D chemical force microscopy indicated a higher overall adhesion force of 50-70 nN and various areas with forces larger 200 nN correlating to the topographical image of the plasma influenced spots were found.

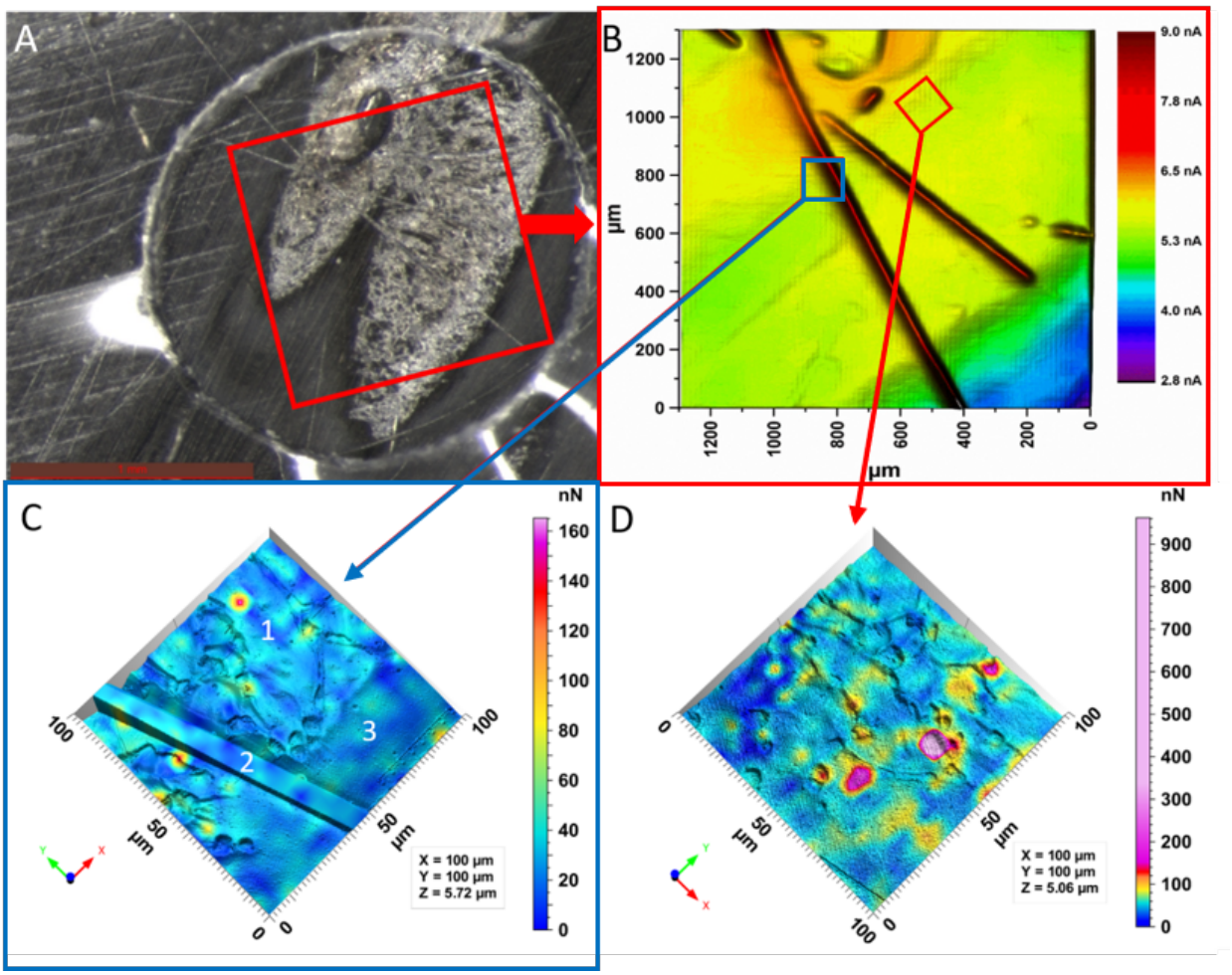

Figure 3.23: Characterization of plasma treated CFRP. (A) Optical image of the CFRP, the red square corresponds to the area imaged by SECM. (B) SECM false color image of the CFRP. AFM topography and adhesion force (false coloring) image before (C) and after (D) chemical activation. The imaged areas correspond to the red squares shown in (B).

Laser pretreated CFRP surface.

Compared to the smooth appearance of the untreated CFRP, the laser pretreatment resulted in exposing single carbon fiber strands and in a grooved surface structure (Fig. 3.24 A). This optical change correlates with the examinations reported in literature[28]. In the SECM image (Fig. 3.24 B) exposed carbon fiber strands are indicated by a positive feedback current of up to 7.8 nA. The line by line pretreatment by the laser is clearly visible, showing the limited effectivity of the method. Smaller currents in wide areas of the image between the fiber strands reflect the rough topography which is also shown in the AFM images (Fig. 3.24 C, Fig. 3.24 D). A reduction of the positive feedback by isolating areas of resin could also decrease the measured current. The adhesion force measured before the chemical

activation (Fig. 3.24 C) was in the same range as with the untreated CFRP. After chemical activation (Fig. 3.24 D) an increased overall adhesion comparable to the untreated CFRP was detected. Interestingly, within the imaged grooves a strong increase in the adhesion force caused by a higher amount of activator could be seen. In all images the line structure of the laser induced impact can be seen.

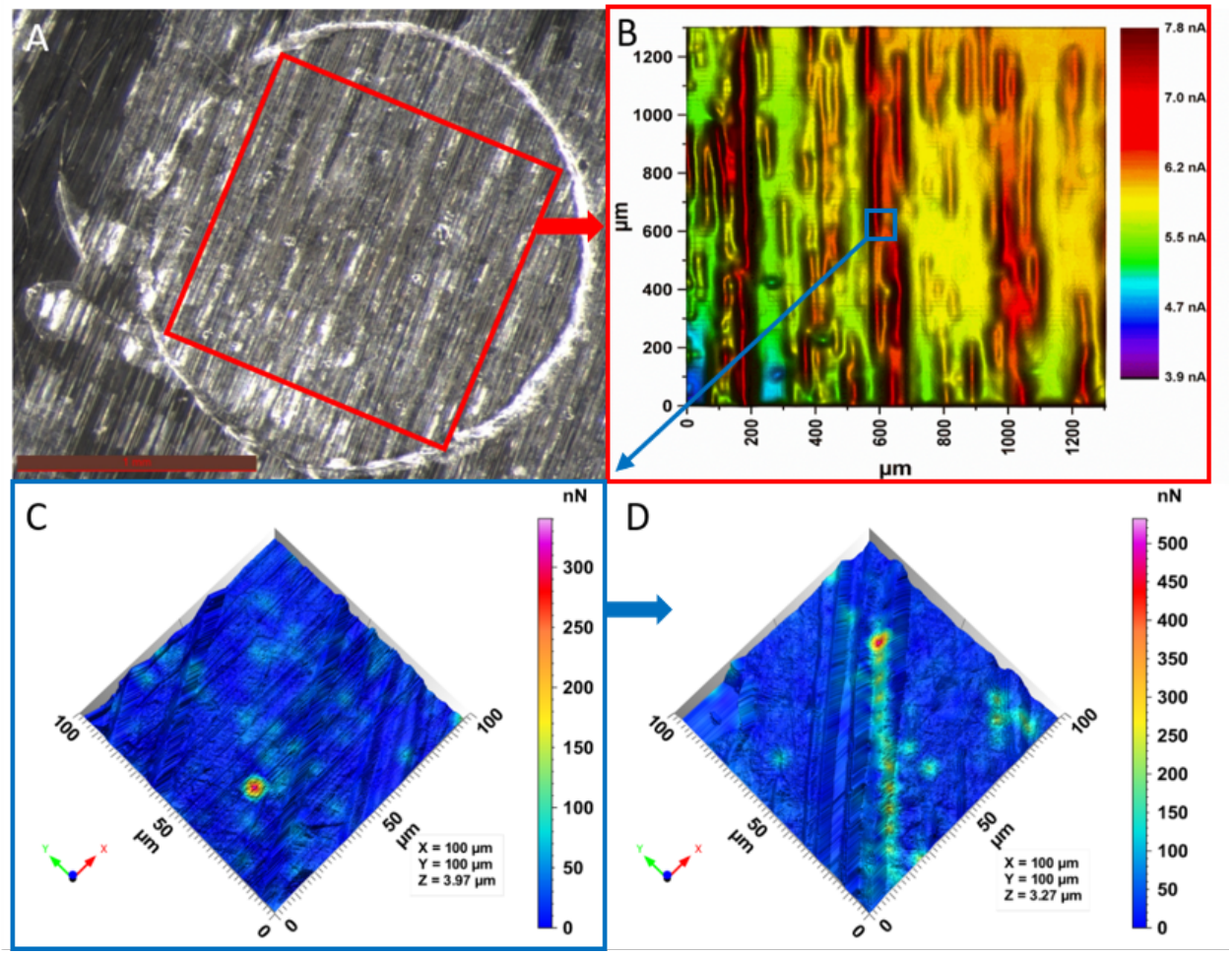

Figure 3.24: Characterization of laser treated CFRP. (A) Optical image of the CFRP, the red square corresponds to the area imaged by SECM. SECM false color image of the CFRP (B). AFM topography and adhesion force (false coloring) image before (C) and after (D) chemical activation.

CFRP surface pretreated by corundum blasting.

With corundum blasting pretreatment a significant mechanical impact can be observed in the microscopic image (Fig. 3.25 A). In contrast to laser pretreatment an increased erratic roughness was found. The electrochemical activity (Fig. 3.25 B) was drastically increased reflected by an average feedback current of 7 nA and maximum currents up to 12 nA. Only

small areas show a negative feedback which can be assigned to regions still covered with epoxy resin. The topographical inhomogeneity is also shown in the AFM images (Fig. 3.25 C, Fig. 3.25 D) with a maximum roughness of 8.4 µm. Compared to the untreated substrate the adhesion increases on several spots to 50-80 nN (Fig. 3.25 C). The positive influence of the corundum blasting pretreatment is shown after applying a chemical activator (Fig. 3.25 D). A maximum of 1.3 µN and an overall increased adhesion force within multiple activated areas of 100-250 nN were measured. Compared to the previously discussed activation techniques the adhesion forces were clearly enhanced and were distributed more homogenously over the surface.

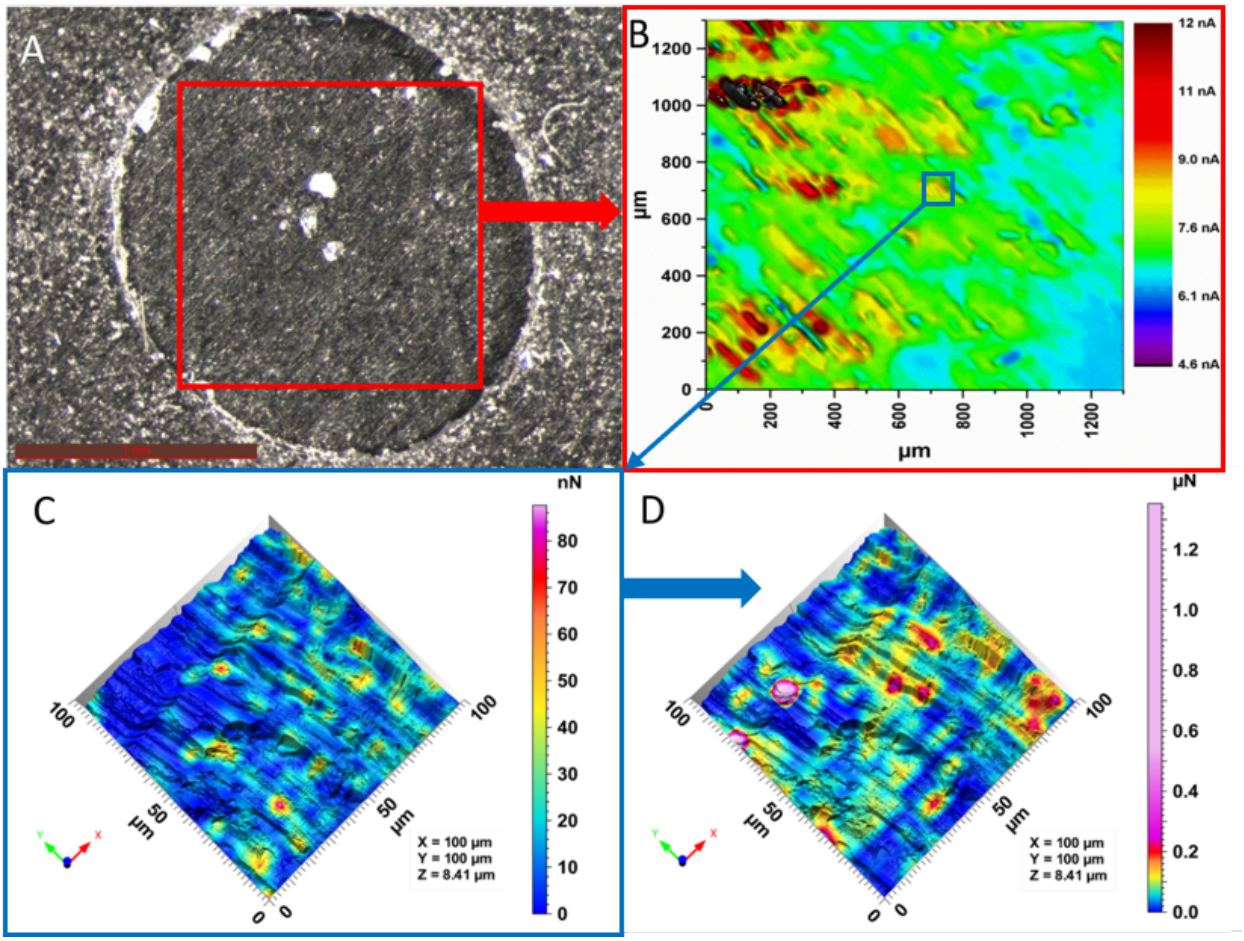

Figure 3.25: Characterization of CFRP treated by corundum blasting. (A) Optical image of the CFRP, the red square corresponds to the area imaged by SECM. (B) SECM false color image of the CFRP. AFM topography and adhesion force (false coloring) image before (C) and after (D) chemical activation.

XPS investigations.

To study the influence of the chemical composition of the CFRP surfaces XPS measure-

ments were carried out (Table 3.3). The reference sample and the corundum blasting pretreated surface showed the highest amount of carbon. It was found that plasma and laser pretreated surfaces exhibited a high amount of oxygen. For further evaluation the binding state of the carbon was examined (Fig. 3.26). Notably, the reference CFRP surface (Fig. 3.26 A) was the only one with an intact epoxy layer represented by bound ester groups. The increased carbon signal can be deduced from surface contamination. Laser and plasma pretreatments (Fig. 3.26 B, Fig. 3.26 C) led to free functional groups, such as alcohol and carboxyl groups. However, the analysis of the binding state of the corundum blasting pretreated surface indicated that the amount of alcohol groups was twice as much compared to the other pretreatments. Without any pretreatment, the surface is non-reactive due to the lack of free functional groups. Laser and plasma pretreatment have a similar impact on the surface, generating reactive carboxyl and alcohol groups. The highest density of functional groups was generated with corundum blasting pretreatment. Depending on the distribution and the density of reactive groups an increased adhesion force is expected.

Table 3.3: Quantification of surface atom distribution by XPS measurements.

XPS quantification

sample	**C1s**	**N1s**	**O1s**	**Si2p**	**Sn3d5**	**C/O**
	Atom.-%	Atom.-%	Atom.-%	Atom.-%	Atom.-%	
reference	83.7	0.8	13.2	2.3	-	6.4
plasma	78.2	1.0	17.5	3.1	0.2	4.5
laser	77.2	1.4	17.5	3.9	-	4.5
corundum	82.7	2.0	14.8	0.5	-	5.6

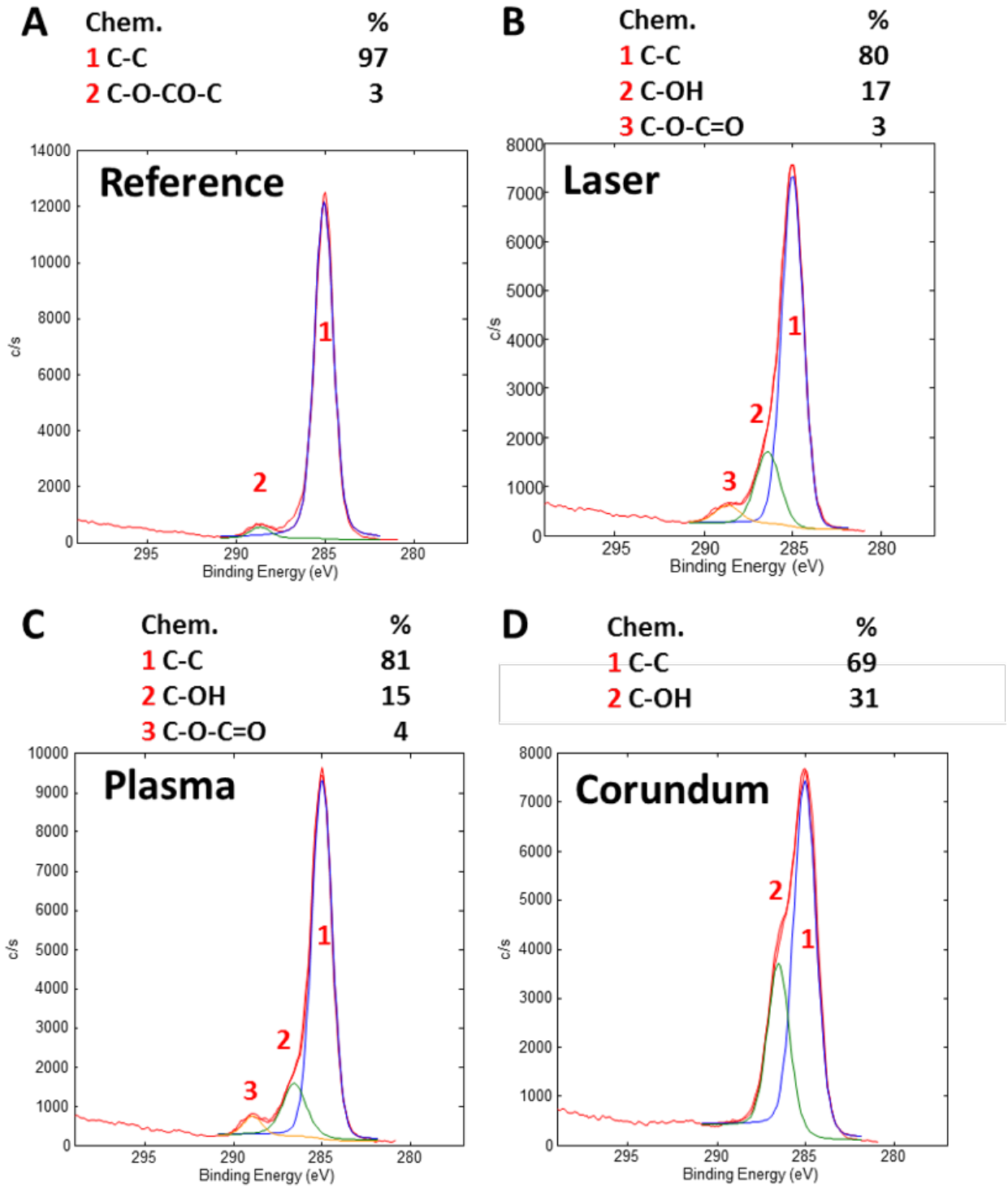

Figure 3.26: XPS measurements of CFRP surfaces with different pretreatment protocols. C1s signals are shown for (A) reference CFRP without pretreatment, (B) laser pretreated CFRP, (C) plasma pretreated CFRP, (D) corundum blasting pretreated CFRP.

Macroscopic mechanical tests.

The tensile shear test was evaluated regarding the fracturing of the adhesive (Table 3.4). The samples without any mechanical pretreatment but with chemical activation (Fig. 3.27 A) showed an adhesive failure of 70 % (n = 5). For plasma pretreatment with chemical activation (Fig. 3.27 B) an adhesive detachment of 15 % (n = 5) was found and for laser pretreatment with chemical activation (Fig. 3.27 C) the test showed an adhesive fracture of 35 % (n = 5). The different pretreatment techniques showed an improvement of the bonding between adhesive and CFRP. For corundum blasting with chemical activation (Fig. 3.27 D) a 100 % cohesive fracturing was found.

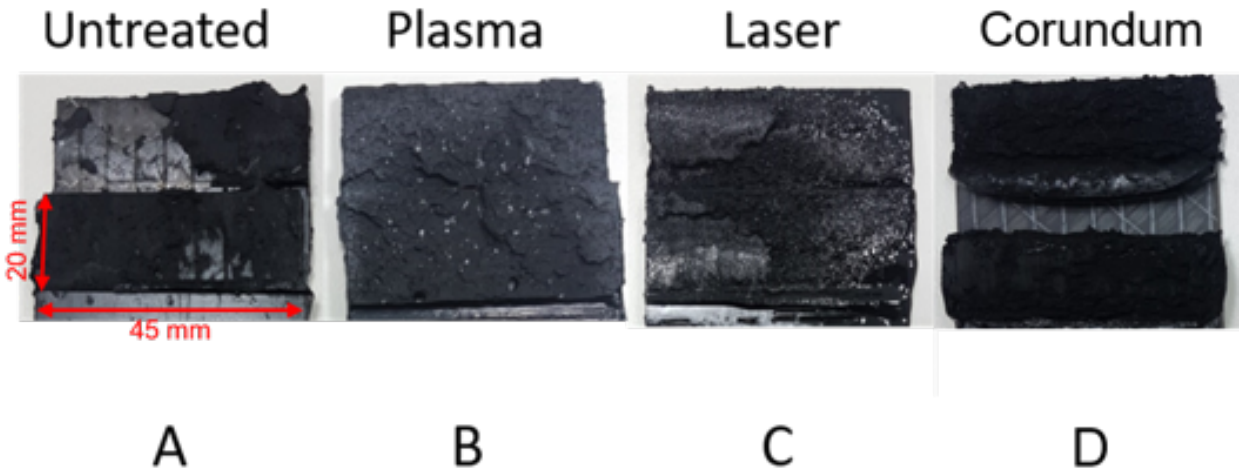

Figure 3.27: Representative examples for fracturing of the CFRP correlated with the different pretreatment methods.

Table 3.4: Tensile shear strength measurements of bonded CFRP samples pretreated with different methods.

Untreated + chemical	Plasma + chemical	Laser + chemical	Corundum blasting + chemical
70 % adhesive	15 % adhesive	35 % adhesive	100 % cohesive

3.4.6 Conclusion

The combination of optical microscopy with electrochemical imaging via SECM and adhesion force imaging via CFM was proven to be suitable for the evaluation of CFRP surface characteristics and for studying the influence of activation techniques in the context of adhesive bonding. With CFM a clear increase of adhesion forces after chemical activation of the substrate was identified and assigned to an enhancement concerning the reaction of the adhesive with the surface. With XPS the chemical activity of the substrate surface was studied supplementing the microscopic characterization. SECM imaging revealed the exposure of carbon fiber strands and enabled the characterization of the pretreatment methods for larger surface regions. The results of the macroscopic fracturing tests correlated well with the results of the advanced microscopic imaging techniques. The corundum blasting pretreatment combined with chemical activation was found to be the most effective pretreatment protocol for reliable adhesive bonding. All imaging techniques applied in this study added information for a better understanding of micro and macroscopic effects influencing the surface characteristics of CFRP substrates. Thus, the effectiveness of a bonding between CFRP substrates and adhesive can be foretold based on combined information derived from the analytical techniques applied in this report.

3.4.7 Appendix

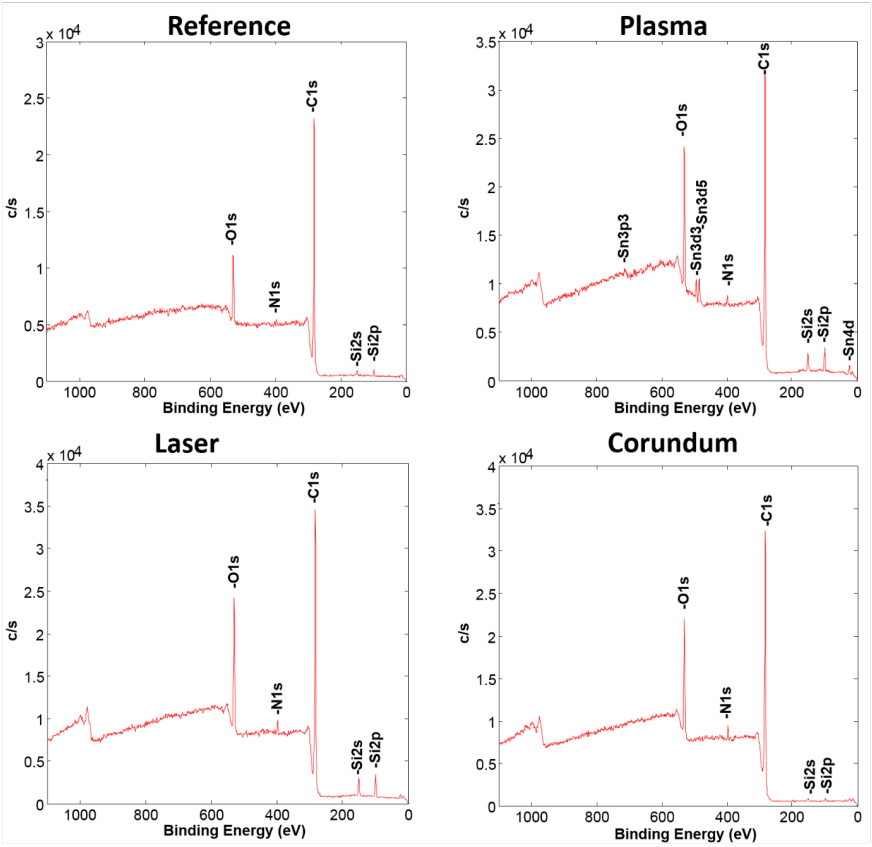

Figure 3.28: XPS spectra of CFRP surfaces after applying different pretreatment methods.

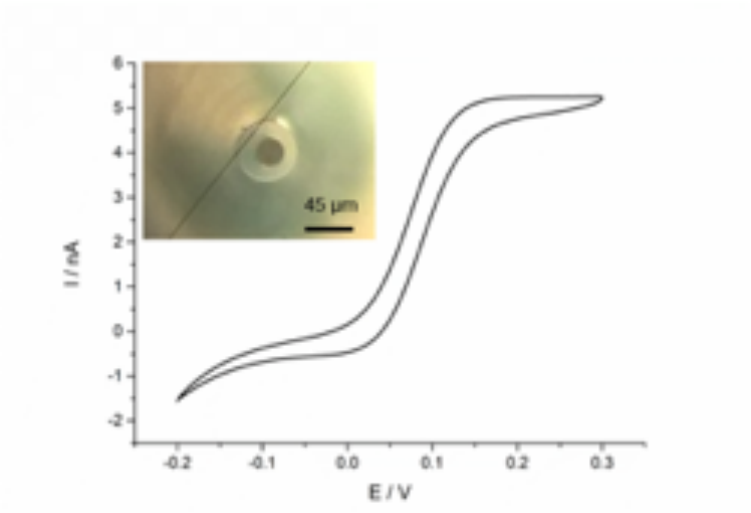

Figure 3.29: Cyclic voltammogram using a SECM probe with a diameter of 25 µm (1.5 mM FcMeOH with 0.2 M KNO_3, Estart= -0.2 V, Evortex= 0.3 V, scan rate: 50 mV s^{-1}). Inset: Optical micrograph of the SECM probe.

3.4.8 References

[1] D. A. Bhagwan and C. K. Lawrence, J. Broutman, *Analysis and performance of fiber composites*. Wiley & Sons, 3rd ed., 2006.

[2] Q. Zhang, "The "black revolution" of sports equipment: Application of carbon fiber reinforced plastics (cfrp)," in *Advanced Materials & Sports Equipment Design*, vol. 440 of *Applied Mechanics and Materials*, pp. 69–73, Trans Tech Publications, 2014.

[3] I. P. T. Rajakumar, P. Hariharan, and L. Vijayaraghavan, "Drilling of carbon fibre reinforced plastic (cfrp) composites - a review," *International Journal of Materials and Product Technology*, vol. 43, no. 1-4, pp. 43–67, 2012. PMID: 47647.

[4] S. Ebnesajjad and A. H. Landrock, "Adhesives Technology Handbook," Boston: William Andrew, 3rd ed., 2015.

[5] R. Wiesendanger, *Scanning Probe Microscopy and Spectroscopy : methods and applications*. Cambridge: Cambridge University Press, 1994.

[6] G. Binnig and C. F. Quate, "Atomic Force Microscope," *Physical Review Letters*, vol. 56, no. 9, pp. 930–933, 1986.

[7] D. Leckband and J. Israelachvili, "Intermolecular forces in biology," *Quarterly Reviews of Biophysics*, vol. 34, no. 2, pp. 105–267, 2001.

[8] S. S. Nair, S. Wang, and D. C. Hurley, "Nanoscale characterization of natural fibers and their composites using contact-resonance force microscopy," *Composites Part A: Applied Science and Manufacturing*, vol. 41, no. 5, pp. 624–631, 2010.

[9] U. Dürig and A. Stalder, "Adhesion on the Nanometer Scale," ch. Physics of Sliding Friction, pp. 299–323, Dordrecht: Springer Netherlands, 1996.

[10] S. Raman, T. Utzig, T. Baimpos, B. Ratna Shrestha, and M. Valtiner, "Deciphering the scaling of single-molecule interactions using Jarzynski's equality," *Nature Communications*, vol. 5, p. 5539, 2014.

[11] M. P. Boneschanscher, J. van der Lit, Z. Sun, I. Swart, P. Liljeroth, and D. Vanmaekelbergh, "Quantitative Atomic Resolution Force Imaging on Epitaxial Graphene with Reactive and Nonreactive AFM Probes," *ACS Nano*, vol. 6, no. 11, pp. 10216–10221, 2012.

[12] D. S. Wastl, A. J. Weymouth, and F. J. Giessibl, "Atomically Resolved Graphitic Surfaces in Air by Atomic Force Microscopy," *ACS Nano*, vol. 8, no. 5, pp. 5233–5239, 2014.

[13] E. V. Dubrovin, M. Schächtele, D. V. Klinov, and T. E. Schäffer, "Time-Lapse Single-Biomolecule Atomic Force Microscopy Investigation on Modified Graphite in Solution," *Langmuir*, vol. 33, no. 38, pp. 10027–10034, 2017.

[14] J. Kwak and A. J. Bard, "Scanning electrochemical microscopy. Theory of the feedback mode," *Analytical Chemistry*, vol. 61, no. 11, pp. 1221–1227, 1989.

[15] S. Bergner, J. Wegener, and F.-M. Matysik, "Simultaneous Imaging and Chemical Attack of a Single Living Cell within a Confluent Cell Monolayer by Means of Scanning Electrochemical Microscopy," *Analytical Chemistry*, vol. 83, no. 1, pp. 169–174, 2011.

[16] S. Bergner, P. Palatzky, J. Wegener, and F. M. Matysik, "High-Resolution Imaging of Nanostructured Si/SiO2 Substrates and Cell Monolayers Using Scanning Electrochemical Microscopy," *Electroanalysis*, vol. 23, no. 1, pp. 196–200, 2011.

[17] P. Vatsyayan, C. Iffelsberger, C. C. Mayorga-Martinez, and F.-M. Matysik, "Imaging of localized enzymatic peroxidase activity over unbiased individual gold nanowires by scanning electrochemical microscopy," *Analytical Methods*, vol. 8, no. 38, pp. 6847–6855, 2016.

[18] A. J. Bard and M. V. Mirkin, *Scanning Electrochemical Micrsocopy*. Boca Raton: CRC Press, 3rd ed., 2012.

[19] M. A. Mezour, R. Cornut, E. M. Hussien, M. Morin, and J. Mauzeroll, "Detection of Hydrogen Peroxide Produced during the Oxygen Reduction Reaction at Self-Assembled Thiol-Porphyrin Monolayers on Gold using SECM and Nanoelectrodes," *Langmuir*, vol. 26, no. 15, pp. 13000–13006, 2010.

[20] L. Christine and C. Renaud, "Analytical Expressions for Quantitative Scanning Electrochemical Microscopy (SECM)," *ChemPhysChem*, vol. 11, no. 3, pp. 547–556, 2010.

[21] D. Polcari, P. Dauphin-Ducharme, and J. Mauzeroll, "Scanning Electrochemical Microscopy: A Comprehensive Review of Experimental Parameters from 1989 to 2015," *Chemical Reviews*, vol. 116, no. 22, pp. 13234–13278, 2016.

[22] J. Thomason and D. Dwight, "The use of XPS for characterisation of glass fibre coatings," *Composites Part A: Applied Science and Manufacturing*, vol. 30, no. 12, pp. 1401–1413, 1999.

[23] R. Tao, M. Alfano, and G. Lubineau, "Laser-based surface patterning of composite plates for improved secondary adhesive bonding," *Composites Part A: Applied Science and Manufacturing*, vol. 109, pp. 84–94, 2018.

[24] C. A. Prickett, A. P. Smith, and F. J. Watts, "ToF-SIMS studies of carbon-fibre composite fracture surfaces and the development of controlled Mode in situ fracture," *Surface and Interface Analysis*, vol. 31, no. 1, pp. 11–17, 2001.

[25] S. Grunder, S. S, and L. A, *Polyurethanklebstoffe zum Kleben von Kunststoffen. Kunststoffe erfolgreich Kleben*. Wiesbaden: Springer Fachmedien Wiesbaden, 2018.

[26] B. Müller and W. Rath, *Formulierung von Kleb- und Dichtstoffen: das kompetente Lehrbuch für Studium und Praxis*. Hannover: Vincentz Network, 2004.

[27] W. J. Blank, Z. A. He, and E. T. Hessell, *Catalysis of the isocyanate-hydroxyl reaction by non-tin catalysts*, vol. 35. 1999.

[28] V. Oliveira, S. P. Sharma, M. De Moura, R. Moreira, and R. Vilar, *Surface treatment of CFRP composites using femtosecond laser radiation*, vol. 94. 2017.

3.5 Characterization of environmental aging effects on industrial carbon fiber reinforced plastic building parts

3.5.1 Introduction

The ideal manufacturing process neglects issues, such as storage time of components and the change of surface properties while aging under environmental conditions[1][2]. Surface changes on the molecular level must be considered, due to environmental contamination, including dust, temperature-dependent migration effects or improper transportation[3][4][5][6]. Therefore, using the previoiusly described methods, the influence of storage under extreme climatic conditions was examined.

3.5.2 Experimental Procedure

For this study optimized industrially manufactured CFRP plates with a water soluble external release agent were used. After removal of the release agent and chemical activation, these samples showed a functioning bond to an adhesive. The influence of storage under extreme environmental conditions was examined by exposing the samples to 80°C for 30 days under the exclusion of light. To evaluate the influence on the aging tensile, shear tests were performed on multiple samples before and after storage. The result was a reproducible 100 % cohesive fracture within the adhesive for the reference surface, and a 100 % adhesive delamination for the sample after storage under extreme environmental conditions. Previously described methods, such as CFM, DART-Q-ToF-MS and XPS, were applied to both samples for the analytical characterization of the surface changes.

3.5.3 Results & Discussion

CFM

The surface differences, using CFM, between the reference CFRP surface (Fig. 3.30) and the CFRP surface after 30 days of storage (Fig. 3.31) are presented below. The adhesion

force of the reference sample showed a homogeneous distribution of the adhesion force (areas with 200 nN), whereas the adhesion on the aged surface decreased 40 nN - 80 nN. Thus, the behavior of the surface changed after storage.

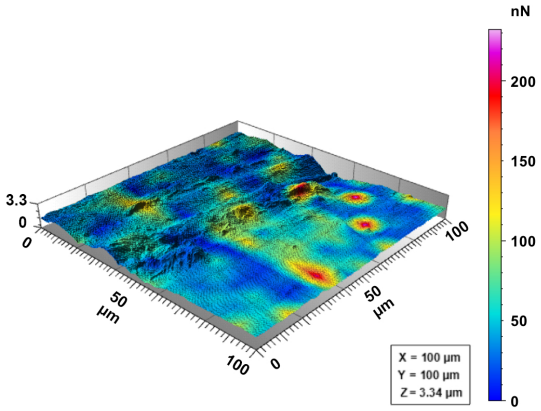

Figure 3.30: Chemical force microscope image of the reference CFRP sample without the influence of extreme climate conditions

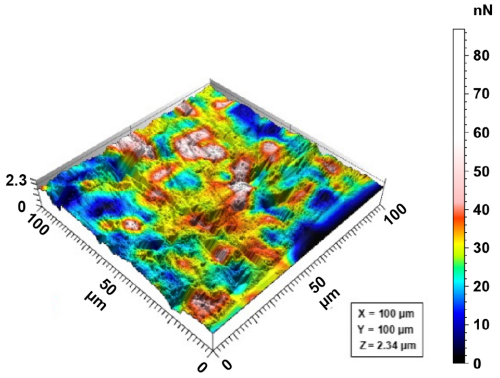

Figure 3.31: Chemical force microscope image of the CFRP sample after 30 days storage at 80° C

DART-Q-ToF-MS

When comparing the chemical composition using DART-Q-ToF-MS, a significant change in the mass distribution was seen. The reference surface (Fig. 3.32) showed multiple components with a molecular weight between 400-600 m/z such as $C_{24}H_{51}N_{11}O_2$ and $C_{20}H_{49}N_7O_7$. In the mass spectrum for the aged surface (Fig. 3.35) the molecular weight of the compounds found was significantly lower (40 - 400 m/z) (Table 3.5). Hence, a degradation of the polymer matrix to fragments with lower molecular weight, such as $C_{12}H_{14}O_4$ and $C_6H_{15}N$ can be seen.

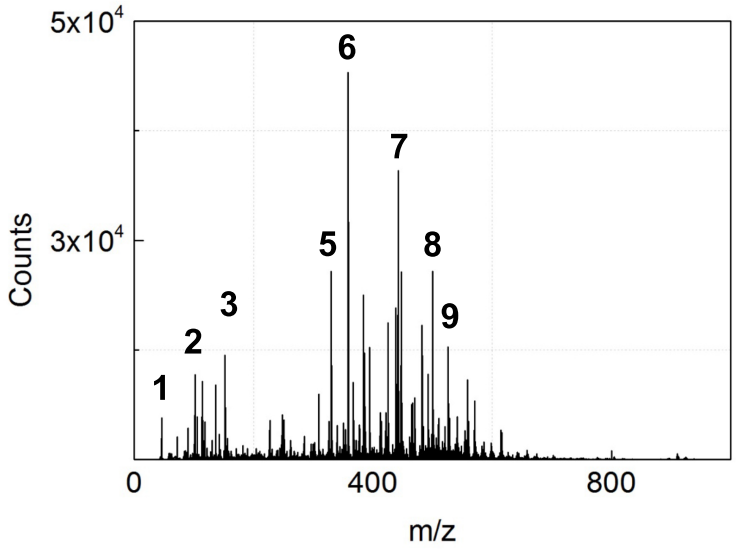

Figure 3.32: DART-Q-ToF-MS mass spectrum of the reference CFRP sample; signals 1 to 9 listed in Table 3.5

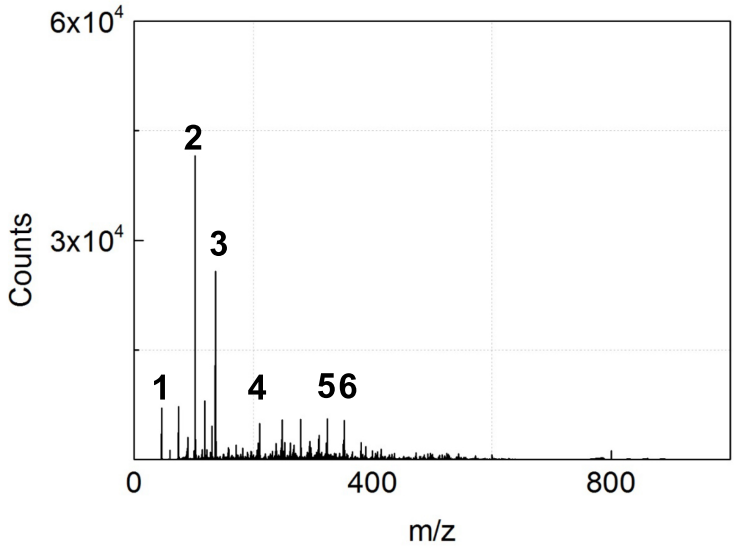

Figure 3.33: DART-Q-ToF-MS mass spectrum of the CFRP sample after 30 days storage at 80°C; signals 1 to 6 listed in Table 3.5

Table 3.5: DART-Q-ToF-MS mass identification

signal number	m/z	**molecular formula**
1	46.0655	C_2H_7N
2	102.1272	$C_6H_{15}N$
3	136.1110	$C_9H_{13}N$
4	223.0965	$C_{12}H_{14}O_4$
5	330,1702	$C_{19}H_{23}NO_4$
6	358,2011	$C_{21}H_{27}NO_4$
7	442,3371	$C_{28}H_{46}O_4$
8	500,3786	$C_{20}H_{49}N_7O_7$
9	526,4305	$C_{24}H_{51}N_{11}O_2$

XPS

Using XPS, carbon, nitrogen and oxygen were detected on both samples. The reference sample showed signals with 81.2 Atom. % carbon, 4.3 Atom. % nitrogen and 14.5 Atom. % oxygen (3.6). The sample after storage had 78.2 Atom. % carbon, 3.6 Atom. % nitrogen and 18.2 Atom. % oxygen. The concentrations of carbon and nitrogen were lower, but that of oxygen was significantly higher.

Table 3.6: Quantification of surface atom distribution by XPS measurements

XPS quantification				
sample	**C1s**	**N1s**	**O1s**	**C/O**
	Atom.-%	Atom.-%	Atom.-%	
reference	81.2	4.3	14.5	5.6
30 days aged	78.2	3.6	18.2	4.3

For the C1s signal of the reference (3.34) and the aged sample (3.35) a difference was seen. The higher amount of oxygen was denoted by the broadening peak of the carbon-to-alcohol bond at 286.7 eV. Both oxidation and degradation of the polymer are responsible for the increase in alcohol groups at the surface. The degradation of the surface, however, lead to the loss of groups that were not stably bonded to the matrix.

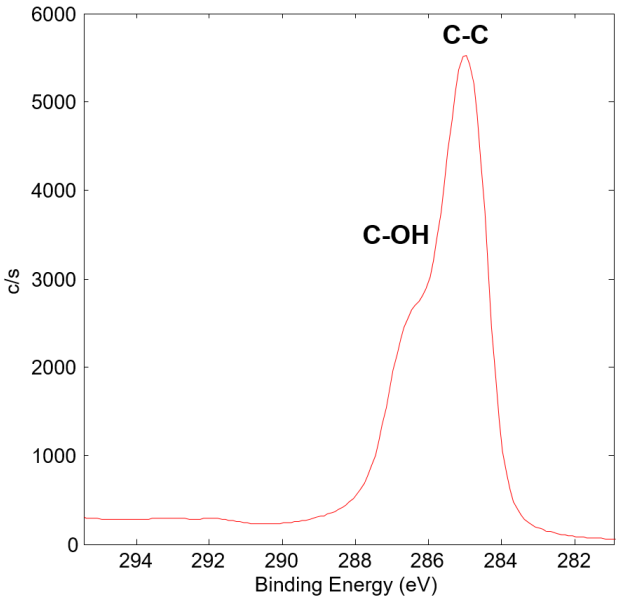

Figure 3.34: XPS spectrum of the reference CFRP sample

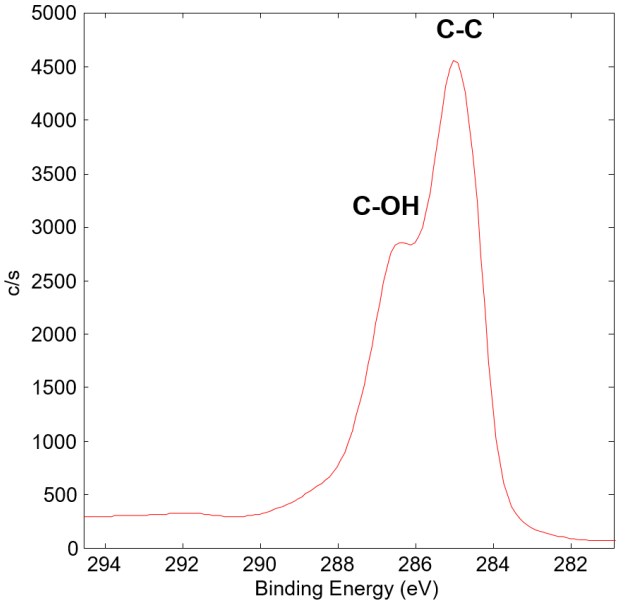

Figure 3.35: XPS spectrum of the CFRP sample after 30 days storage at 80°C

3.5.4 Conclusion

The aging of the CFRP sample influenced the behavior of the surface. The cause of the detachment after aging was identified using the applied methods. As seen with the DART-Q-ToF-MS mesurement, a degradation of the polymeric epoxy resin took place. The XPS measurment showed that a high number of functional groups (e.g. oxygen) does not implicitly lead to good bonding. The XPS measurment showed that a high number of functional groups (e.g. oxygen) does not implicitly lead to good bonding. The bonding to the matrix substrate was also weakened. The combination of microscopic techniques and chemical analysis of the surface resulted in a deeper understanding of the mechanisms at play when storing the samples under extreme environmental conditions. Consequently, parts that are stored for an unscheduled period of time can be evaluated using a combination of the presented methods.

3.5.5 References

[1] T. Gates, "The physical and chemical ageing of polymeric composites," in *Woodhead Publishing Series in Composites Science and Engineering*, pp. 3–33, Woodhead Publishing, 2008.

[2] T. Tsotsis, "Thermo-oxidative ageing of composite materials," in *Woodhead Publishing Series in Composites Science and Engineering*, pp. 130–159, Woodhead Publishing, 2008.

[3] B. C. Ray, "Temperature effect during humid ageing on interfaces of glass and carbon fibers reinforced epoxy composites," *Journal of Colloid and Interface Science*, vol. 298, no. 1, pp. 111–117, 2006.

[4] A. C. de Albuquerque, K. Joseph, L. Hecker de Carvalho, and J. R. M. D'Almeida, "Effect of wettability and ageing conditions on the physical and mechanical properties of uniaxially oriented jute-roving-reinforced polyester composites," *Composites Science and Technology*, vol. 60, no. 6, pp. 833–844, 2000.

[5] D. N. Markatos, K. I. Tserpes, E. Rau, K. Brune, and S. Pantelakis, "Degradation of Mode-I Fracture Toughness of CFRP Bonded Joints Due to Release Agent and Moisture Pre-Bond Contamination," *The Journal of Adhesion*, vol. 90, no. 2, pp. 156–173, 2014.

[6] R. I. Ledesma, F. L. Palmieri, W. T. Yost, J. W. Connell, and J. M. Fitz-gerald, "Surface Monitoring of CFRP Structures for Adhesive Bonding," in *40th 2017 Annual Meeting of the Adhesion Society*, 2017.

3.6 Evaluation of an industrial approach for improving a surface protecting cavity wax with a combination of different analytical techniques

3.6.1 Introduction

Cavity waxes are an important part for manufacturing cars, protecting uncoated metal parts against corrosion. To extend the lifetime and increase the quality of a car, a sustainable and extensive coating (e.g. varnish) must be applied. This is especially true in cavities and flanges, where an overall coating is hard to achieve. Therefore, alternative materials, other than regular varnishes, are used to ensure the protection of the body part. There are different types of cavity waxes with different hardening mechanisms. Waxes can be segmented into solvent-based, water-based and free-of-solvent waxes (Table 3.7).

Table 3.7: Different types of cavity waxes

Type	Solid content	Hardening mechanism
Solvent-based	75 %	Evaporation of solvent
Water-based	40 - 60 %	Primary: Evaporation of water
		Secondary: Resin hardening
Free-of-solvent	100 %	Physical hardening (temperature)

Depending on the type of wax, the application can be realized by spraying or flooding the car part[1]. For large industrial applications, solvent-based waxes are contentious for toxicological reasons. Waxes that are free of solvents have the benefit of controlled hardening, due to temperature dependence. These waxes, however, are costly and the manufacturing process requires an additional step including an oven. Consequently, waxes based on water are the most common and practical option.

To improve the reaction rate of commercially available water-based cavity waxes, the reaction steps of the hardening process were examined. Water evaporation is a crucial step to the hardening of the wax, and the oxidative hardening of an alkyd resin or oil

contributes to the hardening process, albeit slowly. To improve the reaction rate of hardening, an additive used in paints and beeswax was tested for the use with cavity waxes. Following the formation of an oxygen radical, a cross-linking with other unsaturated molecules takes place, and the hardening of the wax is accelerated. With a higher number of double bonds in the oil or alkyd, the chance of oxygen radical formation is increased, preferably taking place on a CH_2 group in the allylic position. The following decay of the hydro peroxide can either be enhanced thermally or with the addition of a catalyst (e.g. siccative). Radicals are thereby formed, and depending on the oxidation state of the siccative the catalyst is oxidized form M(II) to M(III) in one step (Equ. 3.1) and reduced in the next step(Equ. 3.2). For siccatives with the function of "supporting dryers" (metals containing one oxidation state), the metals are bonded between two hydro peroxide groups.[2]

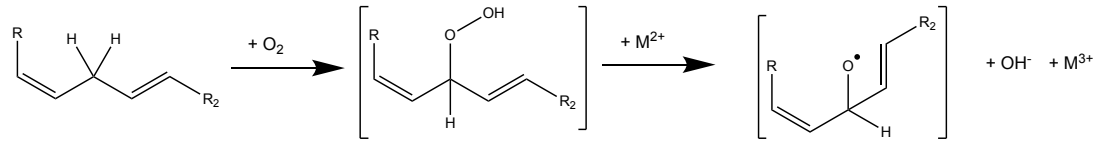

(3.1)

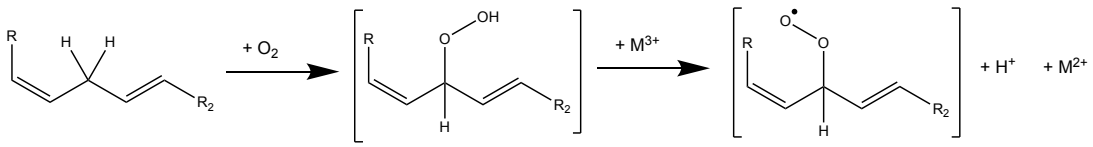

(3.2)

3.6.2 Experimental Procedure

Chemicals
For all experiments, a commercially available water-based cavity wax was used. A mixture of unsaturated oil and siccatives were added to the cavity wax. Different stoichiometric attempts were examined, resulting in two oil/siccative formulations. Formulation A contained 99.3 w.% of linoleic acid, 0.6 w.% of calcium stearate and 0.1 w.% iron(II/III)oxide nano-powder. Formulation B contained 89.5 w.% of linoleic acid, 1.5 w.% potassium permanganate, 8 w.% cobalt(II)acetate tetrahydrate, 0.5 w.% calcium stearate and 0.5 w.% aluminum stearate. All chemicals were purchased at Sigma-Aldrich.

Formulation
Two batches of modified cavity wax were formulated; one with 0.75 w.% Formulation A and the other one with 0.75 w.% Formulation B.

Saucer test
To test the hardening of the wax over time, a plate with an electric coating was modified by five spherical indentations. The plate was positioned horizontally and each indentation was filled with 500 µL of cavity wax. For two hours the wax had the chance to cure in the notches, before the plate was positioned vertically. The evaluation was based on the stability of the wax, since leaking wax would show an insufficient reaction rate.

Application
To evaluate the performance of the modified cavity waxes, a large scale industrial experiment was performed on the doors of an unfinished car (Fig. 3.36). With a nozzle, 35 mL of the wax was applied with a pressure of 100 bar into the cavities of the door (Fig. 3.37).After the application of the wax, the door stayed in place for five minutes. The door was tilted forward for one minute at an angle of 15° and then tilted backward at the same angle. To evaluate the quality of the cavity wax, small bags were placed on the outlet of the door. The amount of wax that leaked was weighed after the idle time of five minutes and again after the tilting procedure. Mixtures of 0.5 w.% and 1.0 w.% of Formulation B with cavity wax were tested, as well as cavity wax with an addition of 0.75 w.% of formulation A. As a reference, a non-modified cavity wax was also used.

Figure 3.36: Application to an unfinished industrial manufactured door of a car

Figure 3.37: Industrial application of cavity wax using a dual-nozzle.

Analytical verification

To validate the influence of the siccative on the cavity wax, the amount of aldehyde formation was measured. Due to the chemical reaction, the amount of aldehyde per time corre-

lates with the increased chemical reaction rate of the wax (Equation 3.3).

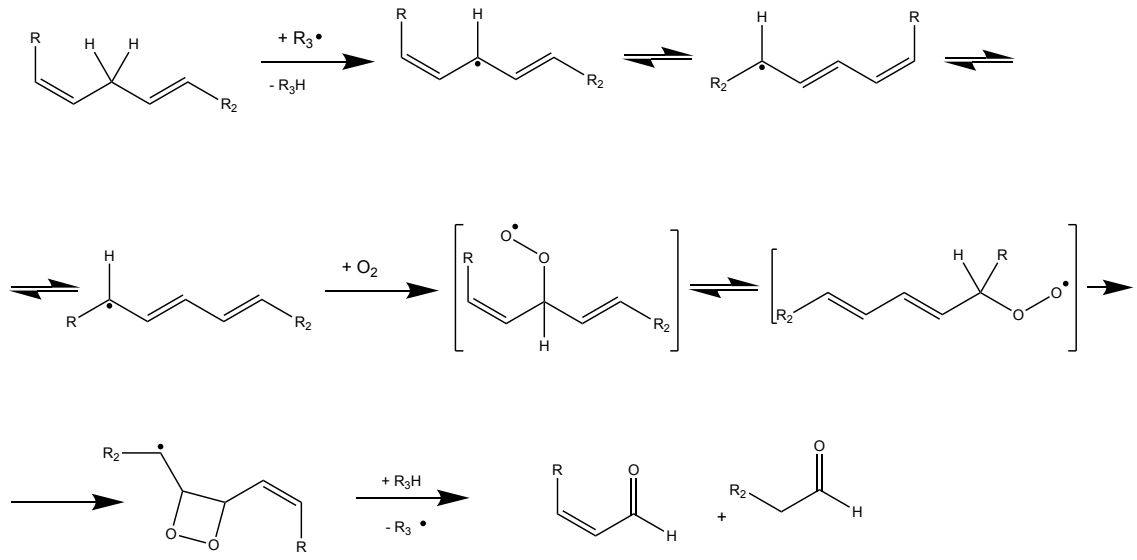

(3.3)

A method was established to reproduce the measurement for different cavity wax formulations. 2 g of cavity wax was weighed in an aluminum plate and placed in a micro chamber (Markes international, M-CTE250, Fig. 3.38)with a volume flow rate of 15 mL/min of synthetic air. The temperature was set to 65°C and a DNPH-cartridge was placed on the outlet. After five days the components in the cartridge were eluted with 5 mL of acetonitrile. The extract was separated with an HPLC (reversed phase C-18 column) before quantifying the aldehydes with a quadrupole-MS (Agilent 6100 series).

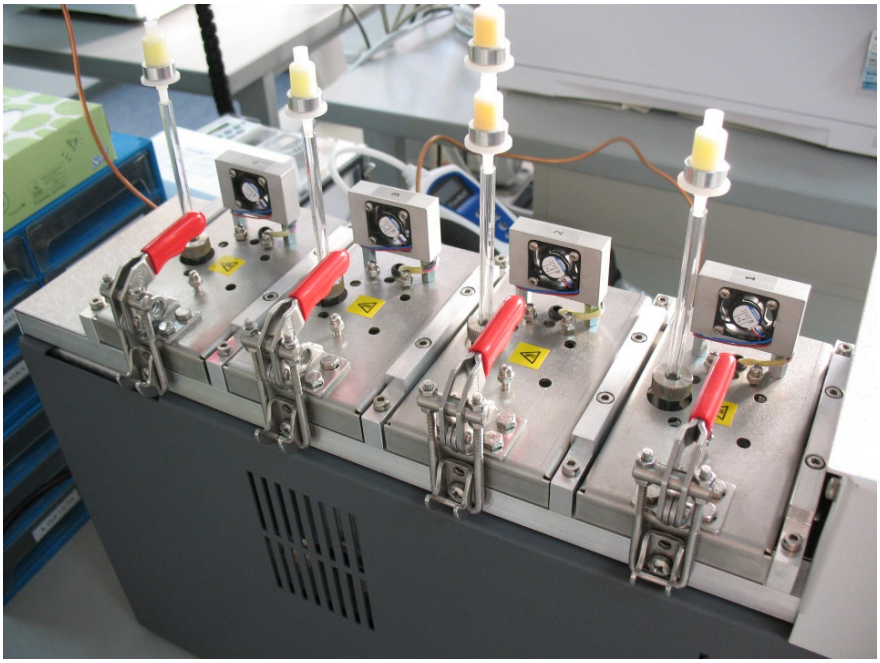

Figure 3.38: Micro chamber with DNPH-catridge for the analysis of aldheyde emission.

3.6.3 Results & Discussion

Saucer test

As seen in Figure (3.39), the reference wax was leaking from the indention, but both formulations A and B formed a stable composition. Whereas both formulations A and B form a stable composition. Especially formulation B shows no sign of creeping. Formulation A, with an iron redox catalyst and a calcium "supporting dryer", saw a significant improvement in the curing rate. Formulation B used cobalt as redox catalyst, aluminum as an efficient dryer and calcium as a supporting dryer effectively. It produced a highly efficient dryer, but its use in industrial applications is doubtful, due to the restrictions for cobalt in the industrial products.

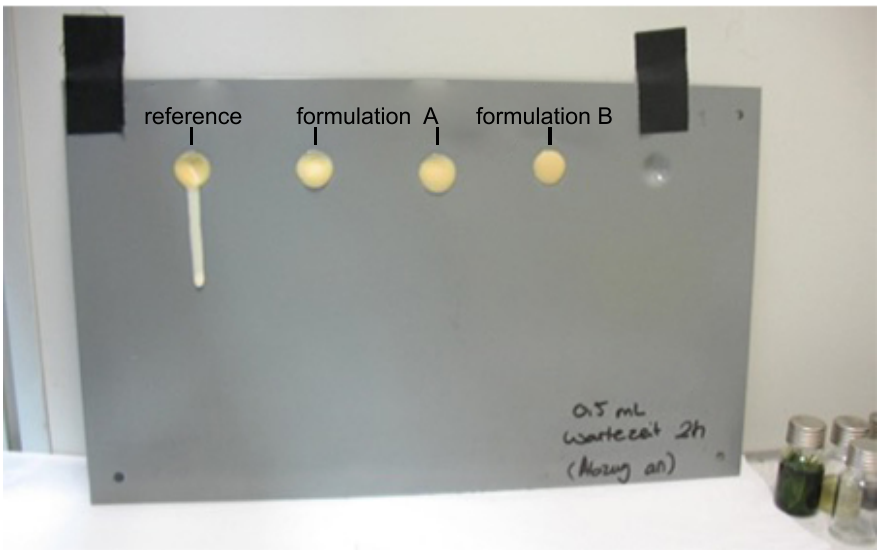

Figure 3.39: Saucer test for the evaluation of the hardening time of the cavity wax after two hours.

Application

The total leakage was measured after the application and a wait time of five minutes, as well as after tilting (Table 3.8, Fig. 3.40). With the reference cavity wax, a total of 22.3 % leaked from the door with 0.8 % leaking after tilting. All three improved cavity waxes showed no sign of leaking after tilting. After the application and wait time of five minutes, 11.4 % dripped from the door for the cavity wax with 0.5 w.% of Formulation B, 3.1 % dripped from 1.0 w.% Formulation B and 2.2 % dripped from 0.75 w.% of formulation A. Thus, cavity wax with formulation A showed the highest effect on the large-scale industrial application.

Table 3.8: Total leakage of the cavity wax before and after tilting

	Reference	Form. B 0.5 w.%	Form. B 1.0 w.%	Form. A 0.75 w.%
before tilting	22.3 %	11.4 %	3.1 %	2.2 %
after tilting	0.8 %	-	-	-

Figure 3.40: Leakage of cavity wax into plastic bags.

Analytical verification

For all cavity wax variations, the same aldehyde products were found, due to auto-oxidation (Fig. 3.41), resulting in formaldehyde, acetaldehyde, propionalaldehyde, butyraldehyde, benzaldehyde, valeraldehyde and hexaldehyde.However, the amount of aldehyde formed over the five days varied with the different cavity wax modifications. For comparative studies and nondisclosure purposes, the results were normalized to the amount of hexaldehyde found in Formulation B. For all three waxes, comparable amounts of formaldehyde and benzaldehyde were found. Slightly increased amounts of acetaldehyde and propinaldehyde were found and both hexaldehyde and valeraldehyde emissions were drastically increased for Formulation A versus the reference wax. For formulation B, acetaldehyde, butyraldehyde, valeraldehyde and hexaldehyde were each over ten times the amount in the reference system. Consequently, the amount of aldehyde emissions showed the enhanced reaction rate of Formulation A and B. Thus a verification for the reaction process was presented with the analytical method utilized.

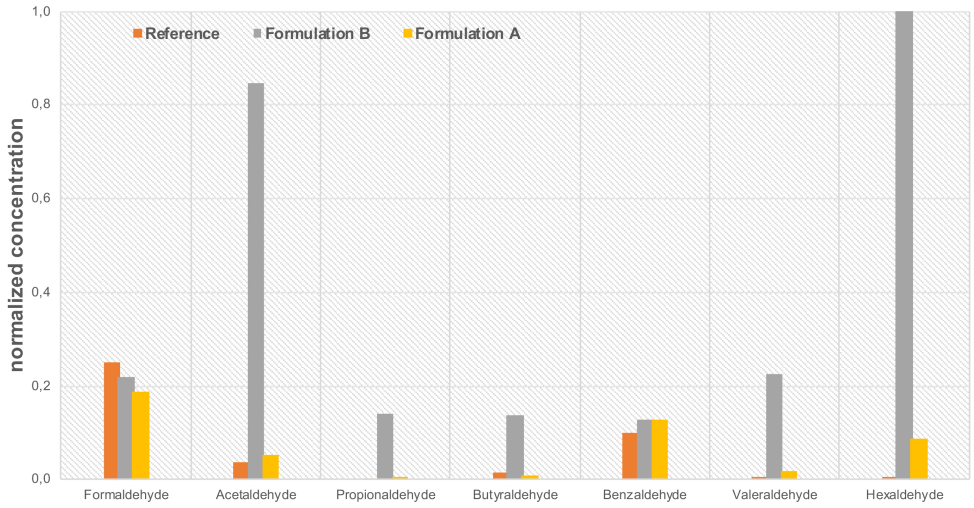

Figure 3.41: Aldehyde emissions for the different wax modifications after the micro chamber.

3.6.4 Conclusion

The combination of laboratory experiments, industrial applications and instrumental analysis led to an improved water-based cavity wax. The mechanism used for drying paints, oils and varnishes was applied to a new field of application. Different approaches were shown, resulting in a formulation with iron and calcium siccative for an easy to use, environmental friendly and highly efficient product. The theoretical approach of increasing the reaction rate of water-based cavity waxes has been validated with the emission test via the micro chamber combined with HPLC-MS analysis. For a final industrial product, several stoichiometric attempts and industrial applications have to be examined. All studies resulted in a patent[3].

3.6.5 References

[1] H.-H. Braess and U. Seiffert, *Vieweg Handbuch Kraftfahrzeugtechnik*. Springer Fachmedien Wiesbaden GmbH: Vieweg +Teubner Verlag, 6 ed., 2011.

[2] B. Müller, *Additive kompakt*. Hannover: Vincentz Network, 2009.

[3] S. Viehbeck, J. Troffer, and M. Günther, "Korrosionsschutzmittel und Verfahren zum Konservieren eines Hohlraumes," 2015.

3.7 Verifaction of urea as aldehyde diminishing component in a newly formulated industrial cavity wax

3.7.1 Introduction

Due to increasing restrictions on industrial manufactured products, companies need to fulfill the demands, making health-relevant topics a priority. In addition to recent topics, such as fuel emission control, in the automotive segment, the total emissions in the interior of a car is just as crucial for the health of the passengers. Therefore, quality control of the components used inside a car is as demanding as the constant optimization of the external body parts implemented on the vehicle. One of these components is the aforementioned (Chapter 3.6) cavity wax. As shown in the previous chapter, certain modifications optimized the rheological behavior of the wax. Yet the issue of aldehyde emission during the oxidative hardening process was neglected. Thus, an analytical approach to optimizing the wax regarding its emission products will be examined.

Based on a polycondensation of urea with formic aldehyde (Equation 3.4), a product was composed of water-based cavity waxes with different urea concentrations.

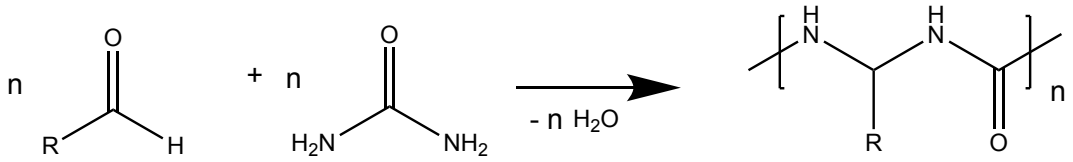

(3.4)

Depending on the pH value of the product, a polymerization with deposition of water takes place. For ideal extended chain polymerization, a pH value below five is required, yet the cavity wax was formulated with a slightly basic pH value. Nonetheless, the polymerization takes place and polymers with a low molecular weight are formed [1]. Thus the highly volatile and health-critical aldehydes are replaced by polymers with low molecular weight.

3.7.2 Experimental Procedure

Chemicals
For all experiments, commercially available water-based cavity wax was used, along with reagent-grade urea (Sigma-Aldrich).

Formulation
An unmodified wax was used as a reference. Two different versions of the cavity wax were formulated. One had 1 w.% urea and the other had 10 w.% urea. After homogenization, 2 g of the three variations were added to a micro chamber with a volume flow rate of 15 mL/min of synthetic air. The temperature was set to 25°C and a DNPH-cartridge was placed on the outlet. After five days, the components in the cartridge were eluted with 5 mL of acetonitrile. The extract was separated with an HPLC (reversed phase C-18 column) before the aldehydes were quantified with a quadrupole-MS.

3.7.3 Results & Discussion

The characterization of the cavity wax regarding emission products using the micro chamber coupled with the Quadrupole-MS is shown in Fig. 1.10. The total amount of aldehyde emission was drastically reduced for the formulation with 1 w.% of urea, especially for formic aldehyde, which was reduced by 50 %. A slight increase in aceticaldehyde was seen, possibly due to the saturation of the DNPH-cartridge for the reference wax, since the amount of formicaldehyde exceeded the capacity of the cartridge. For the formulation with 10 w.%, a further decrease in aldehyde concentration was seen, though it was not linear with respect to the formulation with 1 w.%.

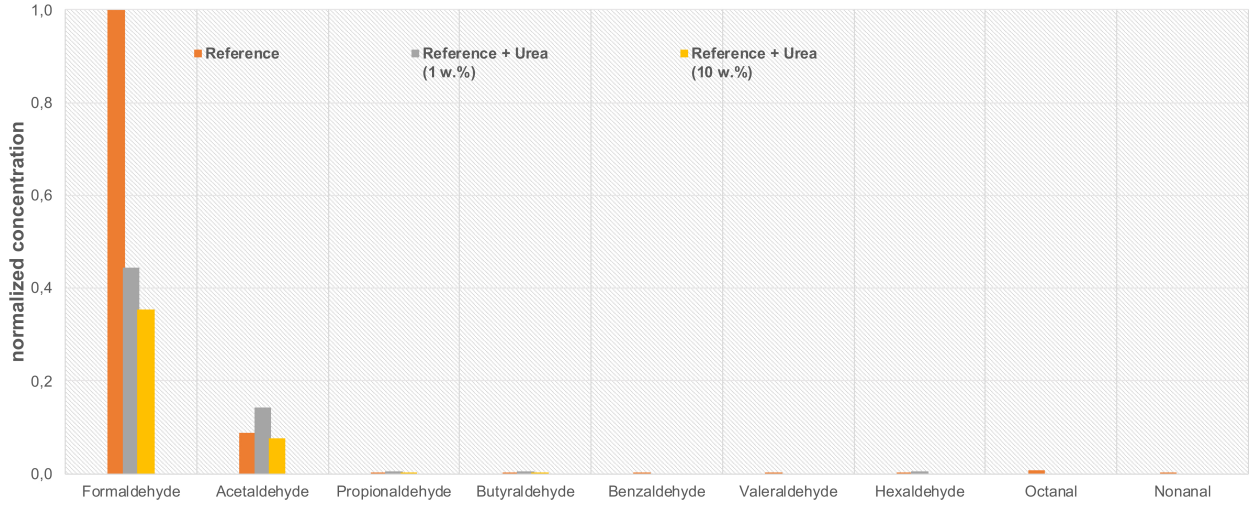

Figure 3.42: Quantitative aldehyde emission of the cavity wax with different urea modifications

3.7.4 Conclusion

The modification of the wax was effective and the total aldehyde emissions decreased by 50 %. Thus, a formulation was presented to optimize the emission of the cavity wax. With this analytical approach, a method was presented for verification and quality control. The studies resulted in a patent[2].

3.7.5 References

[1] U. D. Akpabio, "Effect of pH on the Properties of Urea Formaldehyde Adhesives," *International Journal of Modern Chemist*, vol. 2, no. 1, pp. 15–19, 2012.

[2] S. Viehbeck, G. Mayer, and J. Troffer, "Korrosionsschutzmittel," 2016.

4 Summary

Current analytical techniques lack the ability to specifically characterize issues, such as detachments and adhesive failures regarding newly introduced industrial materials. Therefore, a combination of highly specific surface characterization techniques were successfully introduced and applied to industrial parts.

For correlation with mechanical tests, a model adhesive system was formulated, optimized and analytically characterized. A reference system with known composition was used for all experiments to ensure a reliable and reproducable result.

The surface characterization techniques, such as DART-Q-ToF-MS, AFM and X-ray photoelectron spectroscopy, were implemented as an improvement to understand surface characteristics. DART-Q-ToF-MS was a fast and sensitive technique that was the foundation for the identification of surface contamination, migration effects or degradation of the composite. Its combination with a high resolution Q-ToF mass spectrometer provided the necessary resolution and mass accuracy to reliably identify the relevant components.

The main novelity for industrial composite characterization was presented with the AFM system. Besides topographical mapping and material contrast measurments, adhesion measurements were performed. A reliable and reproducable tip preparation for chemical force measurements was the premise for successful adhesion measurements. A validation process used XPS for each modified batch. Further XPS was used for the characterization of the elemental composition of the surface and the determination of the thicknes of an aluminum oxygen layer. The individual techniques used for surface characterization led to a combination of different techniques, including optical microscopy, AFM, SECM, CFM and XPS to investigate specific adhesion mechanisms and improve the surface quality of new composite materials. Using only one analytical technique to evaluate an adhesive bond and understand the prerequisites for successful surface preparation is simply

not possible. A combination of different factors, including surface roughness, chemical composition of the surface, technical cleanliness of the surface, surface pretreatment and aging all influence the quality of the bond. The applied techniques were validated and compared to mechanical macroscopic tests, such as tensile strength measurements. The effect of aging on materials was investigated in detail with the aforementioned techniques.

In addition to the analytical techniques, two major improvements to an industrially used product were achieved, which resulted in two patents. Due to the modification of the cavity wax, the quality of the material was drastically improved. By using analytical and mechanical techniques, the efficacy of the modification was evaluated and successfully verified.

5 Zusammenfassung in deutscher Sprache

Gegenwärtige analytische Techniken sind nicht in der Lage, Probleme, wie Ablösungen und Klebstoffversagen in Bezug auf neu eingeführte industrielle Materialien, eindeutig zu charakterisieren. Daher wurde eine Kombination von Oberflächencharakterisierungsmethoden erfolgreich eingeführt und auf industrielle Bauteile angewandt.

Zur Korrelation mit mechanischen Tests wurde ein Modellklebstoffsystem formuliert, optimiert und analytisch charakterisiert. Dieses Referenzsystem mit bekannter Zusammensetzung wurde für alle Experimente verwendet, um zuverlässige und reproduzierbare Ergebnisse zu gewährleisten.

Oberflächencharakterisierungstechniken, wie DART-Q-ToF-MS, AFM und Röntgenphotoelektronenspektroskopie, wurden als eine Verbesserung implementiert, um Oberflächenphänomene zu verstehen. DART-Q-ToF-MS überzeugte als schnelle und empfindliche Technik, welche die Grundlage für die Identifizierung von Oberflächenkontaminationen, Migrationseffekte oder den Abbau von Verbundmaterialien bildete. Die Kombination mit einem hochauflösenden Q-ToF-Massenspektrometer lieferte die notwendige Auflösung und Massengenauigkeit, um die relevanten Komponenten zuverlässig zu identifizieren.

Die wichtigste Neuheit für die industrielle Charakterisierung von Verbundwerkstoffen wurde mit dem AFM-System vorgestellt. Neben topographischen Kartierungen und Materialkontrastmessungen wurden Adhäsionsmessungen durchgeführt. Eine zuverlässige und reproduzierbare Präparation der Spitzen für chemische Kraftmessungen war die Voraussetzung für erfolgreiche Adhäsionsmessungen. In einem Validierungsprozess mittels XPS wurden die produzierten Chargen verifiziert. Des Weiteren wurde XPS

zur Charakterisierung der Elementzusammensetzung der Oberfläche und zur Bestimmung der Dicke einer Aluminiumoxidschicht verwendet. Die einzelnen Techniken zur Oberflächencharakterisierung führten zu einer Kombination verschiedener Techniken, einschließlich optischer Mikroskopie, AFM, SECM, CFM und XPS, um spezifische Adhäsionsmechanismen zu untersuchen und die Oberflächenqualität neuer Verbundwerkstoffe zu verbessern. Mit nur einer alleinstehenden Analysenmethode ist es nicht möglich Klebeverbindungen zu bewerten und die Hintergründe für eine erfolgreiche Oberflächenvorbehandlung zu verstehen. Eine Kombination verschiedener Faktoren, einschließlich der Oberflächenrauheit, der chemischen Zusammensetzung der Oberfläche, der technischen Sauberkeit der Oberfläche, der Oberflächenvorbehandlung und der Alterung, beeinflussen die Qualität der Verbindung. Die angewandten Techniken wurden validiert und mit mechanisch-makroskopischen Tests, wie Zugfestigkeitsmessungen, verglichen. Die Auswirkung der Alterung von Materialien wurde im Detail mit den oben genannten Techniken untersucht.

Zusätzlich zu den Analysetechniken wurden zwei wesentliche Verbesserungen für ein industriell verwendetes Produkt erzielt, was zu zwei Patenten führte. Aufgrund der Modifikation des Hohlraumwachses wurde die Qualität des Materials drastisch verbessert. Unter Verwendung analytischer und mechanischer Techniken wurde die Wirksamkeit der Modifikation evaluiert und erfolgreich verifiziert.

6 List of Figures

1.1 Industrial manufacturing process of fibers - polymerization, spinning, washing, drying, elongating, spool, adapted from [2] 8
1.2 Resin transfer molding - industrial approach, adapted from [2] 9
1.3 Wet compression molding - industrial approach, adapted from [2] 10
1.4 Scanning electron microscope (SEM) image of a monolithic silicon Tap-300 Al-G cantilever, force constant 40 N/m, length 125 µm, width 30 µm, radius < 10 nm 14
1.5 Comparison of various microscopic techniques and the resolution (adapted from [12]) 15
1.6 Scheme of a commercially available AFM (Flex AFM - company nanosurf) . 16
1.7 Force-distance curve with contact mode operation in repulsive region, showing cantilever deflection at each regime, adapted from [12] 17
1.8 Force-distance curve for spectroscopic measurements, A to B approach, at B snap-in occurs, C user defined stop, in contact with sample untill D - snap-off occurs, adapted from [12] 19
1.9 Force-distance curve for spectroscopic measurements; illustration of a chemically modified cantilever and the interaction with the surface molecules R-X, adapted from [12] 20
1.10 XPS set up of commercially available Ulvac Phi - Versa Probe II 21
1.11 Photoelectronic effect, formation of a photoelectron with an X-ray and a 1s electron (adapted from [28]) 22
1.12 DART-Ion source functional principle; first chamber: energetic excitement of the gas to a metastable state through glow discharge, second chamber: filtering charged gas molecules, and third chamber: heating process up to 550°C 24
1.13 Scheme of the tensile shear test 30
1.14 Scheme of the peel test 31

2.1 For self assembled monolayer process 11-mercapto-1-undecanol was used . 33

3.1 Thermo - nicolet is50 37
3.2 FT-IR isocyanate signal and reaction over time 37
3.3 Time resolved FT-IR - Isocyanate signal over time, adhesive formulation A - C and industrial adhesive D 38
3.4 Representative samples with delamination phenomena of an e-coat from a car panel 43
3.5 DART ion source functional principle, first chamber: energetic excitement of the gas to a metastable state through glow discharge, second chamber: filtering charged gas molecules, and third chamber: heating process-the gas can be heated up to 550°C 44
3.6 DIP-APCI ion source functional principle, push rod with crucible for liquid and solid samples, APCI chamber with corona needle 45
3.7 DART-Q-ToF-MS mass spectrum of a typical sample; 1 matrix signal from the coating, 2 signal with the m/z of 419.3156 - identified as protonated bis(7-methyloctyl)phthalate 46
3.8 DIP-APCI-Q-ToF-MS mass spectrum of a typical sample; 1 signal with the m/z of 419.3154 - identified as protonated bis(7-methyloctyl)phthalate . . . 47
3.9 Q-ToF-MS/MS mass spectrum of $m/z = 419$; 1 alkyl groups with $m/z =$ 127 $[C_9H_{18} + H]^+$, 2 m/z = 149 $[C_8H_4O_3 + H]^+$ 47
3.10 Pyrolysis-GC-MS recording corresponding to glass wool containing extracted parts of the sample; 1 phthalic acid (pyrolysis product), 2 bis(7-methyloctyl)phthalate 49
3.11 Pyrolysis-GC-EI mass spectrum of the signal from the chromatogram shown in Fig. 3.10 at 35 min, by comparison with a reference library identified as bis(7-methyloctyl)phthalate, fragments: 1 alkyl groups; 2 $m/z = 149$ $[C_8H_4O_3 + H]^+$[13]; 3 $m/z = 293$ $[C_{17}H_{24}O_4 + H]^+$ 50
3.12 AFM camera image of the topographical irregularities after applying varnish 52
3.13 Topographical AFM map of the contaminated area 53
3.14 AFM - Material contrast imaging of the contaminated area due to different adhesion 53
3.15 XPS spectrum of the contaminated area, showing signals of Sn and S 54
3.16 XPS profile: pretreated surface 56
3.17 XPS profile: pretreated surface 57

3.18 Schematic representation of the principle of AFM/CFM measurements (A) and functionalized cantilever (B) 63
3.19 Preparation of self-assembled monolayer on cantilever tips. 63
3.20 XPS spectra of unmodified AFM cantilevers and cantilevers with SAM modification used for CFM measurements. 65
3.21 Measurement with B unmodified gold cantilever and A modified gold cantilever. 66
3.22 Characterization of untreated CFRP. (A) Optical image of the CFRP, the red square corresponds to the area imaged by SECM. (B) SECM false color image of the CFRP. AFM topography and adhesion force (false coloring) images before (C) and after (D) chemical activation. 74
3.23 Characterization of plasma treated CFRP. (A) Optical image of the CFRP, the red square corresponds to the area imaged by SECM. (B) SECM false color image of the CFRP. AFM topography and adhesion force (false coloring) image before (C) and after (D) chemical activation. The imaged areas correspond to the red squares shown in (B). 76
3.24 Characterization of laser treated CFRP. (A) Optical image of the CFRP, the red square corresponds to the area imaged by SECM. SECM false color image of the CFRP (B). AFM topography and adhesion force (false coloring) image before (C) and after (D) chemical activation. 77
3.25 Characterization of CFRP treated by corundum blasting. (A) Optical image of the CFRP, the red square corresponds to the area imaged by SECM. (B) SECM false color image of the CFRP. AFM topography and adhesion force (false coloring) image before (C) and after (D) chemical activation. 78
3.26 XPS measurements of CFRP surfaces with different pretreatment protocols. C1s signals are shown for (A) reference CFRP without pretreatment, (B) laser pretreated CFRP, (C) plasma pretreated CFRP, (D) corundum blasting pretreated CFRP. 80
3.27 Representative examples for fracturing of the CFRP correlated with the different pretreatment methods. 81
3.28 XPS spectra of CFRP surfaces after applying different pretreatment methods. 83
3.29 Cyclic voltammogram using a SECM probe with a diameter of 25 µm (1.5 mM FcMeOH with 0.2 M KNO_3, Estart= -0.2 V, Evortex= 0.3 V, scan rate: 50 mV s^{-1}). Inset: Optical micrograph of the SECM probe. 83

3.30 Chemical force microscope image of the reference CFRP sample without the influence of extreme climate conditions 88
3.31 Chemical force microscope image of the CFRP sample after 30 days storage at 80° C 88
3.32 DART-Q-ToF-MS mass spectrum of the reference CFRP sample; signals 1 to 9 listed in Table 3.5 89
3.33 DART-Q-ToF-MS mass spectrum of the CFRP sample after 30 days storage at 80°C; signals 1 to 6 listed in Table 3.5 89
3.34 XPS spectrum of the reference CFRP sample 91
3.35 XPS spectrum of the CFRP sample after 30 days storage at 80°C 92
3.36 Application to an unfinished industrial manufactured door of a car 97
3.37 Industrial application of cavity wax using a dual-nozzle. 97
3.38 Micro chamber with DNPH-catridge for the analysis of aldheyde emission. 99
3.39 Saucer test for the evaluation of the hardening time of the cavity wax after two hours. 100
3.40 Leakage of cavity wax into plastic bags. 101
3.41 Aldehyde emissions for the different wax modifications after the micro chamber. 102
3.42 Quantitative aldehyde emission of the cavity wax with different urea modifications 106

Erklärung

Ich habe die Arbeit selbstständig verfasst, keine anderen als die angegebenen Quellen und Hilfsmittel benutzt und bisher keiner anderen Prüfungsbehörde vorgelegt. Von den in §27 Abs. 5 vorgesehenen Rechtsfolgen habe ich Kenntnis genommen.

Regensburg, 09.01.2019 ..... Stefan Viehbeck .....

(Stefan Viehbeck)